NSEL Report Series
Report No. NSEL-011
May 2008

Structural Health Monitoring Strategies for Smart Sensor Networks

Yong Gao
and
Billie F. Spencer, Jr.

NEWMARK STRUCTURAL ENGINEERING LABORATORY

Department of Civil and Environmental Engineering
University of Illinois at Urbana-Champaign

UILU-ENG-2008-1805

ISSN: 1940-9826

The Newmark Structural Engineering Laboratory (NSEL) of the Department of Civil and Environmental Engineering at the University of Illinois at Urbana-Champaign has a long history of excellence in research and education that has contributed greatly to the state-of-the-art in civil engineering. Completed in 1967 and extended in 1971, the structural testing area of the laboratory has a versatile strong-floor/wall and a three-story clear height that can be used to carry out a wide range of tests of building materials, models, and structural systems. The laboratory is named for Dr. Nathan M. Newmark, an internationally known educator and engineer, who was the Head of the Department of Civil Engineering at the University of Illinois [1956-73] and the Chair of the Digital Computing Laboratory [1947-57]. He developed simple, yet powerful and widely used, methods for analyzing complex structures and assemblages subjected to a variety of static, dynamic, blast, and earthquake loadings. Dr. Newmark received numerous honors and awards for his achievements, including the prestigious National Medal of Science awarded in 1968 by President Lyndon B. Johnson. He was also one of the founding members of the National Academy of Engineering.

Contact:
Prof. B.F. Spencer, Jr.
Director, Newmark Structural Engineering Laboratory
2213 NCEL, MC-250
205 North Mathews Ave.
Urbana, IL 61801
Telephone (217) 333-8630
E-mail: bfs@uiuc.edu

This technical report is based on the first author's doctoral dissertation under the same title which was completed in July 2005. The second author served as the dissertation advisor for this work.

Financial support for this research was provided in part by the National Science Foundation (NSF) under NSF grant CMS 03-01140 (Dr. S. C. Liu, Program Manager). This support is gratefully acknowledged.

The cover photographs are used with permission. The Trans-Alaska Pipeline photograph was provided by Terra Galleria Photography (http://www.terragalleria.com/).

ABSTRACT

Structural health monitoring (SHM) is an emerging field in civil engineering, offering the potential for continuous and periodic assessment of the safety and integrity of civil infrastructure. Based on knowledge of the condition of the structure, certain preventative measures can be carried out to prolong the service life of the structure and prevent catastrophic failure. However, challenges remain to apply SHM to civil engineering structures.

The research detailed in this report has three complimentary efforts that seek to address some of those challenges. The first component is to experimentally verify an existing damage detection method utilizing a three-dimensional 14-bay truss structure at the Smart Structures Technology Laboratory (SSTL) of University of Illinois at Urbana-Champaign (UIUC). This flexibility-matrix-based method has drawn considerable attention recently; however, only numerical validation had been previously provided. Experimental verification allows assessment of the efficacy of the method in practice.

The second part of the work is directed toward extending the flexibility-matrix-based approach to continuous online SHM employing ambient vibration (*i.e.*, unmeasured input excitations). Continuous online SHM of civil infrastructure is highly desired, because it allows early detection of the damage in a structure and therefore offers the possibility to extend the service life of the structure.

Finally, a new distributed computing SHM strategy, which is suitable for implementation on arrays of densely distributed smart sensors, is proposed for monitoring of civil infrastructure. Recent development of smart sensor technology has the potential to fundamentally change how civil infrastructure will be monitored. Damage detection algorithms which can take advantage of smart sensor technology are highly desired, but currently very limited. The new approach proposed in this research is different from the traditional ones which have relied on central data acquisition and processing, and therefore meshes well with the distributed computing environment offered by smart sensor technology. A strong basis for application of SHM to civil engineering structures using smart sensors has been provided.

CONTENTS

CHAPTER 1

INTRODUCTION

1.1 Importance of Damage Detection of Civil Infrastructure

Our daily lives are becoming more and more dependent on civil infrastructure, including bridges, buildings, pipelines, offshore structures, etc. Much of the existing infrastructure in the United States has been in service for many years. These structures continue to be used, despite aging and the associated accumulation of damage. For example, the George Washington Bridge which crosses the Hudson River between upper Manhattan and Fort Lee, New Jersey has been in service for more than 70 years. This bridge is still in use and deemed as one of the busiest bridges in the world. Any malfunction of this bridge could cause tremendous economic loss. Aktan et al. (2001) pointed out that most of the long-span bridges in the United States, which have 100 meters or longer spans, are over 50 years old and several are even over 100 years old; more than 800 of these kinds of bridges are classified as fracture-critical in the National Bridge Inventory. Monitoring the condition of these structures to provide the necessary maintenance has become critically important to our society. Moreover, evaluation of the condition of critical facilities and civil infrastructure is extremely important after natural hazards such as earthquake, or man-made disasters such as terrorist attack. These emergency facilities have to be evaluated and repaired immediately to minimize the impact of the disaster and to facilitate the recovery of our society.

Structural health monitoring (SHM) is an emerging field in civil engineering, offering the potential for continuous and periodic assessment of the safety and integrity of the civil infrastructure. Based on knowledge of the condition of the structure, certain preventative measures can be carried out to prolong the service life of the structure and prevent catastrophic failure. Damage detection strategies can ultimately reduce life cycle cost.

1.2 Damage in Civil Engineering Structures

In the most general terms, damage can be defined as changes introduced into a system that adversely affects its performance (Farrar et al. 1999). As for civil engineering structures, changes in materials, connections, boundary conditions, etc., which cause deteriorated performance of the structure, can be defined as damage. For example, material aging usually reduces the load capacity of structural elements which leads to stress redistribution in the structure. This stress redistribution can result in loads that are substantially different from those expected based on the original structural design, potentially undermining the safety of the structure and even leading to its failure.

Structural damage can be caused in various ways. Normal activities can introduce damage to the structure. Buildings can be damaged due to corrosion, aging, and daily activities. Traffic and wind loads cause damage on bridges, while offshore structures suffer from wave loading and corrosion due to the seawater. On the other hand, excessive

loads produced by tornados, hurricanes, and earthquakes also can potentially cause damage in structures.

The effect of damage on structures can be classified as linear and nonlinear (Doebling et al. 1996). Linear damage can be defined as the case when structures still behave linear-elastically after damage is introduced, while nonlinear damage causes structures to show nonlinear behavior after damage has occurred. In civil engineering structures, metal corrosion and concrete spalling/scour are typical damage events that may be defined as linear damage. Both corrosion and spalling/scour can significantly reduce the cross section of structural members, and therefore degrade the load capacity of the structure. For example, severe spalling resulted from rapid current often happens at the waterline of bridge piles with a considerable loss of cross-section. Examples of nonlinear damage in civil engineering include cracks formed in concrete or metal members, loose connections of steel members, etc. For example, structural members with fatigue cracks often show nonlinear behaviors due to the open and close of the cracks even under the normal operating vibration environment.

The research detailed in this report only addresses the case of linear damage in structures. In particular, structural damage is simulated by decreasing the elastic modulus in numerical studies and by reducing the cross section of structural members in experimental studies. The methods developed here are expected to be able to accommodate various cases of linear damages that result in a loss of structural stiffness.

1.3 Challenges of Applying Existing SHM Methods to Civil Infrastructure

Numerous SHM methods have been proposed in the past few decades; however, challenges remain before they can be applied to civil engineering structures. Most existing SHM methodologies require direct measurement of the input excitation for implementation. However, in many cases, there is no easy way to measure these inputs – or alternatively, to externally excite the structure. This difficulty has limited the application of existing SHM methods which require the measurements of input excitations. Methods based on ambient vibration have become more important in the field of SHM and damage detection. More research efforts should be directed toward the development of SHM methodologies which minimize the needs to measure the input excitation and can handle the ambient vibration case.

Another challenge results from the fact that damage in structures is an intrinsically local phenomenon. Sensors close to the damaged site are expected to be more heavily influenced than those remote to the damage. Therefore, to effectively detect damage at an arbitrary location in a structure, sensors must be densely distributed throughout the structure. Most existing SHM methods assume the measured data is to be centrally acquired. Using traditionally wired sensors to implement such a SHM system with a dense array of sensors is quite challenging because of the cost and difficulties in deploying and maintaining associated wiring plant. A traditional SHM system employing wired sensors is shown in Fig. 1.1. The wiring system for a large civil infrastructure is obviously much more complicated and therefore more difficult to manage. In addition, a tremendous

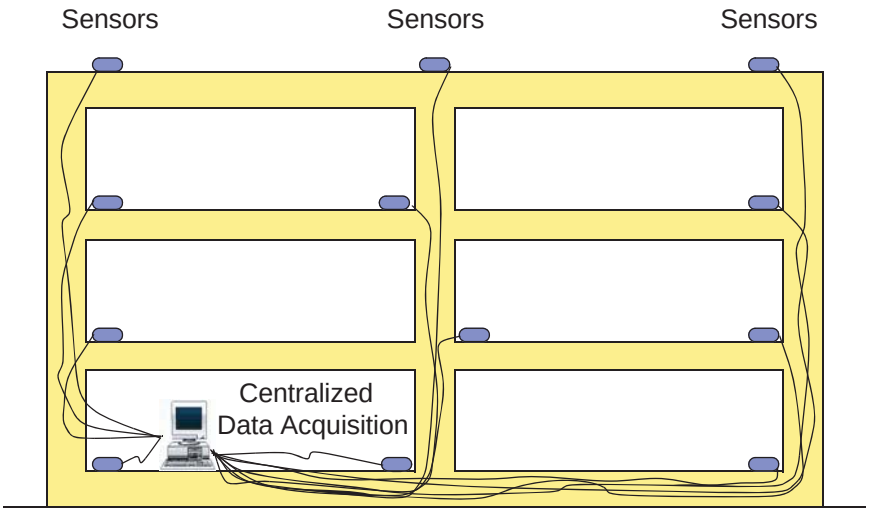

Figure 1.1: Traditional SHM system using centralized data acquisition (Spencer et al. 2004).

amount of data is expected to be generated that would need to be sent to the central station. Managing such a large amount of data is also challenging and is not cost-effective. Therefore, damage detection of large civil infrastructure employing traditionally wired sensors is intractable.

Recent development of smart sensors has made SHM using a dense array of sensors feasible (Spencer et al. 2002, 2004). The essential feature of a smart sensor is the on-board microprocessor, which grants sensors the “smart” characteristics. Programming can be embedded in the sensor’s microprocessor, which allows smart sensors to save data locally, perform desired computation, make “if-then” decisions, scan valuable information, send results quickly, etc. Therefore, a portion of the computation can be done at the local sensor level for damage detection. Extraneous information can be discarded, reducing the information that needs to be transferred back to the central station. Note that all smart sensors to date are wireless as well, with data transmissions based on radio frequency (RF) communications. A typical wireless SHM system using smart sensors is shown in Fig. 1.2. Damage detection algorithms which can take advantage of the distributed computing environment offered by smart sensor technology are highly desired but currently very limited.

1.4 Overview of Report

The research detailed in this report seeks to address some of these challenges, with the final goal of developing a new SHM strategy that is suitable for implementation on a dense array of smart sensors.

Chapter 2 reviews previous research on vibration-based damage detection methods, as well as the smart sensor technology.

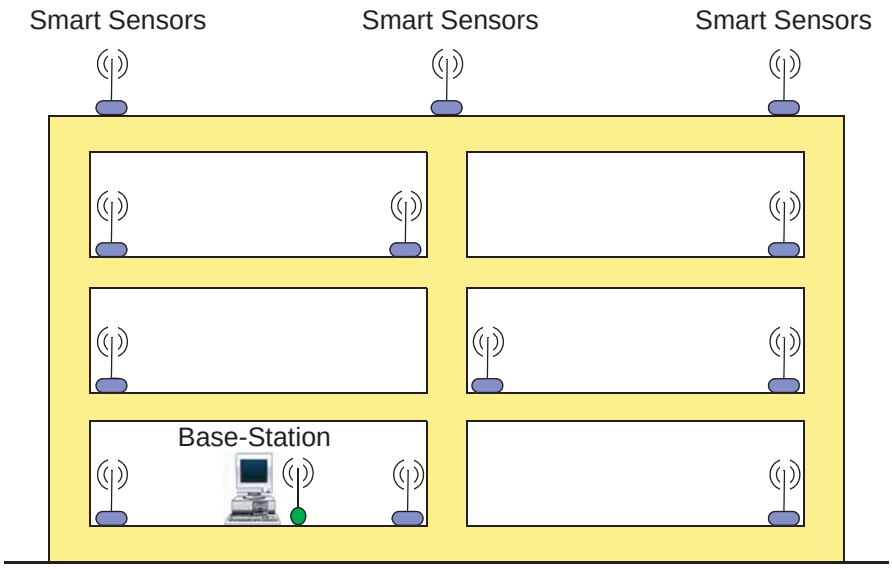

Figure 1.2: Wireless SHM system using smart sensors (Spencer et al. 2004).

Chapter 3 presents the experimental verification of a flexibility matrix based damage detection method, the damage locating vector (DLV) method. The DLV method has drawn considerable attention recently; however, only numerical examples have been provided to date. Experimental verification needs to be conducted to assess the efficacy of the method in practice. Following presentation of the motivation for the flexibility-based methods, the basic concept of the DLV method is introduced. Construction of the flexibility matrix for proportionally damped structure employing forced vibration is then reviewed. Finally, details of the experimental setup and experimental verification results are presented in this chapter.

Extension of the DLV method to continuous online SHM employing ambient vibration is described in Chapter 4. Continuous online monitoring of civil infrastructure is highly desirable, because it allows the damage in the structure to be detected at an early stage so that necessary measures can be carried out in time to prevent further damage to the structure. In this chapter, construction of the flexibility matrix employing forced vibration for structures with general viscous damping and employing ambient vibration for proportionally damped structures is described. Changes of the modal normalization constants due to structural damage are then investigated, which leads to the extension of the DLV method for continuous online SHM. Finally, numerical validation of the proposed approach is presented.

Chapter 5 presents the development of a new distributed computing strategy (DCS) suitable for implementation of SHM on a dense array of smart sensors. The proposed algorithm employs only locally measured sensor information to monitor the portion of the structure which is in the vicinity of the sensors. Measured data are aggregated locally with extraneous information being discarded before sending to a central station. This new approach is therefore different from the traditional algorithms which are reliant on central

data acquisition and processing. The concept of damage localization using local sensor information is first presented. The hierarchical distributed computing SHM strategy is then proposed. Numerical validation of the proposed approach employing a 14-bay planar truss is provided.

In Chapter 6, experimental validation of the proposed DCS strategy is presented using a 6.5 m long truss structure. This three-dimensional 14-bay truss structure is tested at the Smart Structures Technology Laboratory (SSTL) of University of Illinois at Urbana-Champaign (UIUC). Following the discussion of the experimental setup, experimental results for the algorithm initialization are first presented. Damage detection results of different damage scenarios under various excitation conditions are then provided. Finally, preliminary reliability study using experimental data is conducted.

Reference implementation of this distributed computing SHM strategy in a Simulink and Stateflow model is presented in Chapter 7. Numerical and experimental studies of the efficacy of the proposed DCS approach are carried out in Chapter 5 and 6. However, some important issues of implementing the proposed approach on real smart sensor networks have not been studied. A Simulink and Stateflow model which simulates a smart sensor network consisting of eleven sensor communities has been developed in this chapter to better understand the application of the proposed DCS approach in practice. Background knowledge of Simulink and Stateflow is first provided. Detailed description of the proposed Simulink and Stateflow model is then presented, followed by implementation of the proposed DCS approach in the proposed model employing both simulation and experimental data.

Finally, Chapter 8 summarizes the research detailed in this report and presents possible directions for future research on SHM employing smart sensors.

LITERATURE REVIEW

This chapter presents a brief review of some of the existing vibration-based damage detection methods, as well as recent developments in smart sensor technology.

2.1 Vibration Based Damage Detection Techniques

Numerous existing health monitoring methods were carefully reviewed by Doebling et al. (1996) and Sohn et al. (2003). Vibration-based damage detection techniques, which usually do not require a prior knowledge of the damage location and by which damage covered by non-structural elements can still be detected, have been an important research area for SHM. Vibration-based damage detection methods are often classified based on the type of the measured data used and/or the technique used to identify the damage.

One category of these methods uses frequency changes. Vandiver (1975) detected the damage in an offshore light station tower by examining the frequency changes in the first two bending modes and the first torsional mode. By developing an analytical model and systematically removing members from the model to simulate structural damage, the author demonstrated that failure of most members produces a frequency change greater than 1%, and thus, damage in most of the elements is detectable. Adams et al. (1978) and Cawley and Adams (1979) proposed a sensitivity-based damage localization method using only frequency measurements. This method is based on the assumption that the ratio of the frequency change between two modes is only a function of the damage locations. By calculating the theoretical frequency ratios due to the damage in selected locations and comparing them with the measured ones, the damage locations were determined. However, some erroneous results were obtained when implementing this method. Additionally, the accuracy of this method is highly dependent on the accuracy of the analytical model. Stubbs (1985) and Stubbs and Osegueda (1987) presented a method which relates the change of the element stiffness to the change of the modal frequency. This method assumes that the structural stiffness matrix can be expanded in terms of a diagonal element stiffness matrix. This assumption is only valid for simple structures, for example, truss structures. By removing this assumption, Stubbs and Osegueda (1990a, b) gave a more general expression relating the element stiffness matrix and the modal frequencies. For multiple damage scenarios, false damage locations were predicted by this method. Spyrakos et al. (1990), Chen et al. (1995), and Brincker et al. (1995) reported experimental studies on frequency changes due to damage in the structure. As expected, the frequency decreases when the damage extent increases. Messina et al. (1996) and Williams et al. (1997) introduced the damage location assurance criterion (DLAC), which is a correlation criteria between the measured frequency change and the frequency change due to damage in assumed locations.

Although numerous researchers have been working on the techniques only employing frequencies, several limitations exist. Salawu (1997) pointed out that a 5% frequency shift

might be required to detect structural damage with confidence when using frequencies only. In addition, frequency shifts alone might not necessarily indicate that damage has occurred in the structure. As Aktan et al. (1994) reported, significant frequency shifts (exceeding 5%) caused by changes in ambient conditions have been measured for bridges in a single day. Additionally, different damage locations can produce the same degree of the frequency shift; therefore, using only frequency changes might not be sufficient to uniquely determine the damage location. Moreover, damage in low stress regions might be particularly difficult to detect employing frequency data alone (Salawu 1997).

Another category of these methods uses the change in mode shapes. West (1984) was perhaps the first to implement systematic use of mode shape information for damage detection. His technique uses the modal assurance criteria (MAC) to localize structural damage. To implement this method with confidence, numerous sensors appear to be necessary. After numerical and experimental study of a beam, Fox (1992) showed that the MAC value is not so sensitive to damage and suggested that graphical comparison of the mode shapes might be a good way to locate damage. Kim et al. (1992) successfully isolated damage in a structure by employing the Coordinate MAC (COMAC) in conjunction with the Partial MAC (PMAC). Ko et al. (1994), Lam et al. (1995), and Salawu (1995) also did extensive research in this area in the past decade.

Modal strain energy has also been employed to detect structural damage. Carrasco et al. (1997a, b) located and quantified the damage in a truss structure using changes in the modal strain energy before and after damage. However, damage simulated by a cut through half the depth of the element could not be located. Shi et al. (1998, 2000) also applied the concept of modal strain energy change to detect structural damage. Elements with a high modal strain energy change ratio were identified as possibly damaged elements. Then, a damage quantification algorithm was developed by expressing the modal strain energy change in terms of the contributions from the possible damage elements. In this algorithm, iteration is required to obtain a converged damage measure, and results showed that many modes are needed to obtain an accurate estimate of the damage extent. In practice, measuring higher modes is challenging. Shi et al. (2002) improved their quantification algorithm by using only the first few modes. The numerical example showed good results. For experimental verification, the authors assumed that the type of the damage was known a priori, which is usually not the case.

Ricles and Kosmatka (1992) used residue force as an indicator of the damage in the structure. Damage locations are first identified at the degrees of freedom (DOFs) with non-zero residue forces. The damage extent is then determined by expressing the damaged modal parameters as a Taylor series in terms of the structural parameters in the damaged region and the corresponding undamaged modal parameters. The results indicated that this method is quite model dependent. Baruh and Ratna (1993) and Sheinman (1996) also used the residue force to detect the damage with a different quantification algorithms.

Parameter estimation methods have also shown promising. By estimating structural parameters, not only the location but the extent of the damage can be obtained. Yao et al. (1992) successfully performed parameter estimation on a steel frame structure for damage detection using experimental data. Shin and Hjelmstad (1994) proposed a parameter estimation method employing an adaptive element-grouping scheme. This method has

shown to be successful using noisy and limited measurement information. However, errors arise in some of the cases when multiple damage locations exist. Dos Santos and Zimmerman (1996) propose a method employing minimum rank perturbation theory in conjunction with ordinary least-squares estimation for damage detection. Hjelmstad (1996) observed that there will not be a unique solution for structural parameter estimation in some of the cases when measurements are too limited and sparsely distributed. Pothisiri and Hjelmstad (2003) improved the method proposed by Shin and Hjelmstad (1994) by successfully tackling the multiple damage scenario using a new element-group updating scheme. The proposed approach was also shown to be able to handle the nonuniqueness issue in parameter estimation. In this method, errors in the estimated parameters are reduced by selecting a near-optimal measurement set.

Another group of these methods takes advantage of the changes in the flexibility matrix. Because there is an inverse relationship between the flexibility and stiffness matrix, damage in the structure, which leads to a decrease in the stiffness, will increase the flexibility. Pandey and Biswas (1994, 1995b) employed the flexibility matrix to locate damage. First, the flexibility matrices before and after damage are constructed from the measured data. The maximum value in each column (each column corresponding to one DOF) of the flexibility matrix change was then selected as indicator of the damage location. The columns which have larger values are the possible damage locations. However, directly using the flexibility matrix change to do damage localization might be difficult for multiple damage locations. Pandey and Biswas (1995a) further improved the method based on the flexibility matrix to locate and quantify the damage in the structure. A formulation describing the relationship between the change in the flexibility matrix as a function of the change in the elemental stiffness matrix was developed. A pseudo inverse technique was then applied to obtain the change in the elemental stiffness. Toksoy and Aktan (1994) examined the damage on a real bridge based on the measured modal flexibility matrix. The modal flexibility matrices before and after damage were developed from the measurements. Then, these matrices were loaded with different load configurations and the deflection profiles obtained. Comparison of the deflection profiles gave the damage location information in the bridge. More recently, Bernal (2002) proposed a flexibility-matrix-based damage localization method — the damage locating vector (DLV) method. A set of load vectors, designated as damage locating vectors (DLVs), were computed from the change in the flexibility matrix. When the DLVs are applied as static forces on the undamaged structure, the stress field in the structure bypasses the damage areas. This unique characteristic of the DLVs can be employed to localize damage in the structure.

Numerous methods, including mode shape curvatures based methods (Kim et al. 1997; Garcia et al. 1998; Maeck and De Roeck 1999; Ho and Ewins 1999, 2000), neural network techniques (Wu et al. 1992; Chen and Kim 1994; Masri et al. 1996; Luo and Hanagud 1997; Ni et al. 1999**),** genetic algorithms (Friswell et al. 1995; Mares and Surace 1996; Carlin and Garcia 1996; Zimmerman et al. 1997**)**, etc., have also been employed by researchers in the field of damage detection.

2.2 Smart Sensor Technology

Another important research area pertaining to SHM that has attracted significant attentions in the past decade is the smart sensor technology. Indeed, a National Research Council report recently noted that the use of networked systems of embedded computers and sensors throughout society could well dwarf all previous milestones in the information revolution (National Research Council Computer Science and Telecommunications Board 2002). Smart sensors to date have four important characteristics: (1) an on-board microprocessor, (2) wireless communication, (3) a small size, and (4) a low cost. Smart sensing technology may be the only way to fulfill the vision of SHM of civil engineering structures using a densely distributed sensor network. Some of the recently developed smart senors will be reviewed in this section.

Straser and Kiremidjian (1996, 1998) proposed a wireless modular monitoring system (WiMMS) for SHM of civil engineering structures using smart sensor technology. The proposed network provides ease of installation, low cost, portability, and broad functionality. The sensor unit consists of a microprocessor, radio modem, data storage, and batteries. To reduce the battery consumption, the smart sensor can be either in the waiting mode or the operation mode. Agre et al. (1999) presented a prototype smart sensor called “AWAIRS I”. This sensor supports bidirectional, peer-to-peer communications with a small number of neighbors. Brooks (1999) emphasized the importance of the sensor’s computational capacity and defined the fourth-generation sensors as having a number of attributes: bi-directional command and data communication, all digital transmission, local digital processing, preprogramming decision algorithms, user-defined algorithms, internal self-verification and diagnosis, compensation algorithms, on-board storage and extensible sensor object models. Lynch et al. (2001) demonstrated a proof-of-concept smart sensor that uses a standard integrated circuit component. Key features of the unit include wireless communications, high-resolution 16-bit digital conversion of interfaced sensors, and a powerful computational core that can perform various data interrogation techniques in near real-time. The sensor unit was validated through various controlled experiments in the laboratory. Numerous researchers, including Maser et al. (1997), Mitchell et al. (1999, 2001), and Liu et al. (2001), also contributed to this research area.

While substantial research has been conducted, the above-mentioned smart sensor systems are of a proprietary nature. To advance the technology more efficiently, an open hardware/software platform is needed.

The Smart Dust project supported by the US Defense Advanced Research Projects Agency (DARPA) has the ultimate objective of creating massively distributed sensor networks, which consist of hundreds or thousands sensor nodes; these nodes have been termed as Smart Dust or Motes. The goal is to have small dust that is fully autonomous and is cubic millimeter in size (*http://www.darpa.mil/*). The first Smart Dust, termed COTS Dust (Hollar 2000), incorporated communications, processing, sensors, and batteries into a package about a cubic inch in size.

As part of the Smart Dust project, researchers in University of California at Berkeley have developed an open hardware/software platform for smart sensing research. The generation of Motes following COTS Dust was the Rene, which was developed in the

summer of 2000. This version of the Berkeley Mote had 8KB of programming memory and could be reprogrammed over its radio link. Measured data could be communicated over a range of about 15 feet. The Mica node, which increases the radio transmission rate to 40KB per second, was subsequently developed (Hill and Culler 2002). It contains the same expansion bus as the Rene node allowing it to utilize all existing sensor boards. The programming memory and the data storage memory were also improved to 128KB and 4KB, respectively. The Mica has a transmission range over 100 feet, and has been proposed for applications ranging from military vehicle tracking to remote environmental monitoring. a series of development has been carried out to improve Mica platform that results in Mica2, Mica2Dot, and MicaZ (Crossbow Technology Inc., 2004).

In the fall of 2002, the Spec node that is resulted from analyzing the Mica platform was designed. The size of the Spec node was only 2.5x2.5 mm (see Fig. 2.1). The CPU, memory, and RF transceiver are all integrated into a single piece of silicon. It includes an ultra-low power transmitter that drastically reduces overall power consumption. The Spec node also supports the multi-hop mesh networking protocol.

The latest generation of the of Berkeley Mote is Telos platform, that seeks to achieve three major goals: ultra-lower power operation compared with previous Mote generations, easy to use, and robust hardware and software implementation (Polastre et al. 2005). While Spec node provides significant advantages in power consumption, it offers limited interface flexibility. Telos not only achieved the goal of ultra-lower power operation, its integrated design also allows researchers to develop more robust systems.

The hardware design for the Mote can be downloaded from the Berkeley web site (*http://www.tinyos.net/scoop/special/hardware/*) and the components needed for this design can be purchased from Crossbow Inc. (*http://www.xbow.com/*).

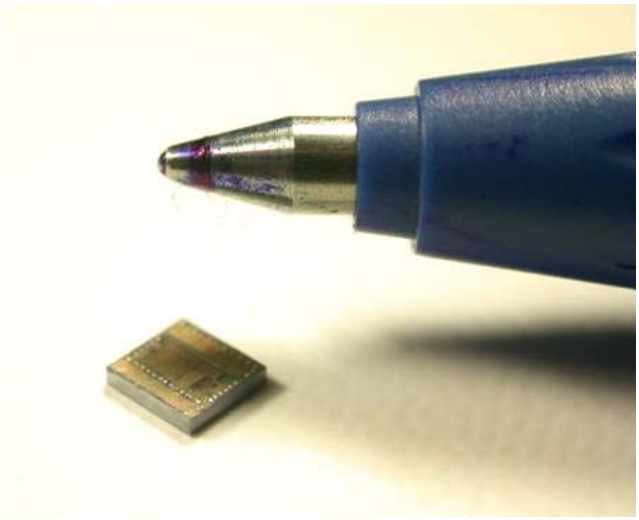

Figure 2.1: Spec node.

Tiny OS is a component based operating environment designed for the Berkeley Mote. More specifically, it is designed to support the concurrency intensive operations required by networked sensors with minimal hardware requirements (*http://today.cs.berkeley.edu/tos/*). The autonomous characteristic of the smart sensor can be realized by developing programs using Tiny OS and then running these program on the on-board microprocessor. This software is open source.

Intel Inc. announced the development of the Intel-Mote platform (Kling 2003). The objective of the Intel-Mote is to create a new platform for smart sensing that provides a high level of integration as well as low-power operation and small physical size. This new platform will fully support Tiny OS. The Berkeley-Mote and Intel-Mote platforms are expected to be an important impetus for smart sensing software and hardware developments.

2.3 Summary

This chapter reviewed some of the vibration-based damage detection methods, as well as recent developments in smart sensor technology. Vibration-based damage detection methods are important because there is no requirement of a prior knowledge of damage location. In addition, damage covered by the non-structural elements can also be detected. Another important research area is the fast-growing smart sensor technology, which is expected to have a significant impact on SHM for civil infrastructure. Development of the vibration-based SHM methods that mesh well with the smart sensor technology is highly desired.

EXPERIMENTAL VERIFICATION OF THE DAMAGE LOCATING VECTOR METHOD

Health monitoring methods based on the flexibility matrix have recently been shown promising. In particular, Bernal (2002) proposed a flexibility-based damage localization method, the damage locating vector (DLV) method. This method has drawn considerable attention recently; however, only numerical validation has been previously provided. Experimental verification needs to be conducted to assess the efficacy of this method in practice.

Following the motivation for flexibility-matrix-based methods, the concept of the DLV method is introduced. Construction of the flexibility matrix for proportionally damped structures employing forced vibration is then provided. Finally, details of the experimental setup and experimental verification results are presented (Gao et al. 2004, 2007).

3.1 Motivation for Flexibility-Based Approach

Because an inverse relationship exists between the flexibility matrix and the square of the modal frequencies, the flexibility matrix is frequently insensitive to high frequency modes, which are typically quite difficult to determine experimentally. This unique characteristic allows the use of a small number of truncated modes to construct a reasonably accurate representation of the flexibility matrix (Gao and Spencer 2002).

To better understand this point, consider the response of a structure described by the following linear equations of motion

$$\mathbf{M}\,\ddot{\mathbf{x}} + \mathbf{C}_d\,\dot{\mathbf{x}} + \mathbf{K}\,\mathbf{x} = \mathbf{f} \tag{3.1}$$

where $\mathbf{M}$ = mass matrix; $\mathbf{C}_d$ = damping matrix; $\mathbf{K}$ = stiffness matrix; $\mathbf{x}$ = displacement vector; and $\mathbf{f}$ = force vector. Assuming proportional damping, the orthogonality property of the mode shapes with respect to the mass and stiffness matrix leads to

$$\overline{\mathbf{M}} = \psi^T \mathbf{M} \psi \quad \text{and} \quad \overline{\mathbf{K}} = \psi^T \mathbf{K} \psi \tag{3.2}$$

in which $\overline{\mathbf{M}}$ = diagonal modal mass matrix; $\overline{\mathbf{K}}$ = diagonal modal stiffness matrix; and ψ = undamped arbitrarily normalized mode shapes. The square of the modal frequencies can be expressed in a matrix sense as

$$\Lambda = \overline{\mathbf{M}}^{-1}\overline{\mathbf{K}} \tag{3.3}$$

in which the square of the modal frequencies ω_j^2 are on the main diagonal of matrix Λ.

Combining Eqs. (3.2) and (3.3) gives

$$\psi^{\mathrm{T}}\mathbf{K}\psi - \psi^{\mathrm{T}}\mathbf{M}\psi\Lambda = 0 \tag{3.4}$$

Let

$$\mathbf{v} = (\psi^{\mathrm{T}}\mathbf{M}\psi)^{1/2} = \overline{\mathbf{M}}^{1/2} \tag{3.5}$$

where $\mathbf{v}$ = diagonal matrix with the mass normalized indices on the main diagonal. Substituting Eq. (3.5) into Eq. (3.4) and keeping in mind that $\mathbf{v}$ is a diagonal matrix, one has

$$\psi^{\mathrm{T}}\mathbf{K}\psi - \mathbf{v}^2\Lambda = 0 \qquad \text{or} \qquad \psi^{\mathrm{T}}\mathbf{K}\psi = \mathbf{v}^{\mathrm{T}}\Lambda\mathbf{v} \tag{3.6}$$

Therefore, the stiffness matrix can be obtained from Eq. (3.6) as

$$\mathbf{K} = (\psi^{\mathrm{T}})^{-1}\mathbf{v}^{\mathrm{T}}\Lambda\mathbf{v}\psi^{-1} \tag{3.7}$$

From Eq. (3.5), one can get

$$(\mathbf{v}^{-2}\psi^{\mathrm{T}}\mathbf{M})\psi = \mathbf{I} \qquad \text{and} \qquad \psi^{\mathrm{T}}(\mathbf{M}\psi\mathbf{v}^{-2}) = \mathbf{I} \tag{3.8}$$

Therefore

$$\psi^{-1} = \mathbf{v}^{-2}\psi^{\mathrm{T}}\mathbf{M} \qquad \text{and} \qquad (\psi^{\mathrm{T}})^{-1} = \mathbf{M}\psi\mathbf{v}^{-2} \tag{3.9}$$

Eq. (3.7) can be rewritten as

$$\mathbf{K} = \mathbf{M}\psi\mathbf{v}^{-1}\Lambda\mathbf{v}^{-1}\psi^{\mathrm{T}}\mathbf{M} \tag{3.10}$$

From the relationship between the stiffness and flexibility matrix $\mathbf{F} = \mathbf{K}^{-1}$, the flexibility matrix is derived from Eq. (3.7) as

$$\mathbf{F} = (\psi\mathbf{v}^{-1})\Lambda^{-1}(\psi\mathbf{v}^{-1})^{\mathrm{T}} \tag{3.11}$$

Equations (3.10) and (3.11) indicate the different influences of the various frequency modes on the stiffness and flexibility matrices, respectively. The influence of the *j*th mode on the stiffness matrix $\mathbf{K}$ increases with the square of the modal frequency ω_j^2, whereas for the flexibility matrix $\mathbf{F}$, the influence decreases with ω_j^{-2}.

To quantitatively see this effect, consider the 53-bar planar truss with 53 DOFs given in Fig. 3.1. The truncated stiffness matrix $\mathbf{K}_n$ at all DOFs, which contains the contribution of the first *n* modes, can be derived from Eq. (3.10) and is written as

$$\mathbf{K}_n = \sum_{j=1}^{n} \mathbf{M}\psi_j\mathbf{v}_j^{-2}\omega_j^2\psi_j^{\mathrm{T}}\mathbf{M}, \qquad n \le N \tag{3.12}$$

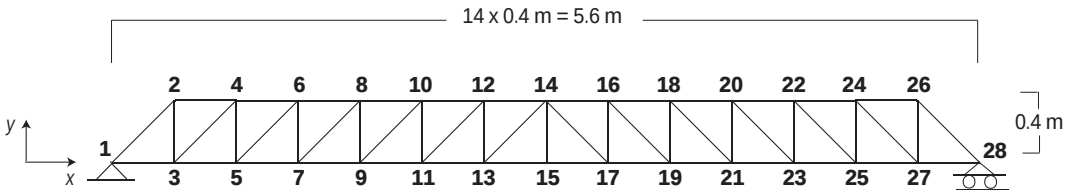

Figure 3.1: 53-bar planar truss.

in which N = number of DOFs of the structure. Two error norms are defined here to measure the difference between the exact and the truncated stiffness matrices at all DOFs. The first is the 2-norm given by the maximum singular value, designated by $\bar{s}$, of the difference matrix

$$\left\| \mathbf{K} - \mathbf{K}_n \right\|_2 = \bar{s}\{ \mathbf{K} - \mathbf{K}_n \} \tag{3.13}$$

The second norm calculated is the Frobenius norm

$$\left\| \mathbf{K} - \mathbf{K}_n \right\|_{\mathrm{F}} = \left[\sum_{i=1}^{N} \sum_{j=1}^{N} (\mathbf{K} - \mathbf{K}_n)_{ij}^2 \right]^{1/2} \tag{3.14}$$

Figure 3.2 shows these two error norms, which are normalized to have a value of 1.0 for $n = 0$. As can be seen from the graph, nearly all of the modes are required to obtain a reasonably accurate representation of the stiffness matrix. Because experimentally obtaining the higher modes of a structure is often challenging, stiffness-matrix-based damage detection strategies may be difficult to implement in practice.

Similarly, the truncated flexibility matrix $\mathbf{F}_n$ can be derived from Eq. (3.11) as

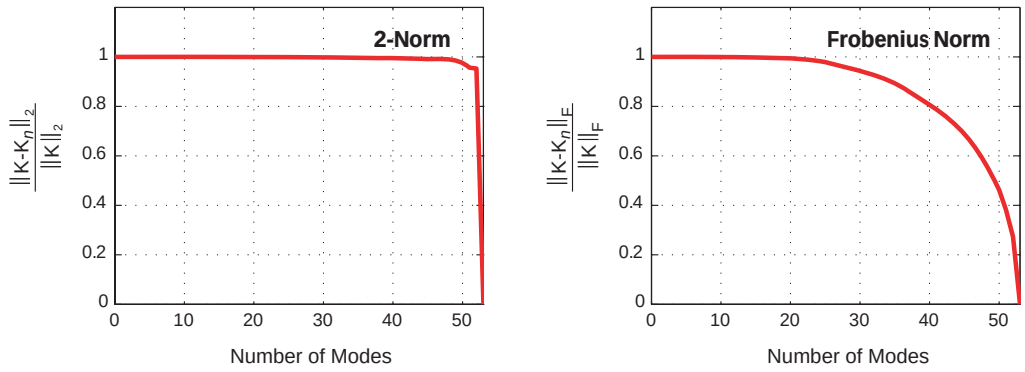

Figure 3.2: Normalized error in truncated stiffness matrix at all DOFs.

$$\mathbf{F}_n = \sum_{j=1}^{n} \psi_j \mathbf{v}_j^{-2} \omega_j^{-2} \psi_j^{\mathrm{T}}, \qquad n \leq N \tag{3.15}$$

The counterparts to the error norms defined in Eqs. (3.13) and (3.14) are then

$$\left\| \mathbf{F} - \mathbf{F}_n \right\|_2 = \bar{s}\{ \mathbf{F} - \mathbf{F}_n \} \tag{3.16}$$

$$\left\| \mathbf{F} - \mathbf{F}_n \right\|_{\mathrm{F}} = \left[\sum_{i=1}^{N} \sum_{j=1}^{N} (\mathbf{F} - \mathbf{F}_n)_{ij}^2 \right]^{1/2} \tag{3.17}$$

These two norms are shown in Fig. 3.3, again normalized to have a value of 1.0 for $n = 0$. As can be seen, only a few modes are required to achieve good accuracy in the flexibility matrix. These results indicate that the truncated flexibility matrix at measured DOFs also can be accurately estimated using the first lower frequency modes.

Because of the high accuracy of the results for the truncated flexibility matrix and its inverse relationship to the stiffness matrix, one might speculate that the truncated stiffness matrix can be recovered by taking the inverse of the truncated flexibility matrix. To investigate this possibility, consider again the planar truss in Fig. 3.1. For this truss, the mode shapes at the DOFs in the *y*-direction at nodes [3, 5, 7, 9, 11] are computed from the analytical model and used to construct the associated stiffness and flexibility matrices.

The truncated flexibility matrix for these DOFs can be obtained using Eq. (3.15) with ψ_j representing the mode shape at the measured DOFs. Denoting the exact flexibility matrix at the measured DOFs as $\mathbf{F}_{\mathrm{m}}$ and the truncated one as $\mathbf{F}_{\mathrm{m},n}$, similar error norms can be computed using Eqs. (3.16) and (3.17) and are shown in Fig. 3.4. These results, of course, are essentially similar to those previously presented in Fig. 3.3 as the number of DOFs does not change the accuracy of the computed flexibility coefficients.

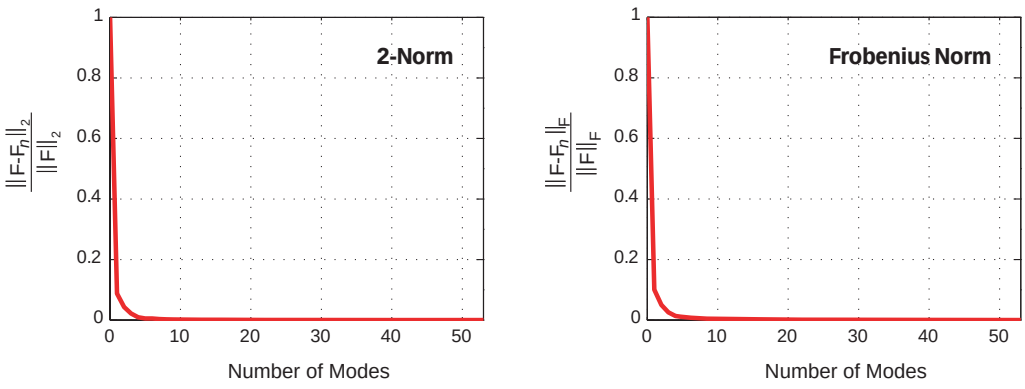

Figure 3.3: Normalized error in truncated flexibility matrix at all DOFs.

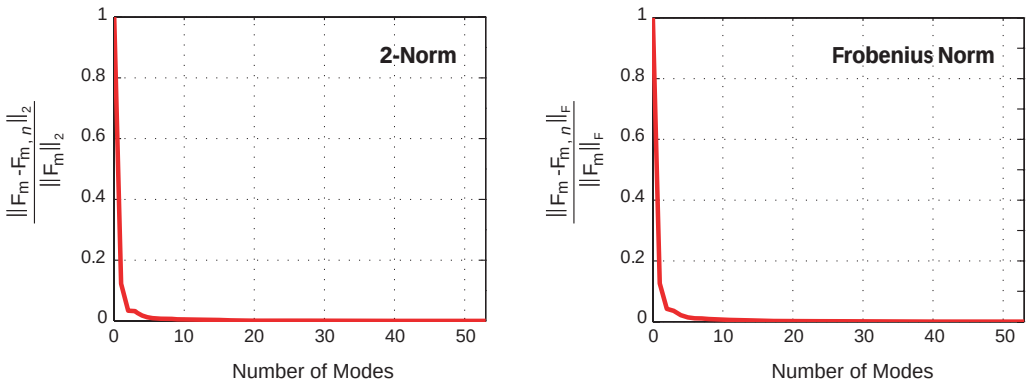

Figure 3.4: Normalized error in truncated flexibility matrix at partial DOFs.

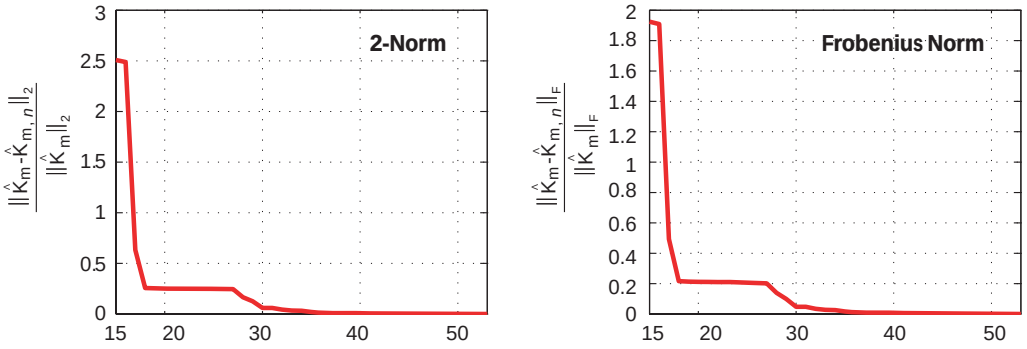

Figure 3.5: Normalized error in condensed truncated stiffness matrix.

The exact condensed stiffness matrices $\hat{\mathbf{K}}_{\mathrm{m}}$ and the truncated condensed stiffness matrix $\hat{\mathbf{K}}_{\mathrm{m},\,n}$ associated with the measured DOFs can be derived from the flexibility matrices, *i.e.*,

$$\hat{\mathbf{K}}_{\mathrm{m}} = \mathbf{F}_{\mathrm{m}}^{-1} \qquad \text{and} \qquad \hat{\mathbf{K}}_{\mathrm{m},\,n} = \mathbf{F}_{\mathrm{m},\,n}^{-1} \tag{3.18}$$

Similar norms for truncated condensed stiffness matrix can be computed from Eqs. (3.13) and (3.14) and are shown in Fig. 3.5. As compared to the flexibility matrix, a larger number of high frequency modes are needed to obtain an accurate estimation of the condensed stiffness matrix.

While these results are problem dependent, they indicate significant potential for practical application of flexibility-based damage detection approaches.

3.2 The DLV Method

3.2.1 General concepts

Bernal (2002) proposed a flexibility-based damage localization method, the DLV method. This technique is based on determination of a special set of load vectors, the so-called damage locating vectors (DLVs). These DLVs have the property that when they are applied to the undamaged structure as static forces at the sensor locations, no stress is produced in the damaged elements. This unique characteristic can be employed to localize structural damage.

Assuming nominally linear structural behavior, the flexibility matrices at sensor locations are constructed from measured data before and after damage and denoted as $\mathbf{F}_u$ and $\mathbf{F}_d$, respectively. Then, all of the linear-independent load vectors $\mathbf{L}$ are collected which satisfy the following relationship

$$\mathbf{F}_d\mathbf{L} = \mathbf{F}_u\mathbf{L} \qquad \text{or} \qquad \mathbf{F}_\Delta\mathbf{L} = (\mathbf{F}_d - \mathbf{F}_u)\mathbf{L} = \mathbf{0} \tag{3.19}$$

This equation implies that the load vectors $\mathbf{L}$ produce the same displacements at the sensor locations before and after damage. From the definition, the DLVs are seen to satisfy Eq. (3.19); that is, because the DLVs induce no stress in the damaged structural elements, the damage of those elements does not affect the displacements at the sensor locations. Therefore, the DLVs are indeed the vectors in $\mathbf{L}$.

To better understand the general concept behind the DLV method, consider the truss shown in Fig. 3.6. Note that the element number has a circle around it. In this structure, assume that three sensors are installed in the *y*-direction at nodes [2, 3, 4]. Therefore, the dimension of the flexibility matrix at the sensor locations is 3×3 and the DLVs are 3×1 vectors. For the case when element 8 is damaged, the DLVs are shown in Fig. 3.7. As can be seen, both DLVs have a zero force in the *y*-direction at node 3. As a result, there will be no stress in element 8 under either of the DLVs, which indicates that element 8 is the damage location.

However, damage in elements for which no stresses are induced by any combination of loads applied at the sensor locations can not be determined by the DLV method. To understand this situation more clearly, refer to Fig. 3.6 again. If the sensor at node 3 is moved to node 7, then the damage in element 8 cannot be located by the DLV method.

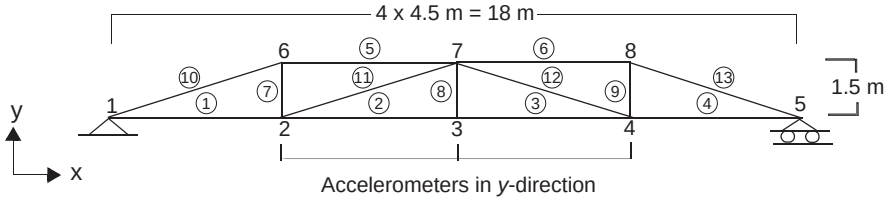

Figure 3.6: 13-bar planar truss.

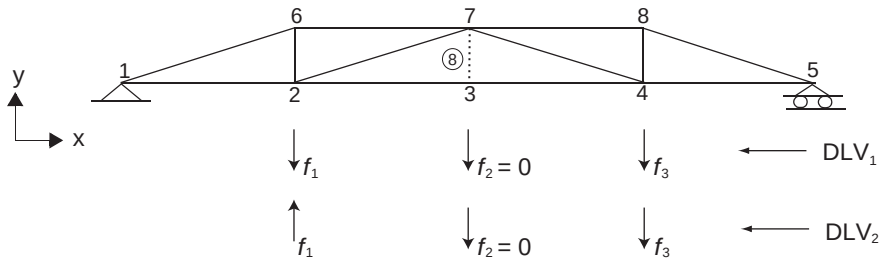

Figure 3.7: Illustration of the DLVs.

This result is due to the fact that no matter what combination of the loads at nodes [2, 4, 7], there is always zero stress in element 8. Therefore, it is important to point out that, for a specific sensor configuration and damage extent, there can be elements that are not damaged but also have small stresses under DLVs. The DLV method identifies a small group of damaged elements that contains the actually damaged elements (Bernal 2002).

3.2.2 Calculation of DLVs

To calculate the load vectors $\mathbf{L}$, the singular value decomposition (SVD) is employed. The SVD of the flexibility difference matrix $\mathbf{F}_\Delta$ leads to

$$\mathbf{F}_\Delta = \mathbf{USV}^T = \begin{bmatrix}\mathbf{U}_1 & \mathbf{U}_0\end{bmatrix}\begin{bmatrix}\mathbf{S}_1 & 0\\ 0 & 0\end{bmatrix}\begin{bmatrix}\mathbf{V}_1 & \mathbf{V}_0\end{bmatrix}^T \tag{3.20}$$

Recall from the properties of the SVD

$$\begin{bmatrix}\mathbf{V}_1 & \mathbf{V}_0\end{bmatrix}^T\begin{bmatrix}\mathbf{V}_1 & \mathbf{V}_0\end{bmatrix} = \mathbf{I} \tag{3.21}$$

Equation (3.20) can be rewritten as

$$\begin{bmatrix}\mathbf{F}_\Delta\mathbf{V}_1 & \mathbf{F}_\Delta\mathbf{V}_0\end{bmatrix} = \begin{bmatrix}\mathbf{U}_1\mathbf{S}_1 & 0\end{bmatrix} \tag{3.22}$$

From Eq. (3.22), one obtains

$$\mathbf{F}_\Delta\mathbf{V}_0 = 0 \tag{3.23}$$

Eqs. (3.19) and (3.23) indicate that $\mathbf{L} = \mathbf{V}_0$, *i.e.*, DLVs can be obtained from the SVD of the difference matrix $\mathbf{F}_\Delta$.

In Eq. (3.20), because of noise and computational errors, the singular values corresponding to $\mathbf{V_0}$ are generally not exactly zero. To select the DLVs from the SVD of the matrix $\mathbf{F}_\Delta$, an index *svn* was proposed by Bernal (2002) and defined as

$$svn_i = \sqrt{\frac{s_i c_i^2}{\max_k (s_k c_k^2)}} \tag{3.24}$$

in which s_i = ith singular value of the matrix $\mathbf{F}_\Delta$; c_i = constant that is used to normalize the maximum stress in the structural element, which is induced by the static load $c_i \mathbf{V}_i$, to have a value of one; and $\mathbf{V}_i$ = right singular vector of the matrix $\mathbf{F}_\Delta$. Bernal (2002) suggested that a value of 0.2 might be a good cutoff for the index *svn*; that is to say, the singular vectors corresponding to the singular values having the index *svn* smaller than 0.2 can be selected as the DLVs.

Each of the DLVs is then applied to an undamaged analytical model of the structure. The stress in each structural element is calculated and a normalized cumulative stress is obtained. If an element has zero normalized cumulative stress, then this element is a possible candidate of damage. The normalized cumulative stress $\bar{\sigma}_j$ for the jth element is defined as

$$\bar{\sigma}_j = \frac{\sigma_j}{\max_k (\sigma_k)} \qquad \text{where} \qquad \sigma_j = \sum_{i=1}^{m} \text{abs}\left(\frac{\sigma_{ij}}{\max_k (\sigma_{ik})} \right) \tag{3.25}$$

In Eq. (3.25), σ_j = cumulative stress in the jth element; σ_{ij} = stress in the jth element induced by the ith DLV; and m = number of DLVs. In practice, the normalized cumulative stresses induced by the DLVs in the damaged elements may not be exactly zero due to noise and uncertainties. Reasonable thresholds should be chosen to select the damaged elements (Bernal 2002).

3.2.3 Numerical example

To quantitatively illustrate the idea of the DLV method, a simple numerical example is given. The 13-bar planar truss, shown in Fig. 3.6 is selected as the test structure. In this structure, each bar has a pipe cross section with an outer diameter of 1.0 cm, and a wall thickness of 0.2 cm. The elastic modulus of the material is 2×10^{11} N/m^2 and the mass density is 7.86×10^3 kg/m^3. The bars are connected at pinned joints. The total length of this truss is 18 m, with 4.5 m in each bay, and the height of the truss is 1.5 m. There are two supports in this truss structure — a pin support at the left end and a roller support at the right end of the lower chord. The roller support at the right end is constrained in the y-direction (vertical direction).

A finite element model consisting of 13 bars, 8 nodes, and 13 DOFs is developed using Matlab. In this numerical example, sensor locations are in the y-direction of nodes [2, 3, 4]. Modal parameters of the lowest three modes before and after damage are obtained from the finite element model. The case when element 12 (*i.e.*, node 4–7) has a 20% stiffness reduction is studied to illustrate the idea of the DLV method.

After the modal parameters are obtained before and after damage, the corresponding flexibility matrices at the sensor locations with a dimension of 3×3 are constructed using Eq. (3.15). The SVD is then applied to obtain the DLVs. To select the DLVs from the results of the SVD, index *svn* is calculated according to Eq. (3.24). Results are shown in Table 3.1. Because the 2nd and 3rd singular values in Table 3.1 have the index *svn* smaller than 0.2, the corresponding singular vectors are selected as the DLVs. These two DLVs are then applied as static forces to the undamaged structure at the sensor locations, *i.e.*, in the *y*-direction of nodes [2, 3, 4]. The normalized cumulative stress for each element is calculated using Eq. (3.25). The results are shown in Fig. 3.8. As can be seen, element 12 has a small normalized cumulative stress, which indicates that element 12 is damaged.

Table 3.1: Results for index *svn.*

	1st singular value	*2nd singular value*	*3rd singular value*
svn	1.0	0.0341	0.0081

3.3 Construction of Flexibility Matrix Using Limited Sensor Information

As shown in the previous section, the flexibility matrix needs to be constructed from the measurement data to implement the DLV method. When the input excitation is measured, there is a least one co-located sensor and actuator pair, and the measured responses are either displacements or velocities, the experimental data can be used to obtain the mass normalized mode shapes (Alvin and Park 1994). Then the flexibility matrix can be computed. Bernal (2000) presented an approach to construct the flexibility matrix at the sensor locations that can employ displacement, velocity, and acceleration responses. This approach will be reviewed in this section.

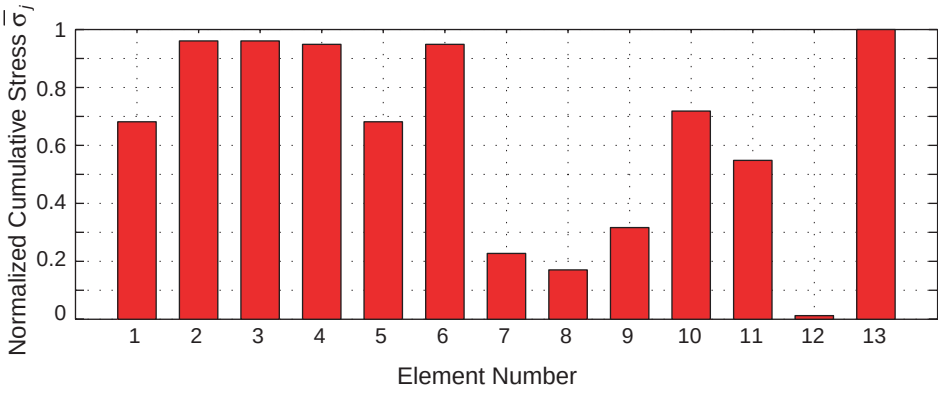

Figure 3.8: Normalized cumulative stress when element 12 is damaged.

First, a state space representation of the structure is obtained using a system identification algorithm, such as the Eigensystem Realization Algorithm (ERA) (Juang and Pappa 1985; Juang 1994). By converting the discrete time state space representation identified from the measured data to continuous time, one obtains

$$\begin{aligned} \dot{\mathbf{z}} &= \mathbf{A}\mathbf{z} + \mathbf{B}\mathbf{u} \\ \mathbf{y} &= \mathbf{C}\mathbf{z} + \mathbf{D}\mathbf{u} \end{aligned} \tag{3.26}$$

where $\mathbf{A}$ = system matrix; $\mathbf{B}$ = input influence matrix; $\mathbf{C}$ = output influence matrix; $\mathbf{D}$ = direct transmission matrix; $\mathbf{z}$ = state vector; $\mathbf{u}$ = input excitation vector; and $\mathbf{y}$ = output vector. Taking the Fourier Transform of Eq. (3.26) yields the following relationship between the inputs and outputs

$$\mathbf{y}(\omega) = \{\mathbf{C}[\mathbf{I} \cdot i\omega - \mathbf{A}]^{-1}\mathbf{B} + \mathbf{D}\}\mathbf{u}(\omega) \tag{3.27}$$

Based on the type of the sensors used in the experiment, the displacement vector $\mathbf{y}_{\mathrm{D}}(\omega)$ can then be expressed as

$$\mathbf{y}_{\mathrm{D}}(\omega) = \frac{1}{(i\omega)^p}\{\mathbf{C}[\mathbf{I} \cdot i\omega - \mathbf{A}]^{-1}\mathbf{B} + \mathbf{D}\}\mathbf{u}(\omega) \tag{3.28}$$

where p = 0, 1, and 2 when measured outputs are displacement, velocity, and acceleration, respectively. If we note that the flexibility matrix relates the inputs to the outputs at $\omega = 0$, the flexibility matrix can be obtained as

$$\mathbf{F}_{\mathrm{f}} = \lim_{\omega \to 0}\left[\frac{1}{(i\omega)^p}\{\mathbf{C}[\mathbf{I} \cdot i\omega - \mathbf{A}]^{-1}\mathbf{B} + \mathbf{D}\}\right] = -\mathbf{C}\mathbf{A}^{-(p+1)}\mathbf{B} \tag{3.29}$$

Therefore, the ith column of $\mathbf{F}_{\mathrm{f}}$ represents the displacements of the structure at the sensor locations due to a unit force being applied at the ith excitation location, u_i.

Let's denote the flexibility matrix at the sensor locations as $\mathbf{F}_{\mathrm{m}}$, then the jth column of $\mathbf{F}_{\mathrm{m}}$ represents the displacements of the structure at the sensor locations due to a unit force being applied at the jth sensor location. If any of the inputs are co-located with sensors, then the corresponding columns in the matrices $\mathbf{F}_{\mathrm{f}}$ and $\mathbf{F}_{\mathrm{m}}$ will be equal. Defining two Boolean matrices $\mathbf{q}_{\mathrm{f}}$ and $\mathbf{q}_{\mathrm{m}}$ which pick out these columns from $\mathbf{F}_{\mathrm{f}}$ and $\mathbf{F}_{\mathrm{m}}$, respectively, we have

$$\mathbf{F}_{\mathrm{m}}\mathbf{q}_{\mathrm{m}} = \mathbf{F}_{\mathrm{f}}\mathbf{q}_{\mathrm{f}} \qquad \text{and} \qquad \mathbf{F}_{\mathrm{m}}\mathbf{q}_{\mathrm{m}} = -\mathbf{C}\mathbf{A}^{-(p+1)}\mathbf{B}\mathbf{q}_{\mathrm{f}} \tag{3.30}$$

Expressing the flexibility $\mathbf{F}_{\mathrm{m}}$ and the system matrix $\mathbf{A}$ in terms of their eigenvalues and eigenvectors gives

$$(\psi_{\mathrm{m}}\mathbf{v}^{-1})\omega^{-2}(\psi_{\mathrm{m}}\mathbf{v}^{-1})^{\mathrm{T}}\mathbf{q}_{\mathrm{m}} = -\mathbf{C}\phi\lambda^{-(p+1)}\phi^{-1}\mathbf{B}\mathbf{q}_{\mathrm{f}} \tag{3.31}$$

where ψ_m = undamped mode shapes at the measured DOFs; $\mathbf{v}$ = matrix of mass normalized indices; λ and ϕ = eigenvalue and eigenvector matrices of the system matrix $\mathbf{A}$, respectively. For classical damping, a mode-by-mode equality holds and Eq. (3.31) can be written as

$$[\psi_m]_j(\omega_j v_j)^{-2}[\psi_m^T]_j \mathbf{q}_m = -2 \cdot \text{real}(\mathbf{C}\phi_j \lambda_j^{-(p+1)} \phi_j^{-1} \mathbf{B}\mathbf{q}_f) \tag{3.32}$$

In Eq. (3.32), only v_j, the diagonal terms of $\mathbf{v}$, are unknown. After v_j is calculated (*i.e.*, the diagonal matrix $\mathbf{v}$ is obtained), the flexibility matrix at the sensor locations can be constructed from the relationship

$$\mathbf{F}_m = (\psi_m \mathbf{v}^{-1})\omega^{-2}(\psi_m \mathbf{v}^{-1})^T \tag{3.33}$$

The DLV method can then be applied to localize damage in the structure. A flow chart for implementing the DLV method for the case when inputs are measured is shown in Fig. 3.9.

3.4 Experimental Verification

The DLV method is experimentally verified using a three-dimensional truss structure (Gao et al. 2004, 2007). In this section, the experimental setup is first described and the experimental results are then presented.

3.4.1 Experimental setup

This 5.6 m long, three-dimensional truss structure (see Fig. 3.10) is tested at the Smart Structures Technology Laboratory (SSTL) of the University of Illinois at Urbana-Champaign (*http://cee.uiuc.edu/sstl/*). It is originally designed at the Structural Dynamics and Control/Earthquake Engineering Lab in the University of Notre Dame (Clayton and Spencer 2001). The length of each bay of the truss is 0.4 m on each side. The truss sits on two rigid supports. One end of the truss is pinned to the support, and the other is roller-supported (see Fig. 3.11). The pinned end can rotate freely with all three translations restricted. The roller end can move in the longitudinal direction.

The truss members are steel tubes with an inner diameter of 1.09 cm and an outer diameter of 1.71 cm. The joints of the elements are specially designed so that the truss member can be easily removed or replaced to simulate damage without dissembling the entire structure. A detailed picture of the joint is shown in Fig. 3.12. As can be seen, the truss member can be removed by unscrewing the collars at the both ends of the member towards the joint. On the other hand, if the collar is screwed away from the joint, this member can be easily installed.

The truss is excited vertically by a Ling Dynamic Systems permanent magnetic V408 shaker (see Fig. 3.13) that can generate a maximum force of 20 lbs with a dynamic performance ranging from 5 Hz to 9000 Hz. A band-limited white noise is sent from the

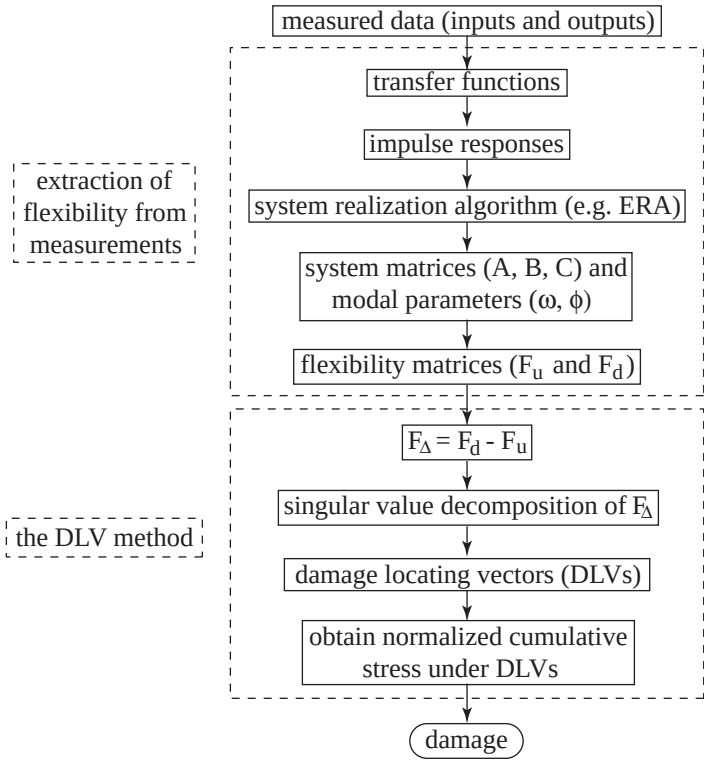

Figure 3.9: Implementation of the DLV method.

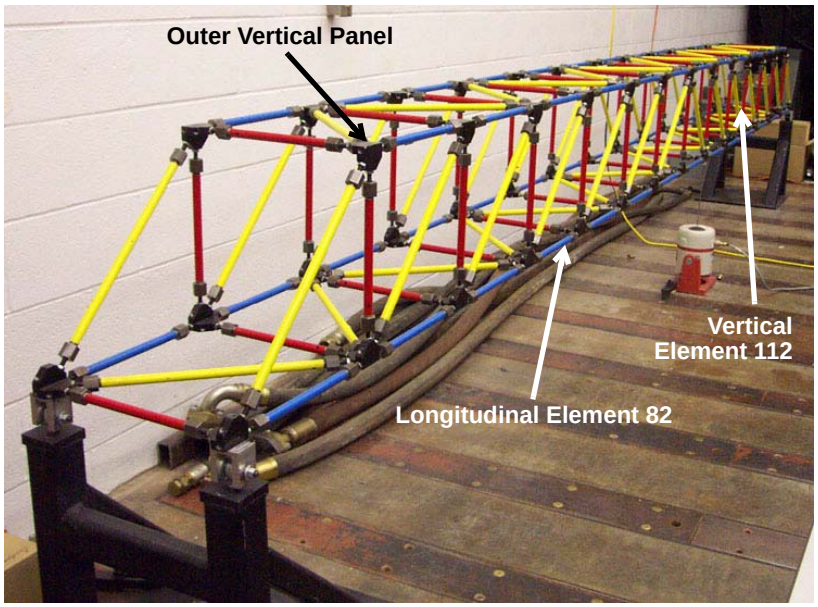

Figure 3.10: Three-dimensional 5.6 m long truss structure.

Figure 3.11: Pin and roller ends.

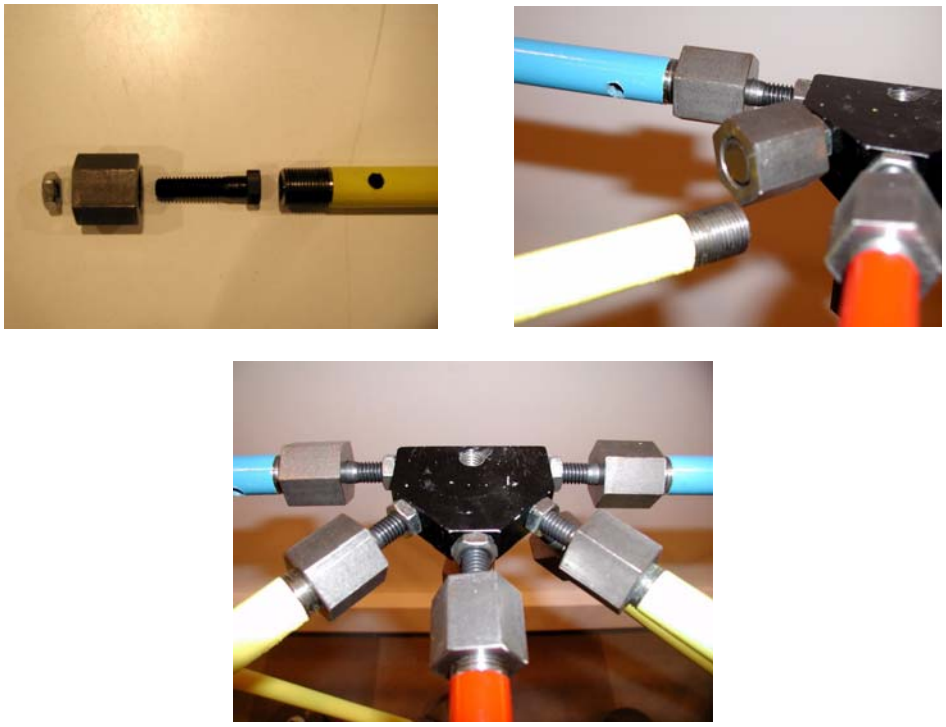

Figure 3.12: Details of the joint.

computer to the shaker to excite the truss structure up to 200 Hz. The shaker is connected to the bottom of the outer panel using a small steel rod. A PCB piezotronics load cell (model 208B02) is installed between the steel rod and the bottom of the joint to monitor and measure the input to the structure. This load cell has a sensitivity of 50 mV/lb, a frequency range of 0.001 to 36000 Hz, and a measurement range of 100 lbs in both compression and tension. A picture depicting the load cell and the connection between the steel rod to the joint node is shown in Fig. 3.14.

PCB high sensitivity piezotronics accelerometers (model 353B33, see top left of Fig. 3.15) are used to measure the response of the structure. These accelerometers have a

Figure 3.13: Magnetic shaker.

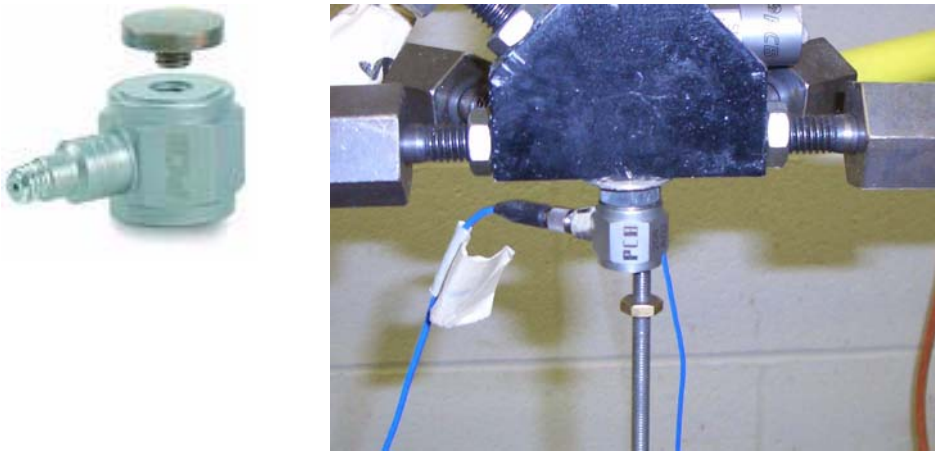

Figure 3.14: Load cell.

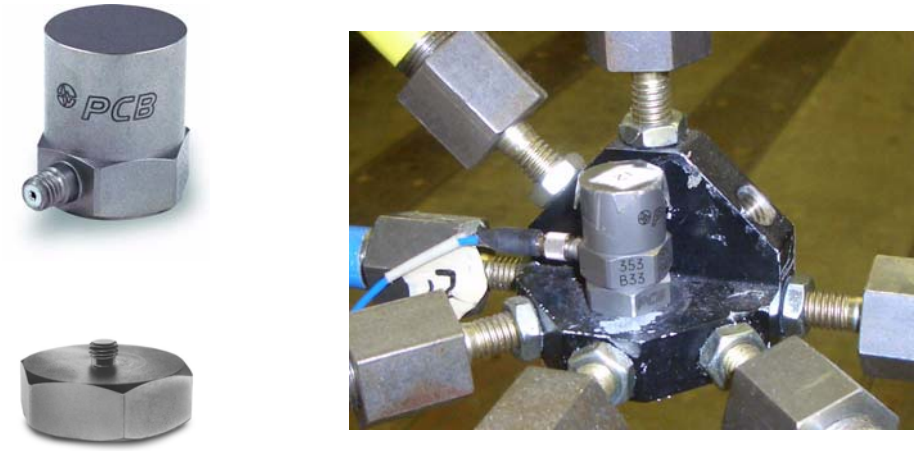

Figure 3.15: Accelerometer and magnetic base.

sensitivity of 100 mV/g, a frequency range of 1 to 4000 Hz, and a measurement range of $\pm 50\,\mathrm{g}$. These accelerometers are mounted on the structure through a magnetic base (see bottom left of Fig. 3.15). These magnetic bases significantly facilitate the relocation of the accelerometers during testing.

Using a limited number of sensors to monitor all members in a complex structure might be difficult. In this experimental verification, the 53 elements in the outer panel (see Fig. 3.16), which are elements 14 through 25 and 79 through 119, are monitored using 13 accelerometers, which are installed vertically at the joints of the lower chord with magnetic bases. A picture of the accelerometer mounted on the structure is shown at the right side of Fig. 3.15.

Two four-channel 20-42 Siglab spectrum analyzers (see Fig. 3.17) are used to drive the shaker and measure the inputs and responses. The spectrum analyzers are synchronized to measure eight channels of data simultaneously, one for the load cell and the other seven channels for the accelerometers. Due to the fact that only eight channels

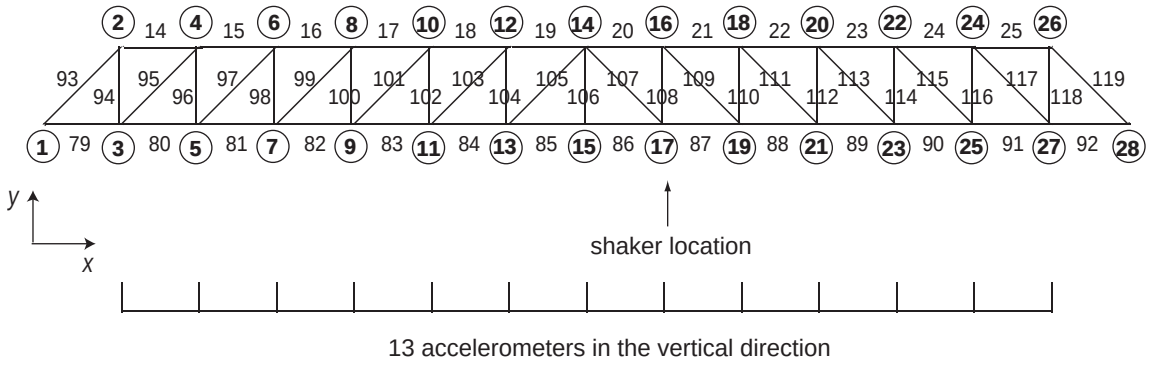

Figure 3.16: Sketch of the outer vertical panel (elements 14 through 25 and 79 through 119).

Figure 3.17: 20-42 Siglab spectrum analyzer.

are available, these thirteen accelerations are measured in two sequential experiments. In this way, thirteen transfer functions between the shaker and different accelerations can still be measured for system identification, by which mode shapes at these thirteen DOFs can be obtained. The shaker is connected to one of the joints at the bottom, so there is one co-located sensor and actuator pair.

Eight-pole elliptical anti-aliasing filters are employed for both the input and output measurements with a cutoff frequency of 200 Hz. The sampling rate for all the measurements is 512 Hz. Measured transfer functions, ranging from 0 to 200 Hz, have a length of 8192 spectra lines with the frequency resolution as 0.0625 Hz. The Hanning window with a 50% overlap is used to compute the transfer functions in the Siglab spectral analyzer. The final transfer function is the average of 30 realizations.

Other equipment used during the testing consist of:

- Amplifier: a Sony STR-D315 amplifier (see Fig. 3.18) is used to magnify the input voltage from the Siglab spectrum analyzer to drive the magnetic shaker.
- Signal conditioner: PCB 4-channel signal conditioners (model 441B104) with AC power supply (model 441A101), as well as single-channel battery powered signal conditioners (model 480E09) have been used in this experiment.

3.4.2 Experimental results

Different damage scenarios have been studied. Damage is simulated by replacing the original member with one having a 52.7% cross section reduction. Results from two of these damage cases (see Table 3.2) in this experimental verification will be presented in the remainder of the chapter.

The use of a single cut-off value of *svn* index (Bernal and Gunes 2004) to select the DLVs has difficulties in the detection of some of the damage cases. For this truss structure and current sensor configuration, a total of five DLVs corresponding to the smallest singular values have been found working well and therefore are used to identify damage for different damage scenarios.

Figure 3.18: Amplifier.

Table 3.2: Two damage cases.

Cases	*Damaged element*	*Cross section reduction*	*Equivalent axial stiffness reduction*
Case 1	longitudinal element 82	52.7%	44%
Case 2	vertical element 112	52.7%	43.5%

Case 1

In this case, longitudinal element 82 (see Figs. 3.10 and 3.16) in the lower chord is replaced by a tube with a 52.7% cross section reduction.

The transfer functions are measured first. Four typical experimentally-measured transfer functions, which are associate the input excitation with measurements from four accelerometers at nodes [2, 5, 8, 11], are shown in Fig. 3.19. The modal parameters are then obtained from the measured transfer functions before and after damage using the ERA method. Here, the first five dominant natural frequencies, which are numbered in Fig. 3.19, are identified. The corresponding mode shapes are also extracted as shown in Fig. 3.20. As noted, there is very little change in the frequencies and mode shapes. Direct comparison between the frequencies and mode shapes to detect damage is difficult if not impossible in this case. Herein, the DLV method is employed to detect the damage.

Once the modal parameters before and after damaged are obtained, the flexibility matrix at the sensor locations can be constructed following the procedure described above. The DLVs are then computed from the difference matrix $\mathbf{F}_{\Delta}$ using Eq. (3.20), and applied as vertical loads at the sensor locations to the undamaged analytical model for static computation. The normalized cumulative stress can then be obtained and employed to locate the damage in the structure.

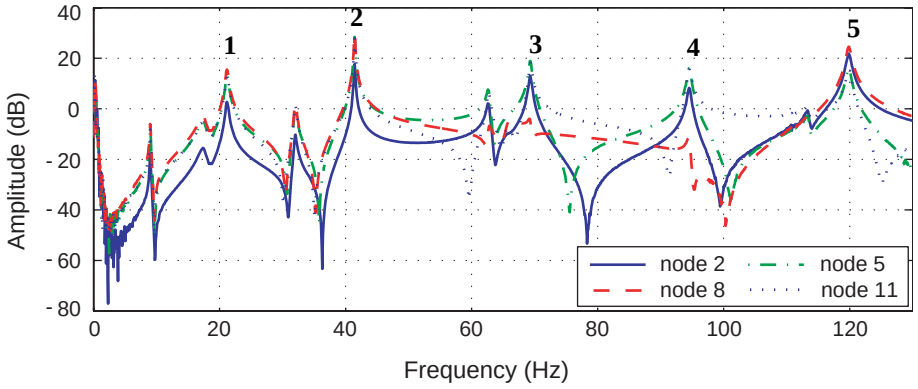

Figure 3.19: Experimentally measured transfer functions.

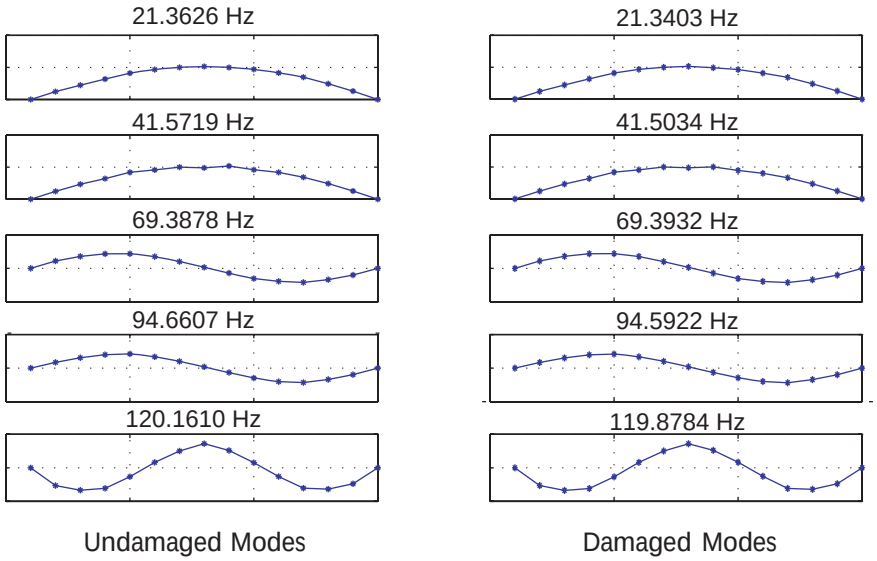

Figure 3.20: Modal parameters identified from experimental data.

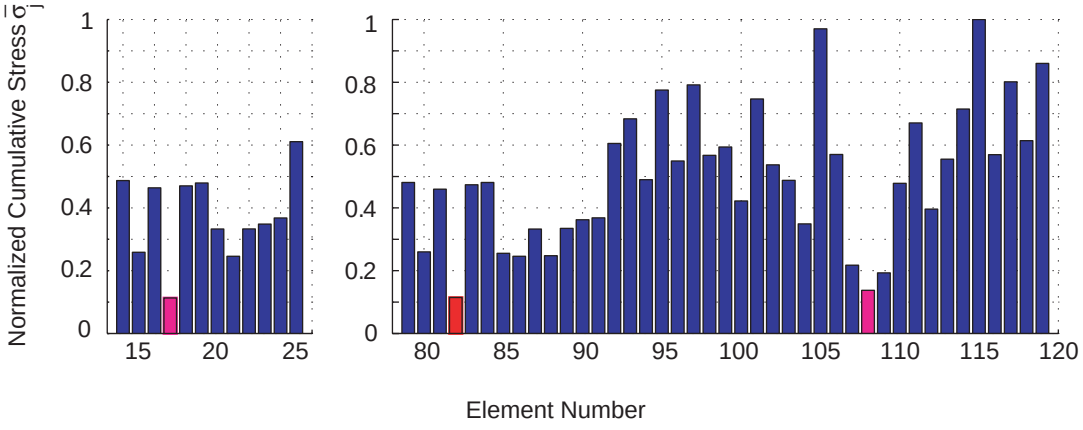

Figure 3.21: Normalized cumulative stress when element 82 is damaged.

The results of the normalized cumulative stress are shown in Fig 3.21. As can be seen, the normalized cumulative stress for element 82 is considerably smaller than others elements, so element 82 is correctly identified as the damage candidate. However, elements 17 and 108, which are not a damaged element, also have a small value of normalized cumulative stress. Therefore, the DLV method identifies a small group of potentially damaged candidates that contain the damaged elements. However, as will be shown later on, when number of sensors increases, the likelihood of false identification of damaged elements is significantly reduced.

More specifically, the reason why element 17 has a small cumulative stress is apparent by looking at the force balance of the truss structure at the horizontal direction if we cut the truss through 82, 100, and 17, and consider the right portion of the truss. The current sensor configuration indicates that the DLVs are only applied in the vertical directions at the lower chord joints in the outer vertical panel; the structural member force which is not in the outer vertical panel (see Fig. 3.10) are indeed very small. Therefore, if we consider the horizontal force balance of the right portion of the truss structure, the axial force in elements 82 and 17 have to be equal and opposite (note that the normalized cumulative stress defined in Eq. (3.25) is always positive). Therefore, if either of these two elements has a small stress, so does the other. A detailed discussion on the theoretical limitations of the spatial resolution of damage that can be obtained from examination of changes in flexibility for a given sensor set is presented in Bernal (2002).

Case 2

In this case, the vertical element, element 112, is replaced by one with a 52.7% cross section reduction instead of a longitudinal element as presented in Case 1. The results are shown in Fig. 3.22, in which elements 107, 112, and 113 have a small normalized cumulative stress compared with others. Obviously, with the current sensor configuration and resulting DLVs, if either one of the two elements (112 and 113) has a small axial force, so does the other. This can be seen from the force balance in the vertical direction of the joint 20 (see Fig. 3.16). Therefore, the DLV method successfully detects element 112 as a possibly damaged location.

3.5 Summary

In this chapter, the flexibility-based damage localization method, the DLV method, was experimentally verified employing a 5.6 m long truss structure. Motivation of the flexibility-based damage detection method was first discussed. The numerical example shows that a reasonably accurate flexibility matrix can be constructed using only a limited

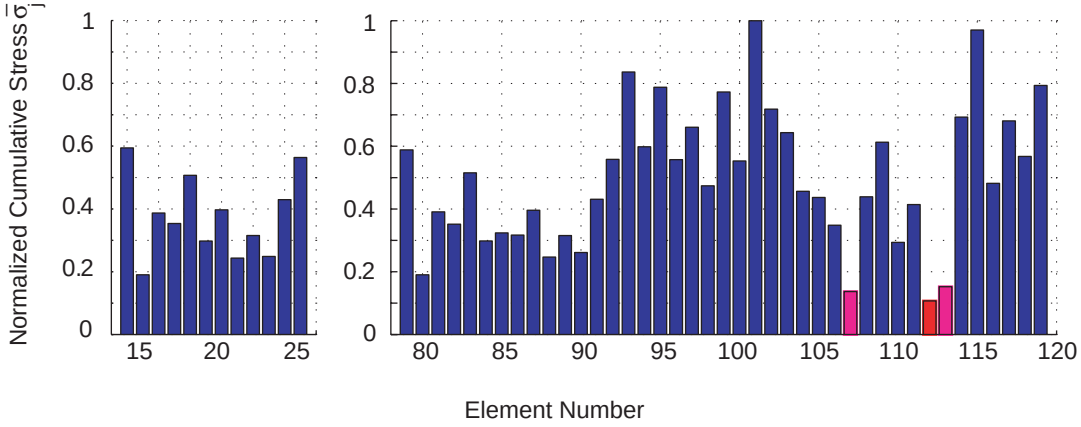

Figure 3.22: Normalized cumulative stress when element 112 is damaged.

number of lower frequency modes, which is a desirable characteristic for vibration-based damage detection methods. The concepts of the DLV method were then introduced and numerical examples were provided to better understand this method.

To assess the efficacy of the DLV method in practice, this method was successfully verified using experimental data. Experimental results show that the change of modal properties subjected to a 52.7% cross section reduction (equivalent to around a 44% axial stiffness reduction) of a single member is very small. Direct comparison of the modal properties to detect damage is difficult if not impossible for this truss structure. By using the flexibility-based DLV method, damage in this truss can be correctly located using only a limited number of sensors and truncated modes.

CONTINUOUS STRUCTURAL HEALTH MONITORING EMPLOYING AMBIENT VIBRATION

Numerous vibration-based damage detection methods have been proposed recently. Although these methods can be effective, they are not yet easily employed for continuous, online SHM. Most of these methods require measurement of the input excitation to be implemented. However, in numerous cases, externally exciting the structure (e.g., with an impactor or a rotating imbalance vibrator) is difficult, especially for large complicated civil infrastructure systems. In addition, Peeters et al. (2001) pointed out that the price of a shaker and the additional manpower to install it on a structure makes it cost-prohibitive and suggested that only ambient vibration should be employed for long-term, continuous monitoring. SHM strategies employing ambient vibration that are suitable for continuous online diagnosis are currently limited.

In this chapter, an approach is proposed for continuous online SHM that is an extension of the DLV method (Gao and Spencer 2005a, 2006). The essence of the proposed approach is to construct an approximate flexibility matrix for the damaged structure utilizing the modal normalization constants from the undamaged structure. This extended DLV method can then be applied for online damage diagnosis employing ambient vibration. Following an overview of the construction of the flexibility matrix based on both forced and ambient vibration, extension of the DLV method for the continuous online SHM is proposed and then numerically validated using a 14-bay planar truss structure.

4.1 Construction of the Flexibility Matrix

As shown in Chapter 3, the flexibility matrices before and after damage need to be constructed to implement the DLV method. Depending on whether or not the input excitations are measured, different formulations are needed to construct the flexibility matrix from the measured data. For the case when the inputs are measured and there is at least one co-located sensor and actuator pair, the flexibility matrix at the sensor locations can be constructed for structures with general viscous damping. For the ambient vibration case (*i.e.* the input excitation is not measured), a formulation is utilized that requires the structure to have classical damping. Both approaches are reviewed in this section.

4.1.1 Formulation of the flexibility matrix based on forced vibration

Consider the homogeneous equations of motion for a linear structure

$$\mathbf{M}\ddot{\mathbf{x}} + \mathbf{C}_d\dot{\mathbf{x}} + \mathbf{K}\mathbf{x} = \mathbf{0} \tag{4.1}$$

where $\mathbf{M}$, $\mathbf{C}_d$, and $\mathbf{K}$ = mass, damping, and stiffness matrix, respectively; and $\mathbf{x}$ = displacement vector. A state space representation of the structure can be expressed as

$$\mathbf{E}\dot{\eta} = \mathbf{G}\eta \tag{4.2}$$

$$\mathbf{E} = \begin{bmatrix} \mathbf{C}_d & \mathbf{M} \\ \mathbf{M} & 0 \end{bmatrix} \qquad \mathbf{G} = \begin{bmatrix} -\mathbf{K} & 0 \\ 0 & \mathbf{M} \end{bmatrix} \qquad \eta = \begin{bmatrix} \mathbf{x} \\ \dot{\mathbf{x}} \end{bmatrix} \tag{4.3}$$

Solving the standard eigenproblem of Eq. (4.2) yields the eigenvalues Λ_E and eigenvectors Φ_E

$$\Lambda_E = \begin{bmatrix} \Lambda & \mathbf{0} \\ \mathbf{0} & \Lambda^* \end{bmatrix} \qquad \Phi_E = \begin{bmatrix} \varphi & \varphi^* \\ \varphi\Lambda & \varphi^*\Lambda^* \end{bmatrix} \tag{4.4}$$

where * represents complex conjugate. Orthogonality of the eigenvectors yields

$$\mathbf{D}_g^{-1} = \Phi_E^T \mathbf{G} \Phi_E \qquad \mathbf{G}^{-1} = \Phi_E \mathbf{D}_g \Phi_E^T \tag{4.5}$$

From Eq. (4.5), one obtains

$$\mathbf{K}^{-1} = -\Psi \mathbf{D}_g \Psi^T \tag{4.6}$$

$$\mathbf{F} = -\Psi \mathbf{D}_g \Psi^T \tag{4.7}$$

where $\Psi = [\varphi \ \varphi^*]$, arbitrarily normalized complex mode shapes; $\mathbf{D}_g = \mathrm{diag}([d_1, d_2, \ldots, d_j, \ldots])$; and d_j = modal normalization constant.

Determination of modal normalization constants

When the input is measured and there is at least one co-located sensor and actuator pair, the experimental data can be used to obtain the modal normalization constant d_j for structures with general viscous damping (Bernal and Gunes 2004).

First, the flexibility matrix related the input locations to the output locations is constructed from measured data following the same procedure presented in section 3.3 and expressed as

$$\mathbf{F}_f = -\mathbf{C}\mathbf{A}^{-(p+1)}\mathbf{B} \tag{4.8}$$

where all the variables have been defined in section 3.3. Again, expressing the system matrix **A** in terms of its eigenvalues and eigenvectors yields

$$\mathbf{F}_f = -\mathbf{C}\phi\lambda^{-(p+1)}\phi^{-1}\mathbf{B} = -\Psi_m\lambda^{-(p+1)}\phi^{-1}\mathbf{B} \tag{4.9}$$

where $\Psi_m = \mathbf{C}\phi$ and Ψ_m = complex mode shapes at sensor locations.

Similar as the derivation in section 3.3, we denote the flexibility matrix at the sensor locations as $\mathbf{F}_{\mathrm{m}}$. If any of the inputs are co-located with sensors, then the corresponding columns in the matrices $\mathbf{F}_{\mathrm{f}}$ and $\mathbf{F}_{\mathrm{m}}$ will be equal. Defining two Boolean matrices $\mathbf{q}_{\mathrm{f}}$ and $\mathbf{q}_{\mathrm{m}}$ which pick out these columns from $\mathbf{F}_{\mathrm{f}}$ and $\mathbf{F}_{\mathrm{m}}$, respectively, we have

$$-\Psi_{\mathrm{m}}\mathbf{D}_{\mathrm{g}}\Psi_{\mathrm{m}}^{\mathrm{T}}\mathbf{q}_{\mathrm{m}} = -\Psi_{\mathrm{m}}\lambda^{-(p+1)}\phi^{-1}\mathbf{B}\mathbf{q}_{\mathrm{f}} \tag{4.10}$$

The modal normalization constant d_j can then be solved from Eq. (4.10) as

$$d_j = \lambda_j^{-(p+1)}\bar{\phi}_j^{\mathrm{T}}\mathbf{B}\mathbf{q}_{\mathrm{f}}[\mathrm{diag}(\Psi_{\mathrm{m},j}^{\mathrm{T}}\mathbf{q}_{\mathrm{m}})]^{-1} \tag{4.11}$$

where $\bar{\phi}_j^{\mathrm{T}}$ = jth row of matrix ϕ^{-1}; and $\Psi_{\mathrm{m},j}^{\mathrm{T}}$ = jth row of matrix $\Psi_{\mathrm{m}}^{\mathrm{T}}$. When there is more than one co-located sensor and actuator pair, multiple estimations of d_j will be obtained. Bernal and Gunes (2004) suggested that the d_j corresponding to the component in vector $\Psi_{\mathrm{m},j}^{\mathrm{T}}\mathbf{q}_{\mathrm{m}}$ with the largest magnitude might be used.

4.1.2 Formulation of the flexibility matrix based on ambient vibration

Consider again Eq. (4.1) for a linear structure. Recall that for classical damping, the stiffness matrix can be expressed as

$$\Phi^{\mathrm{T}}\mathbf{K}\Phi = \Lambda \qquad \text{and} \qquad \mathbf{K} = (\Phi^{\mathrm{T}})^{-1}\Lambda\Phi^{-1} \tag{4.12}$$

Therefore the flexibility matrix takes the form

$$\mathbf{F} = \Phi\Lambda^{-1}\Phi^{\mathrm{T}} = (\psi\alpha)\Lambda^{-1}(\psi\alpha)^{\mathrm{T}} \tag{4.13}$$

where Φ = mass normalized mode shapes and $\Phi = \psi\alpha$; ψ = undamped arbitrarily normalized mode shapes; Λ and ψ = solutions of the eigenproblem $\mathbf{K}\psi = \mathbf{M}\psi\Lambda$; $\alpha = \mathrm{diag}([\alpha_1, \alpha_2, \ldots, \alpha_j, \ldots])$; and α_j = modal normalization constant, which can be obtained from the output measurements for structures with classical damping. When input excitations are not measured, Eq. (4.13) can be used to construct the flexibility matrix.

Determination of modal normalization constants

For the ambient vibration case, the approach presented in the previous section can't be employed to obtain the modal normalization constant α_j because of the lack of a co-located sensor and actuator pair. To overcome this difficulty, researchers (Parloo etc. 2001, 2002; Brinker and Pade 2003; Bernal 2004) have proposed methods based on testing of the structure with known modification masses. The mass perturbation method provided by Bernal (2004) for a linear structure with proportional damping will be presented in the remainder of this section.

The mass matrix of the modified structure can be expressed as

$$\mathbf{M}_1 = \mathbf{M}_0 + \Delta\mathbf{M} \tag{4.14}$$

in which $\mathbf{M}_0$ = mass matrix of the original structure; $\mathbf{M}_1$ = mass matrix of the modified structure; $\Delta\mathbf{M}$ = matrix describing the mass perturbation. The eigenvalue problem for the modified structure is

$$\mathbf{K}\psi_{1,j} = \lambda_{1,j}(\mathbf{M}_0 + \Delta\mathbf{M})\psi_{1,j} \tag{4.15}$$

where $\lambda_{1,j}$ = jth eigenvalue of the modified structure; and $\psi_{1,j}$ = jth eigenvector of the modified structure. The corresponding eigenvalues and eigenvectors for the original structure are $\lambda_{0,j}$ and $\psi_{0,j}$, respectively. The mode shape $\psi_{1,j}$ can be written as

$$\psi_{1,j} = \psi_0\mathbf{q}_j + N(\psi_0)\mathbf{g}_j \tag{4.16}$$

where $\psi_0 = [\psi_{0,1}, \psi_{0,2}, \ldots, \psi_{0,j}, \ldots]$; $N(\psi_0)$ = column null space of ψ_0; $\mathbf{q}_j$ and $\mathbf{g}_j$ = coefficient vectors.

Substituting Eq. (4.16) into Eq. (4.15) and multiplying both sides by ψ_0^{T} yields

$$\alpha^2(\mathbf{R}_j + \varepsilon_j) = \mathbf{E}_j \tag{4.17}$$

where

$$\begin{aligned}
\mathbf{R}_j &= \lambda_{1,j}\psi_0^{\mathrm{T}}\Delta\mathbf{M}\psi_{1,j} \\
\varepsilon_j &= \lambda_{1,j}\psi_0^{\mathrm{T}}\mathbf{M}_0 N(\psi_0)\mathbf{g}_j - \psi_0^{\mathrm{T}}\mathbf{K}N(\psi_0)\mathbf{g}_j \\
\mathbf{E}_j &= \Lambda_0\mathbf{q}_j - \lambda_{1,j}\mathbf{q}_j
\end{aligned} \tag{4.18}$$

with $\Lambda_0 = \mathrm{diag}[\lambda_{0,1}, \lambda_{0,2}, \ldots, \lambda_{0,j}, \ldots]$ and $\mathbf{q}_j = (\psi_0^{\mathrm{T}}\psi_0)^{-1}\psi_0^{\mathrm{T}}\psi_{1,j}$. By neglecting the error term ε_j, Eq. (4.17) can be rewritten as

$$\alpha^2\lambda_{1,j}\psi_0^{\mathrm{T}}\Delta\mathbf{M}\psi_{1,j} = \Lambda_0\mathbf{q}_j - \lambda_{1,j}\mathbf{q}_j \tag{4.19}$$

which can be de-coupled to solve for the unknown α_i as

$$\alpha_i^2 = \frac{\lambda_{0,i} - \lambda_{1,j}}{\lambda_{1,j}} \frac{q_{ij}}{\psi_{0,i}^{\mathrm{T}}\Delta\mathbf{M}\psi_{1,j}} \tag{4.20}$$

Equation (4.20) indicates that there is one set of $[\alpha_1, \alpha_2, \ldots, \alpha_i, \ldots]$ for each $\psi_{1,j}$ (*i.e.*, there are various estimations for different $\psi_{1,j}$). Bernal (2004) pointed out that the most accurate estimation for the normalization index α_i is when $i = j$ in Eq. (4.20).

The modal parameters for both the original and modified structure can be obtained employing the Natural Excitation Technique (NExT) (James et al. 1993) in conjunction with the ERA method. To apply the NExT, the first step is to measure responses. Then auto- and cross-spectral density functions of these responses can be calculated. Afterwards, the inverse Fourier transform is applied to obtain the auto- and cross-correlation functions, which are in turn used by the ERA to extract the modal parameters.

To obtain expected modal parameters, the reference output selected in calculating correlation functions should include the information on all modes of interest (Dyke et al. 2000).

4.2 Extension of the DLV Method for Online Damage Diagnosis

The DLV method is not easily employed for continuous online damage diagnosis. Eqs. (4.7) and (4.13) show that the modal normalization constants d_j or α_j need to be obtained to construct the flexibility matrix. As suggested in the derivation of Eqs. (4.11) and (4.20), a certain degree of interruption of structural operation will be needed to obtain these normalization constants from measured data. The method based on forced vibration requires employing an external exciter, e.g. an impactor or a rotating imbalance vibrator, to shake the structure. The method based on ambient vibration requires adding mass to the structure to conduct dynamic testing. These methods can be used to constructed the undamaged flexibility matrix. However, computing the damaged flexibility matrix by one of these methods each time the health of the structure is assessed is intractable. An approach which can take the advantage of the DLV method and is more suitable for continuous online monitoring is highly desired.

Gao and Spencer (2005a, 2006) proposed an extension of the DLV method to handle the continuous online damage diagnosis employing ambient vibration and will be presented in the remainder of this chapter.

4.2.1 Evaluation of modal normalization constant change due to damage

The main difficulty in applying the DLV method for continuous online damage diagnosis is the computation of the modal normalization constants for the damaged structure. For complex civil infrastructure, the local damage is not expected to significantly change the global structural characteristic, including the modal normalization constants, which leads to the conjecture that the undamaged normalization constants possibly can be employed for constructing an approximate damaged flexibility matrix for the purpose of damage detection.

To understand the situation better, the 14-bay planar truss shown in Fig. 4.1 is considered. A Matlab finite element model consisting of 53 bars and 28 nodes has been

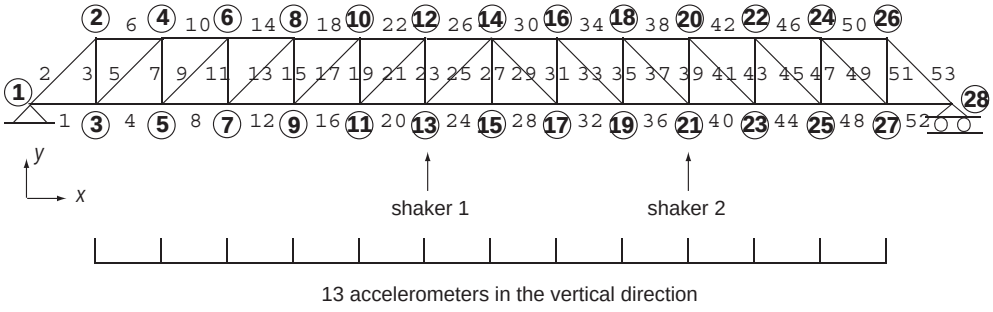

Figure 4.1: 14-bay planar truss.

developed. Structural nodes are numbered starting from left to right, with all the odd numbers at the lower chord, and all the even numbers at the upper chord, except node 28 which is at the right support. Each structural node number has a circle around it. Mode shapes in the *y*-direction of all the lower chord nodes except the supports, and in the *x*-direction for node 7, are used to construct the flexibility matrix in this example.

Now, let's evaluate the change in the modal normalization constants due to damage on this truss structure. Because the mode shapes obtained from system identification based on measured data are arbitrarily normalized, the mode shapes before and after damage have to be properly scaled to make a meaningful comparison of the modal normalization constants. The idea is to have the mode shape at the measured DOFs scaled in such a way that they have a unit magnitude, *i.e.*

$$\Psi_j^T \Psi_j = 1.0 \qquad \text{or} \qquad \psi_j^T \psi_j = 1.0 \tag{4.21}$$

The ratios between the damaged and undamaged normalization constant are evaluated here for various damage scenarios.

The sample results when element 13 is damaged are shown in Fig. 4.2. Another example when element 16 and 33 are damaged are displayed in Fig. 4.3. Both of these

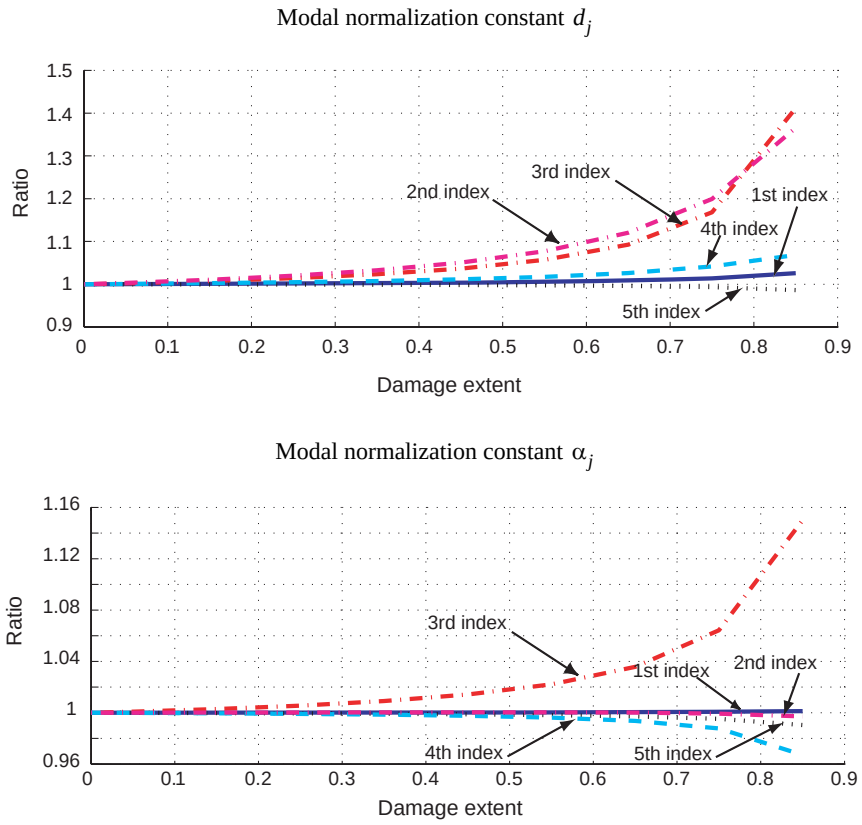

Figure 4.2: Ratio between the damaged and undamaged normalization constants when element 13 is damaged.

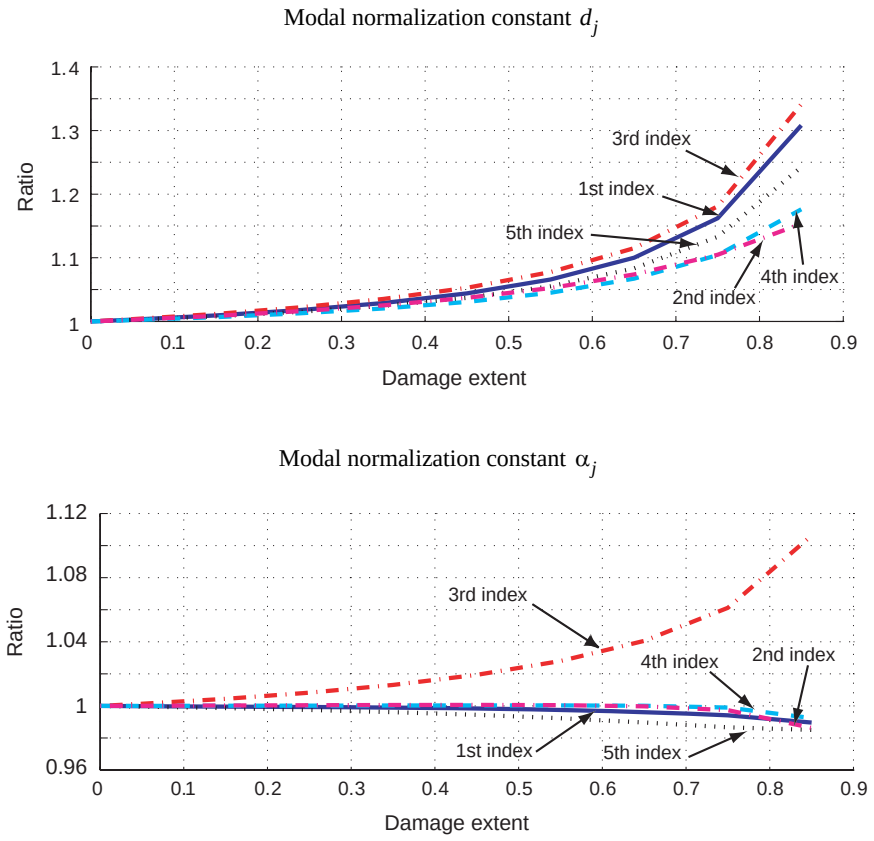

Figure 4.3: Ratio between the damaged and undamaged normalization constants when elements 16 and 33 are damaged.

results indicate a small change of modal normalization constants for the first five modes, especially for small damage. This result implies that the undamaged normalization constants may provide a reasonable approximation to the damaged ones when damage is small. Note that, if the damping in the forced vibration case is proportional, the normalization constant d_j can be easily associated with α_j for each mode by comparing Eqs. (4.7) and (4.13).

4.2.2 Algorithm initialization

The first step of the proposed algorithm is to compute the undamaged normalization constants and then the undamaged flexibility matrix from the measured data. Herein, this step is termed as algorithm initialization. Based on how the undamaged normalization constants are obtained, there are two different initialization approaches (see Fig. 4.4).

Initialization based on forced vibration

To obtain the undamaged normalization constant d_j from forced vibration, the modal parameters of the undamaged structure are first identified using the ERA method; the

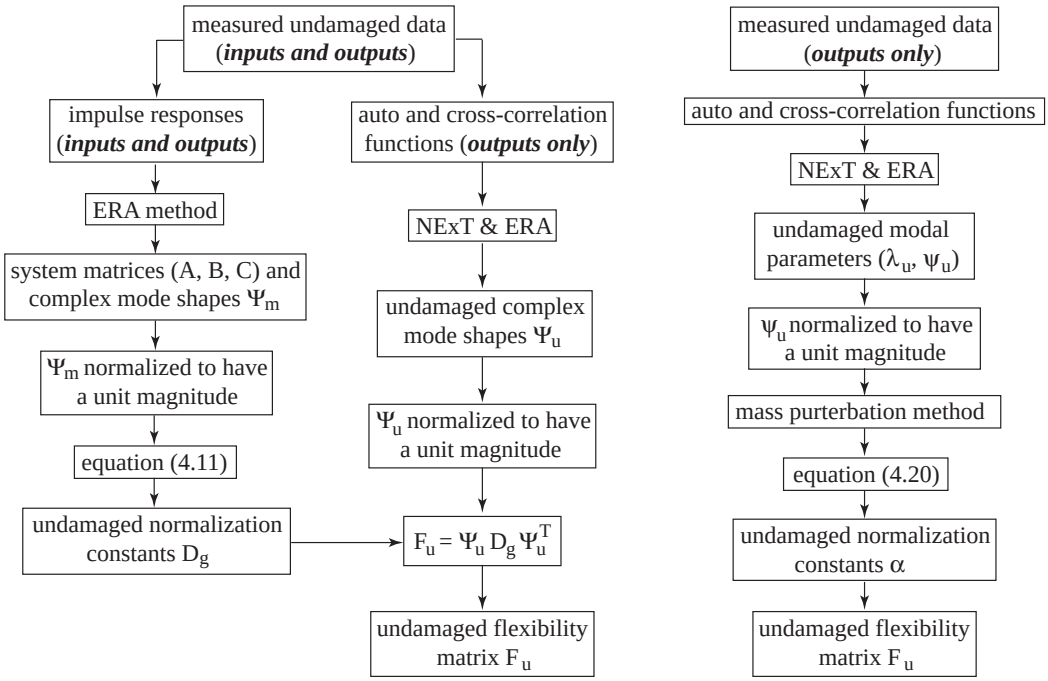

Figure 4.4: Algorithm initialization.

normalization constant d_j is then computed from Eq. (4.11) with the mode shapes normalized to have a unit magnitude.

Because the mode shapes for the damaged structure will be identified from output measurements employing the NExT algorithm in conjunction with the ERA method, system identification using the same approach is applied on the output measurements to obtain the undamaged mode shapes. These mode shapes are then normalized to have a unit magnitude to compute the undamaged flexibility matrix employing Eq. (4.7).

Initialization based on ambient vibration

To obtain the undamaged normalization constant α_j from ambient vibration, the NExT algorithm in conjunction with the ERA method is employed for system identification. Again, the identified mode shapes are normalized to have a unit magnitude. α_j can then be computed employing the mass perturbation method outlined above; and the undamaged flexibility matrix is then constructed by Eq. (4.13).

4.2.3 Algorithm operation – detecting damage

Once the initialization is completed, the second step of the proposed approach is to construct an approximate flexibility matrix for the potentially damaged structure

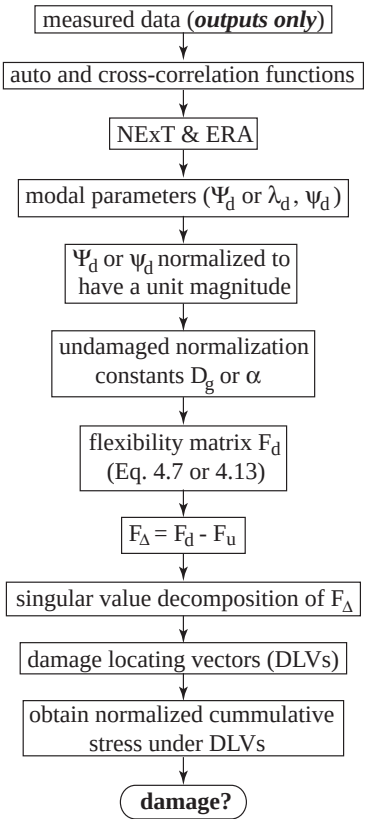

Figure 4.5: Algorithm operation.

employing ambient vibration and then to apply the DLV method to detect damage in the structure. Herein, this step is referred as algorithm operation (see Fig. 4.5).

During the operation of the SHM system, only outputs are measured and used to identify the modal parameters. The NExT algorithm in conjunction with ERA method is applied for system identification. The identified mode shapes are then normalized to have a unit magnitude. The flexibility matrix is computed employing these identified modal parameters and the undamaged normalization constants $\mathbf{D}_g$ or α obtained during the algorithm initialization. After the flexibility matrices for the undamaged and potentially damaged structures are constructed, the DLV method can be applied to detect damage. The DLVs are first calculated from the difference of the flexibility matrices, and then statically applied to undamaged structure at the sensor locations. A small value of the normalized cumulative stress in an element indicates that this element is a damage candidate.

4.3 Numerical Validation

The proposed damage diagnosis approach is verified using the 14-bay planar truss structure shown in Fig. 4.1. This planar truss consists of 53 steel circular bars, which have

a cross section of $1.122 \times 10^{-4}\text{m}^2$ and an area moment of inertia of $2.111 \times 10^{-9}\text{m}^4$. The elastic modulus of the material is $2 \times 10^{11}\ \text{N}/\text{m}^2$, and the mass density is $7.83 \times 10^3\ \text{kg}/\text{m}^3$. The total length of this truss is 5.6 m, with each bay being $0.4\text{m} \times 0.4\text{m}$.

A total of 13 accelerometers are installed in the *y*-direction at all the lower chord nodes except at the supports; and there is one accelerometer installed in the *x*-direction of node 7. A band-limited white noise with RMS amplitude about 5% of the measured signal is added to each of the measurements to simulate measurement noises. The truss is excited using two independent band-limited white noises in the *y*-direction at nodes 13 and 21. To obtain the undamaged normalization constants from forced vibration, excitation at node 13 is measured as the input. For the case of computing undamaged normalization constants from ambient vibration, these two inputs are not measured.

4.3.1 Algorithm initialization

Algorithm initialization based on forced vibration

To obtain the modal normalization constant d_j from forced vibration, the ERA method is employed for system identification. The sample identification results are shown in Fig. 4.6. As can be seen, system identification using the impulse responses shows good agreement with the exact results. The undamaged normalization constants $\mathbf{D}_\text{g}$ are then computed using Eq. (4.11).

After the undamaged normalization constants $\mathbf{D}_\text{g}$ are obtained, system identification employing the NExT algorithm in conjunction with the ERA method is applied on the output measurements only to obtain the undamaged mode shapes. First, acceleration measurements are collected. The auto- and cross-spectral density functions are then computed by selecting a reference output. The sample spectral density function between *y*-direction acceleration at node 3 and node 9 (reference output location) is shown in Fig. 4.7; and the corresponding correlation function is shown in Fig. 4.8. These correlation functions can then be used in the ERA method to extract the modal parameters. Sample results are shown in Fig. 4.9. As can be seen, system identification using correlation functions of outputs shows a good agreement with the exact results. This figure also indicates that the difference between the natural frequencies before and after damage is as small as 0.1% when element 13 has a 20% stiffness reduction for this specific truss.

The undamaged flexibility matrix is then constructed using Eq. (4.7) with Ψ being the identified complex mode shapes at the sensor locations. Comparison of portion of the identified and exact flexibility matrices constructed using the first four modes is shown in Table 4.1. As can be seen, accurate results have been obtained for the flexibility matrix associated with the first four sensor locations, *i.e.*, *y*-direction of nodes [3 5], *x*- and *y*-direction of node 7.

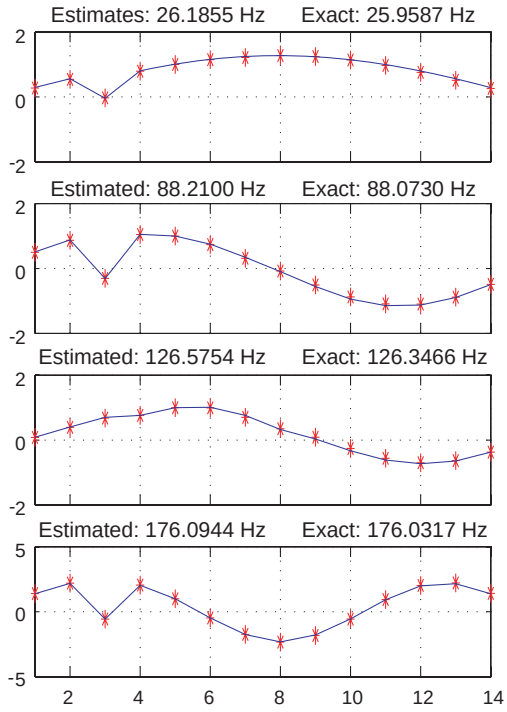

Figure 4.6: Undamaged mode parameters from ERA method ($*$: identified mode shapes; —: exact mode shapes).

Algorithm initialization based on ambient vibration

For the case of ambient vibration, system identification is conducted by employing the NExT algorithm in conjunction with the ERA method. The undamaged normalization constants α are obtained utilizing the mass perturbation method. These normalization constants are then used to construct the undamaged flexibility matrix from Eq. (4.13) with ψ being the identified undamped mode shapes at the sensor locations. A comparison of the identified and exact flexibility matrices is shown in Table 4.1. Again, reasonably accurate results have been obtained.

Table 4.1: Comparison of undamaged flexibility matrices using the first four modes ($\mathrm{x}10^{-5}$ m/N)

Exact flexibility matrix				*Estimated flexibility matrix*							
				Forced vibration				*Ambient vibration*			
0.0160	0.0299	-0.0042	0.041	0.0159	0.0298	-0.0042	0.0403	0.0167	0.0312	-0.0042	0.0420
0.0299	0.0560	-0.0069	0.0760	0.0298	0.0562	-0.0071	0.0765	0.0312	0.0587	-0.0070	0.0799
-0.0042	-0.0069	0.0031	-0.0082	-0.0042	-0.0071	0.0029	-0.0086	-0.0042	-0.0070	0.0030	-0.0084
0.0401	0.0760	-0.0082	0.1046	0.0403	0.0765	-0.0086	0.1052	0.0420	0.0799	-0.0084	0.1101

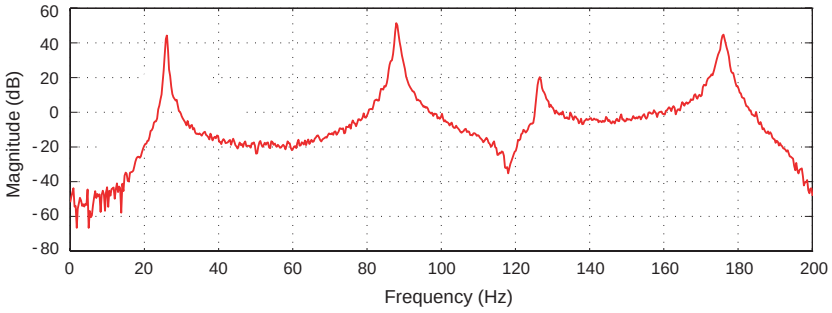

Figure 4.7: Cross-spectral density function.

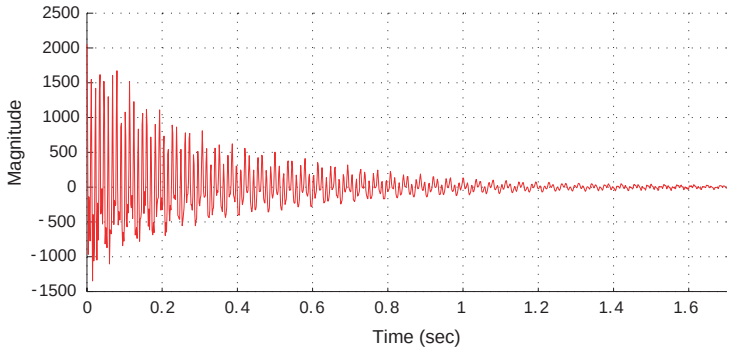

Figure 4.8: Correlation function.

4.3.2 Damage diagnosis results

Once the algorithm initialization is completed, the sensors on the structure can start collecting data to monitor the structural condition. The approximate flexibility matrix is constructed from the output measurements using the undamaged normalization constants. The DLV method is then applied to detect damage in the structure. A cut-off value of 0.15 for normalized cumulative stress while using a total of six DLVs associated with the smallest singular values yields good results for a wide range of damage cases; and therefore will be used here to select the damaged candidates.

The damage cases considered in this numerical example are shown in Table 4.2. Case 1-1 demonstrates performance of the extended DLV method under the situation when only a single element is damaged. Cases 2-1 and 2-2 illustrate the multiple damage scenarios. These three cases are selected to illustrate the effectiveness of the method for damage in different types of elements, including longitudinal, diagonal, and vertical elements.

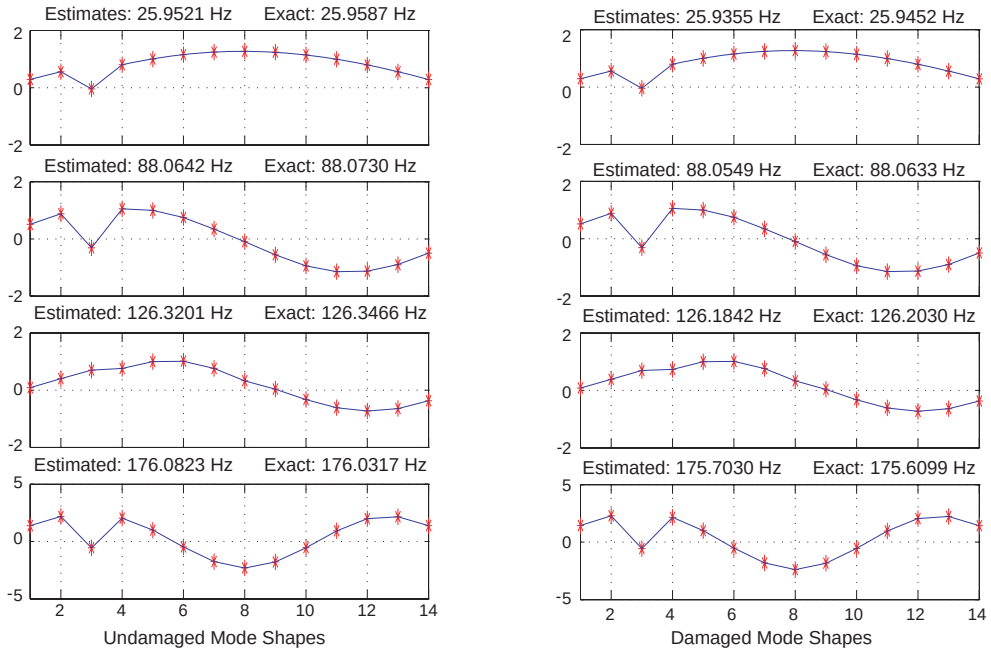

Figure 4.9: Identified modal parameters from NExT & ERA method ($*$: identified mode shapes; —: exact mode shapes).

Table 4.2: Two damage scenarios: three damage cases.

Cases		*Damage extent (stiffness reduction)*	*Damaged elements*
Single damage	Case 1-1	20%	diagonal element 13
Multiple damage	Case 2-1	20%	longitudinal element 12 and diagonal element 33
	Case 2-2	20%	longitudinal element 20 and vertical element 39

Case 1-1

The results of the normalized cumulative stress induced by the DLVs, when element 13 is damaged, are shown in Fig. 4.10. As can be seen, for both cases of initialization from forced and ambient vibration, elements 13 and 15 have a considerably smaller normalized cumulative stress compared with other elements and smaller than the threshold. The reason why element 15 has a small cumulative stress is apparent by looking at the force balance at node 8 in Fig. 4.1. Under the current load configuration where the vertical forces are only applied at the lower chord nodes, if either of these two elements has small stress, so does the other. Therefore, element 13 is successfully identified as a possibly damaged element in this truss structure employing the extended DLV method.

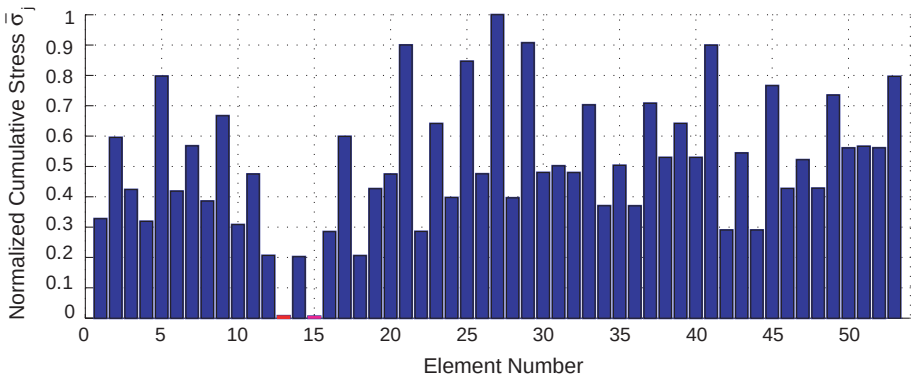

Initialization based on forced vibration

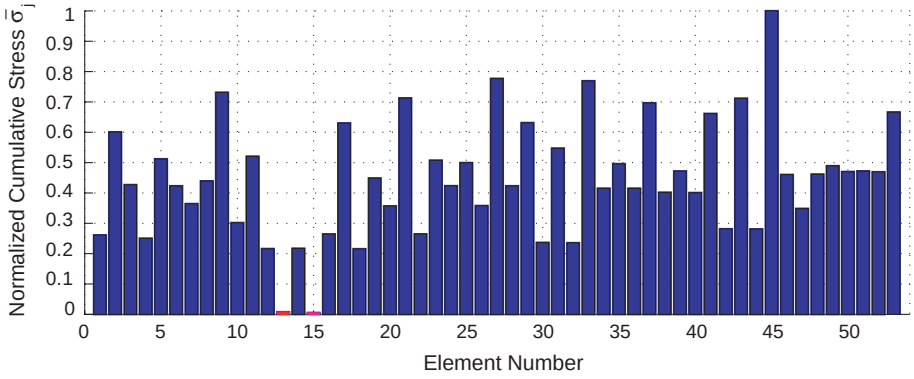

Initialization based on ambient vibration

Figure 4.10: Normalized cumulative stress when element 13 is damaged.

Case 2-1

For the case in which elements 12 and 33 are damaged, the results are shown in Fig. 4.11. As can be seen, the damaged elements have a comparatively smaller stress which is smaller than the threshold. Obviously, under the current load configuration, if element 12 has a small stress, element 18 should have a small stress as well. Similarly for elements 31 and 33, both of them will have a small stress, if either of them does. Therefore, elements 12 and 33 are determined as the candidates of the damage locations in both cases.

Case 2-2

The results when elements 20 and 39 are damaged are shown in Fig. 4.12, in which the damaged elements have a comparatively smaller stress. Similarly, if element 20 or 39

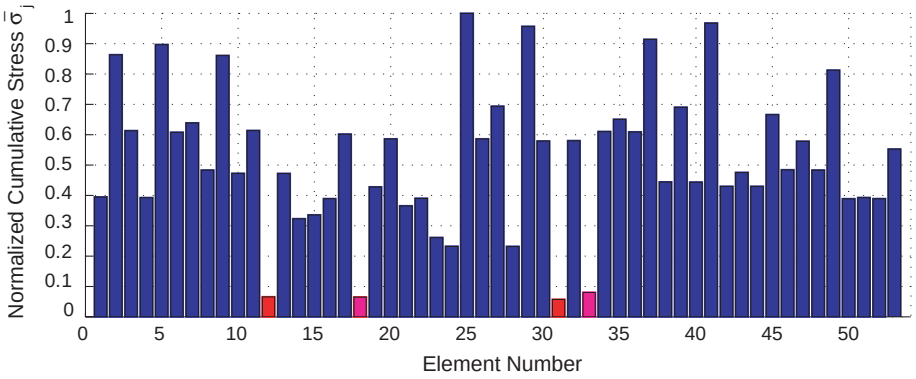

Initialization based on forced vibration

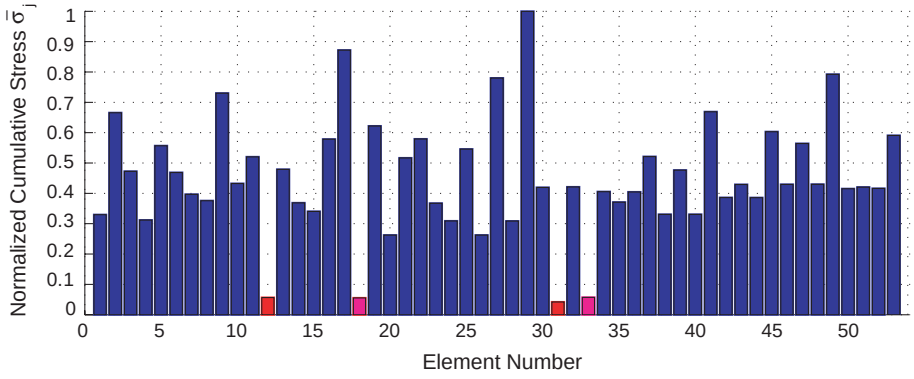

Initialization based on ambient vibration

Figure 4.11: Normalized cumulative stress when elements 12 and 33 are damaged.

is damaged, so does the element 26 or 41. Therefore, elements 20 and 39 are determined as potentially damaged elements for both cases.

4.4 Summary

In this chapter, an approach extending the DLV method to continuous online damage diagnosis was proposed. Different formulations of the flexibility matrix were reviewed. The flexibility matrix for a structure with general viscous damping can be constructed when there is at least one co-located sensor and actuator pair; while for the case when only output measurements are available, flexibility matrix can be computed by employing a mass perturbation method for structures with proportional damping. Changes in the modal normalization constants due to structural damage were investigated. Results for a planar truss structure indicate that modal normalization constants of lower frequency modes may not change significantly when damage is small. This results lead to the extension of the DLV method for continuous online monitoring.

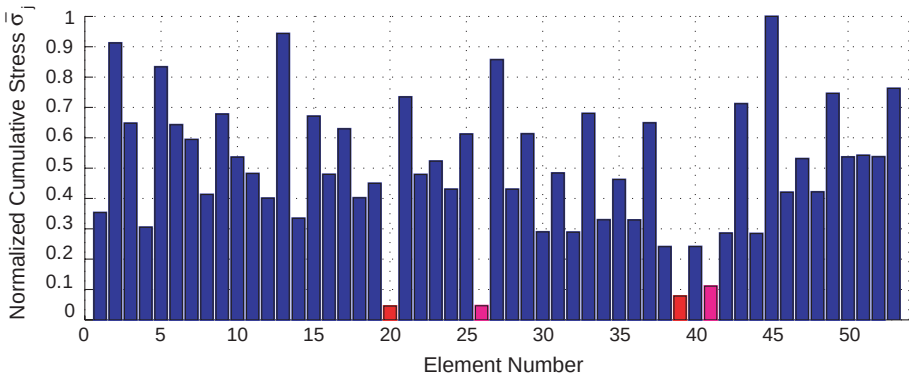

Initialization based on forced vibration

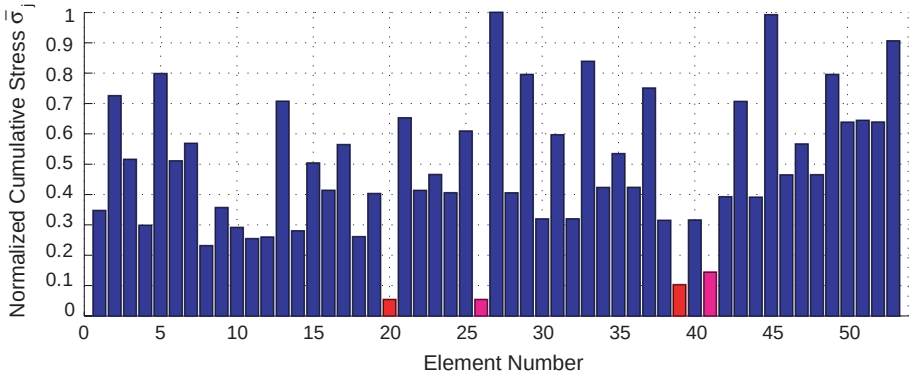

Initialization based on ambient vibration

Figure 4.12: Normalized cumulative stress when elements 20 and 39 are damaged.

The essence of the extended DLV method is to construct an approximate flexibility matrix for the potentially damaged structure utilizing the modal normalization constants from the undamaged structure. The DLV method can then be applied for online damage diagnosis employing ambient vibration. The proposed approach was numerically validated using a 14-bay planar truss structure, with results showing it working well for both single and multiple damage scenarios.

DISTRIBUTED COMPUTING SHM STRATEGY USING SMART SENSORS

As shown in Chapter 4, good results have been obtained using a limited number of sensors distributed throughout the structure; however, questions arise about whether the sensor information away from the damaged region is needed. Could the information from the sensors in the vicinity of the damaged region alone be used to locate the damage? This question will be addressed in this chapter.

Following the introduction of the necessary background knowledge, the concept of damage detection using localized sensors is demonstrated. Development of a new distributed computing strategy (DCS) for SHM is then proposed that is suitable for implementation on a network of densely distributed smart sensors. Finally, numerical validation of the DCS approach is provided with results showing the proposed approach promising (Spencer and Gao 2005; Gao et al. 2006).

5.1 Background

Monitoring of complex structures to provide real-time safety and reliability information of the structure poses significant technical challenges. To detect damage in large civil infrastructure systems, densely distributed sensors are expected to be required. Use of traditional wired sensors is challenging for such applications because of the cost and difficulty in deploying and maintaining a large wiring plant. Using a wireless sensor network is also difficult because large amounts of measured data need to be transferred to a central station. The bandwidth and power requirement to transfer these data may easily exceed the limit of the wireless sensor. In both cases, a tremendous amount of data is expected to be generated that would need to be sent to a central station. Managing this large amount of data is challenging. Unnecessary information needs to be eliminated to efficiently utilize the network.

Recently rapid advances in smart sensor technology have made damage detection using a dense array of sensors feasible (Spencer et al. 2002, 2004). The essential feature of a smart sensor is the on-board microprocessor, which allows smart sensors to make decisions, perform computation, save data locally, etc. By conducting a portion of the computation at the sensor level, only limited information needs to be transferred back to a central station. Damage detection algorithms which can take advantage of the distributed computing environment offered by smart sensors are highly desired but currently very limited.

5.2 Locating Damage Using Local Sensor Information

In this section, damage detection using localized sensors to monitor the local elements is investigated, which directly leads to the proposed DCS approach in the next section.

This concept is demonstrated through a numerical example employing the DLV method. The flexibility matrices before and after damage are constructed using the first four modes from the analytical model. The planar truss shown in Fig. 4.1 is utilized in this numerical example. For convenience, a picture of this truss structure is re-displayed in Fig. 5.1.

For this specific structure, assume there are two sensors at every structural node except the supports, one in the *x*-direction and the other in the *y*-direction. Sensors on every three consecutive lower chord nodes and the corresponding upper chord nodes are grouped together to monitor those elements connected to these nodes. A total of 11 different localized sensor groups are formed from left to right in this truss structure. To allow some computational redundancy, every two adjacent groups have some overlap. For example, group 1 includes nodes [2, 3, 4, 5, 6, 7], and group 2 includes structural nodes [4, 5, 6, 7, 8, 9], etc. Therefore, for each group of localized sensors there are a total of 12 sensors that are installed in the *x*- and *y*-direction at six structural nodes.

In this initial example, system identification is not employed; rather, the exact modal parameters (*i.e.*, mode shapes and frequencies) are used to construct the truncated flexibility matrix which is then employed in the DLV method. The flexibility matrix at the sensor locations is constructed using the first four modes. For the case when element 5 has a 20% stiffness reduction, the normalized cumulative stress when using a total of seven DLVs associated with the smallest singular values is computed for each localized sensor group and shown in Fig. 5.2. Results from group 1 to 11 are shown in the order from top to the bottom. In each plot, a circle is used to mark elements in which both nodes are members of the group, and a cross signifies the elements in which only one of its nodes is a member of a group. Only the condition of elements in which both nodes are in a given group are evaluated here for damage by the localized sensor group.

In Fig. 5.2, results in group 1 shows that element 5 has a very small normalized cumulative stress compared with other elements in the group, which indicates that element 5 is a possibly damaged element. The results from all other groups indicate that there is no other damaged element in this truss. Similar results when elements 11 and 33 are damaged

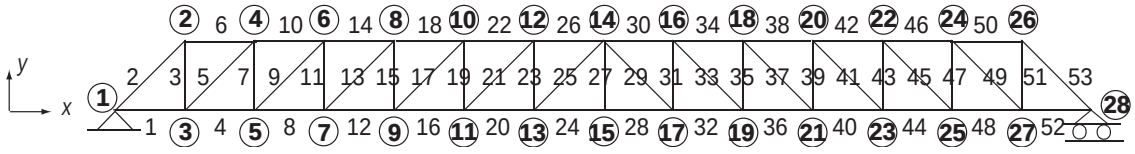

Figure 5.1: 14-bay planar truss.

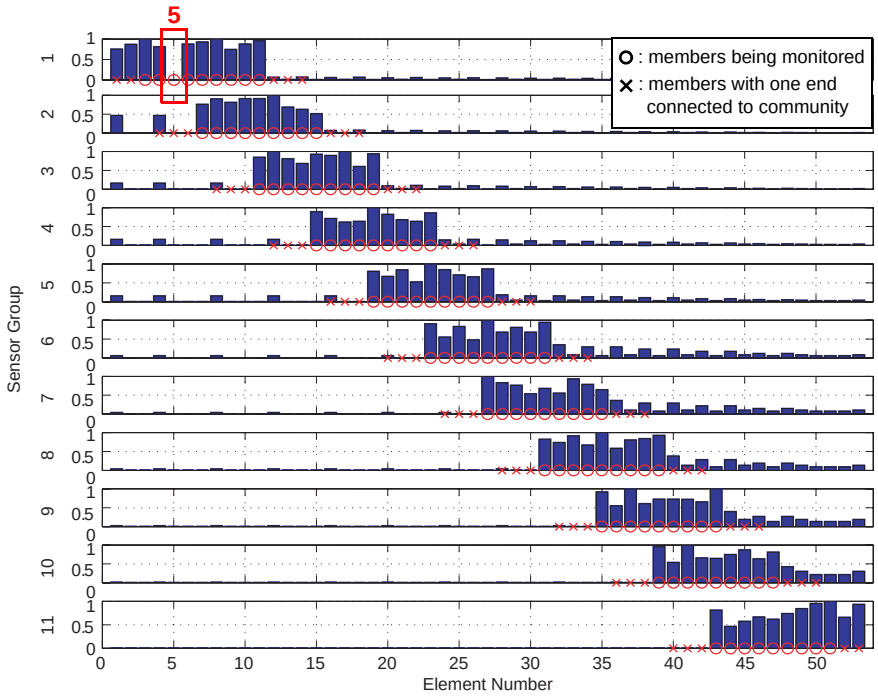

Figure 5.2: Normalized cumulative stress when element 5 has a 20% stiffness reduction.

are shown in Fig. 5.3, in which element 11 is identified as having damage by local groups 1, 2, and 3; and element 33 is determined as a damage candidate by local groups 7 and 8.

It has been demonstrated that the damaged elements can be determined based on information of a small group of sensors localized in the damaged region. This implies that the information away from the damage location might not be necessary for damage detection. This concept can be employed for damage localization for structures with a dense array of sensors.

5.3 Distributed Computing Strategy (DCS)

The previous section provides the basis for development of the scalable SHM strategy presented in this section (Spencer and Gao 2005; Gao et al. 2006).

5.3.1 Hierarchical organization

The conceptual hierarchical organization of the proposed DCS approach is shown in Fig. 5.4. Different hierarchical organizations have been proposed by researchers for different applications in recent years (Frampton 2001; Akyildiz et al. 2002; Lynch 2002). Note that Fig. 5.4 is just a simple example to demonstrate the concept of the DCS approach. In contrast to traditional SHM algorithms which require all the measured information to be transferred to a central station, the measured information is aggregated locally by a selected sensor within the sensor group, termed the manager sensor, and only

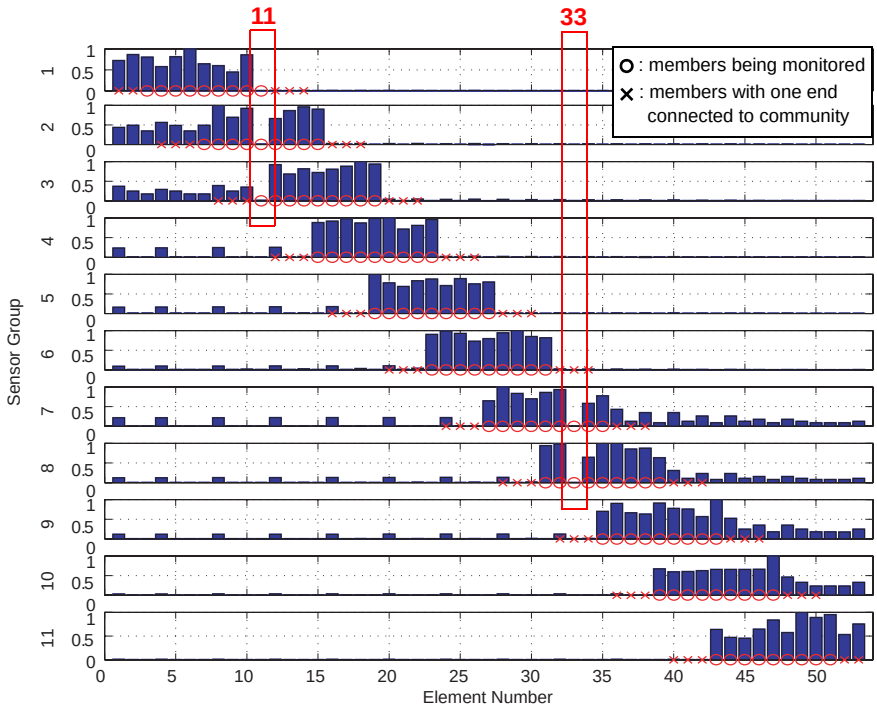

Figure 5.3: Normalized cumulative stress when elements 11 and 33 have a 20% stiffness reduction

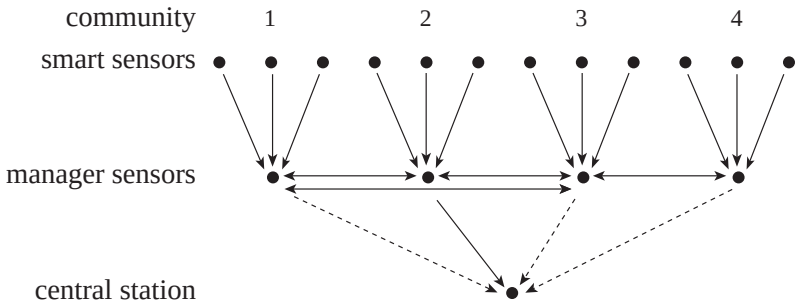

Figure 5.4: Sketch of hierarchical organization.

limited information is sent back to the central station to provide the condition of the structure. Small numbers of smart sensors are grouped to form different communities. For clarity, this figure shows each sensor as being included in only one community; however, in the proposed approach, each sensor can participate in multiple communities. For each community, the manager sensor collects measured responses and implements the damage detection algorithm for this community. Adjacent manager sensors need to interact with each other to exchange information. Referring again to Fig. 5.4, manager sensors in communities 1, 2, and 3 interact with each other while community 4 only interacts with community 3.

After the measured information is aggregated, the manager sensor determines what information needs to be sent back to the central station. In the proposed approach, each of the communities, in which damage has not occurred only transmits an “ok” signal to the central station, which is reflected by the dotted line connection in Fig. 5.4. The communities in which damage has occurred need to send information about the damaged elements, which is reflected by the solid line connection in Fig. 5.4. In this way, only limited information needs to be transferred between sensors throughout the entire structure. This approach will significantly reduce the communication traffic in the sensor network.

5.3.2 Strategy implementation

The planar truss structure shown in Fig. 5.1 is employed to illustrate details of the implementation of the proposed SHM strategy.

Community development

First, different communities are formed. A single community includes a set of adjacent structural nodes, sensors on these nodes, and members. These structural members have both ends connected to the structural nodes in the same community. Fig. 5.5 shows an example how communities can be formed. Different communities are developed from left to right in the truss structure. To facilitate communication among the smart sensors, the structural nodes within the same community should be close to each other. As an example, community 6 in Fig. 5.5 includes nodes [12, 13, 14, 15, 16, 17] and elements [23, 24, 25, 26, 27, 28, 29, 30, 31].

Only the elements which have both ends connected to community nodes are monitored by the manager sensor for this community. There is an exception for those communities close to the supports. If a structural member has one end connected to the support and the other end connected to a community node, then this structural member can also be monitored by this community. For example, in Fig. 5.5, elements 1 and 2 only have one end connected to the community nodes, but they both have the other end connected to a support; therefore these two elements will be investigated by the smart sensors in community 1.

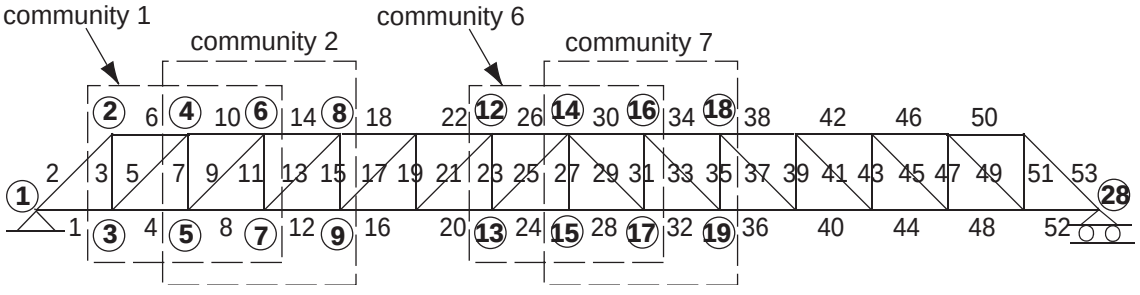

Figure 5.5: Forming communities for damage detection.

To allow some computational redundancy, adjacent communities are recommended to have some overlaps so that each structural member is monitored by more than a single community.

Computing undamaged normalization constants for communities

Once the community is formed, the modal normalization constants for the undamaged structure have to be computed based on either forced or ambient vibration. For this purpose, one sensor from each community, named as the reference sensor, will be required to send the recording data to the central station. These reference sensors are selected so that their mode shape magnitudes will not be zero for the modes interested. The modal parameters associated with these reference sensors, denoted as $\hat{\Psi}_j$ or $\hat{\lambda}_j$ and $\hat{\psi}_j$ respectively, are identified using the ERA method or the NExT in conjunction with the ERA method. The undamaged normalization constants can then be computed based on the methods presented in Chapter 4, and denoted as $\hat{d}_j$ or $\hat{\alpha}_j$.

However, the normalization constants $\hat{d}_j$ or $\hat{\alpha}_j$ cannot be employed directly by each community for damage detection, because the scalar for the j mode shape $\hat{\Psi}_j$ or $\hat{\psi}_j$ and the mode shape in ith community Ψ_j^i or ψ_j^i can be different. The jth undamaged normalization constant for the ith community d_j^i or α_j^i can be obtained as

$$d_j^i = \hat{d}_j \cdot \left(\frac{\hat{\Psi}_j(i)}{\Psi_j^i(k)} \right)^2 \qquad \text{and} \qquad \alpha_j^i = \hat{\alpha}_j \cdot \frac{\hat{\psi}_j(i)}{\psi_j^i(k)} \tag{5.1}$$

where j = jth mode; i = ith community; and k = reference sensor location in the ith community. The undamaged normalization constants for the ith community are $\mathbf{D}_g^i = [d_1^i, d_2^i, \ldots d_j^i]$ or $\alpha^i = [\alpha_1^i, \alpha_2^i, \ldots \alpha_j^i]$.

Data aggregation

To minimize the communication traffic in the sensor network, measured data need to be transferred to the manager sensor for data processing.

Clocks of smart sensors in the same community are first synchronized with each other and these sensors can then start measuring data. The measurements are transferred to the manager sensor for computation. To facilitate communication, the manager sensor should have an overall shorter distance to other sensors in the community. For example, in Fig. 5.6, the sensor on structural node 15 is selected as the manager sensor for community 6. As can be seen from the figure, there are smart sensors which may need to transfer information to more than one manager sensors. This happens when the smart sensors participate in different communities. For example, if communities are developed as shown in Fig. 5.5, sensors at node 6 need to send measured data to the manager sensor on node 5 for community 1, node 7 for community 2, as well as node 9 for community 3.

After the data has been transferred to the manager sensor, computation can be conducted using the on-board microprocessor to locate the damage within the community.

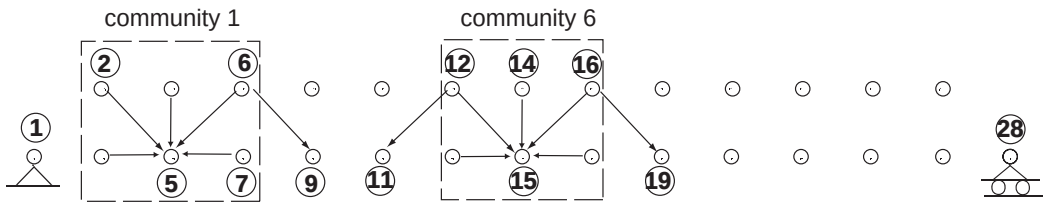

Figure 5.6: Data collection.

The extended DLV method presented in Chapter 4 is incorporated in this DCS approach to localize the damage in each community. The flow chart for data aggregation in a community is shown in Fig. 5.7. Note that the undamaged flexibility matrix F_u in Fig. 5.7 is constructed using Eq. (4.7) or (4.13) once the undamaged normalization constants d_j^i or α_j^i for community *i* are computed from experimental data.

Decision making

Actions need to be taken after the data aggregation is done for a community. If there is no damage detected in a community, the manager sensor does not initiate the interaction with other manager sensors and just sends an “ok” signal back to the central station. If there is damage identified in a community, the manager sensor needs to send queries to its counterpart in adjacent communities. There are three possibilities after sending the queries:

- The damage candidate in community *i* does not participate in adjacent communities. The manager sensor in community *i* sends the damage information back to the central station.
- The damage candidate in community *i* participates in other communities and is identified as the potentially damaged location in all of these communities. This damage candidate is confirmed and reported to the central station by these communities.
- The damage candidate in community *i* participates in other communities, but not all of the communities identify it as the potentially damaged element. These communities then need to retake data, and re-conduct data aggregation and decision making.

A flow chart for the decision making is shown in Fig. 5.7.

To better illustrate how decision making works in a smart sensor network, a simple example is shown in Fig. 5.8. The manager sensors in each community first conduct damage detection locally. Those communities having no damage send “ok” signal back to the central station. Because damage is detected in communities 3, 4, and 8, these communities interact with the surrounding communities. As a result, communities 3 and 4 confirm that element 16 is the damage location and send this damage information back to the central station. Communities 7 and 8 are required to retake data and re-conduct damage detection as inconsistent information has been obtained regarding element 33.

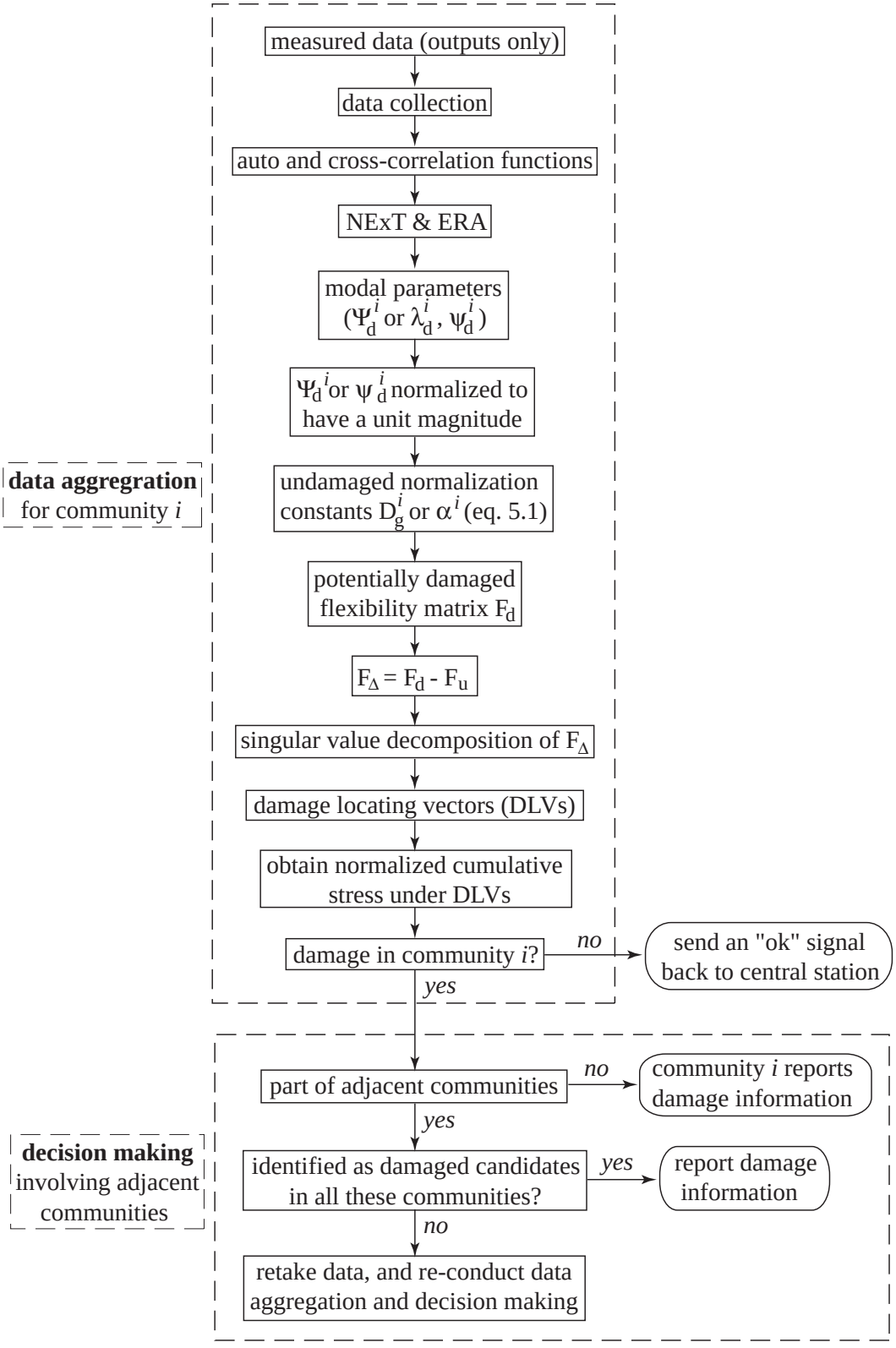

Figure 5.7: Data aggregation and decision making.

	damage	action		action		action		
		send	receive	send	receive	send	receive	
G1	No	**S "ok" B**	-	SLEEP →				
G2	No	**S "ok" B**	R ?16 G3	S "0" G3	-	SLEEP →		
G3	**Yes**	S ?16 G2	-	-	R "0" G2	**S "D16" B**	-	SLEEP
		S ?16 G4	R ?16 G4	S "1" G4	R "1" G4			
G4	**Yes**	S ?16 G3	R ?16 G3	S "1" G3	R "1" G3	**S "D16" B**	-	SLEEP
		S ?16 G5	-	-	R "0" G5			
G5	No	**S "ok" B**	R ?16 G4	S "0" G4	-	SLEEP →		
G6	No	**S "ok" B**	-	SLEEP →				
G7	No	**S "ok" B**	R ?33 G8	S "-1" G8	-	-	R "C" G8	**P "C"**
G8	**Yes**	S ?33 G7	-	-	R "-1" G7	S "C" G7	-	**P "C"**
		S ?33 G9	-	-	R "0" G9	**S "I33 7-8" B**		
G9	No	**S "ok" B**	R ?33 G8	S "0" G8	-	SLEEP →		
G10	No	**S "ok" B**	-	SLEEP →				
G11	No	**S "ok" B**	-	SLEEP →				

Notes:

G1	Manager sensor in community 1.
S	Send.
R	Receive.
B	Base station.
P	Perform.
SLEEP	Sleep mode.
"-"	Idle or listening mode.
?	Query.
"0"	No. It is not a member of our group.
"1"	Yes. It is a member of our group and is damaged.
"-1"	Yes. It is a member of our group but is NOT damaged.
"D"	Damage information.
"ok"	No damage found in this group.
"C"	Cycle: cycle of retaking data and re-conducting damage evaluation.
"I"	Inconsistent.

Examples

S ?16 G2	Send query about element 16 TO group 2.
S "1" G2	Send signal "1" TO group 2.
S "ok" B	Send ok signal TO base station.
S "D16" B	Send damage information about element 16 TO base station.
S "I33 7-8" B	Send signal to base station indicating that inconsistent information regarding element 33 has been obtained by groups 7 and 8.
S "C" G3	Send "Cycle" signal TO group 3 advising it to retake data and re-conduct damage evaluation.
R ?16 G2	Receive query about element 16 FROM group2.
R "1" G2	Receive signal "1" FROM group 2.
R "C" G4	Receive "Cycle" signal FROM group 4.
P "C"	Perform another cycle of retaking data and re-conducting damage evaluation.

Figure 5.8: Decision making example (element 16 is consistently identified as having damage in communities 3 & 4; and inconsistent information has been obtained by communities 7 & 8 regarding element 33).

Damage detection results regarding element 33 need to be reported to the central station after retaking data.

5.4 Numerical Validation

The proposed DCS approach is verified using the planar truss structure shown in Fig. 5.1. Properties of this truss structure have been presented in section 4.4 of the previous chapter.

In this numerical example, assume that accelerometers are installed in the *x*- and *y*-direction at all the nodes except the supports. Communities are developed as described in section 5.3.2. A band-limited white noise with an RMS amplitude around 5% of the measured signal is added to each measurement to simulate measurement noises. Only the first three modes identified from the measured data are utilized for damage detection.

This truss structure is excited in the *y*-direction using two independent band-limited white noises. These excitations are not measured except for the case of algorithm initialization employing forced vibration. To better assess efficacy of the proposed approach in practice, both excitation location and magnitude have been changed before and after damage. These excitation conditions are shown in Table 5.1.

Table 5.1: Excitation conditions before and after damage.

	Location	*Magnitude (height of Power Spectral Density function)*
Before damage	nodes 7 and 11	0.12 and 0.18
After damage	nodes 9 and 23	0.18 and 0.09

5.4.1 Constructing undamaged flexibility matrix in communities

The undamaged normalization constants $\hat{d}_j$ or $\hat{\alpha}_j$ in Eq. (5.1) are first obtained from forced or ambient vibration. Then the SHM system can start measuring data to construct the undamaged flexibility matrix employing ambient vibration.

First, the acceleration measurements are collected and the auto- and cross-spectral density functions are computed by selecting a reference output, which are used to compute the corresponding auto- and cross-correlation functions. The sample correlation function, between the acceleration in the *y*-direction of node 5 and node 7 (reference output in community 1), is shown in Fig. 5.9. These correlation functions can then be used by the ERA method to extract the modal parameters and sample results are shown in Fig. 5.10. In this figure, the star represents the identified mode shape, and the solid line represents exact mode shape from the undamaged analytical model. As can be seen, system identification using only outputs has shown good agreement with the analytical model.

Once the undamaged modal parameters in each community are identified, the associated normalization constants can be obtained using Eq. (5.1), and the undamaged flexibility matrix can then be constructed employing Eq. (4.7) or (4.13). Comparison of

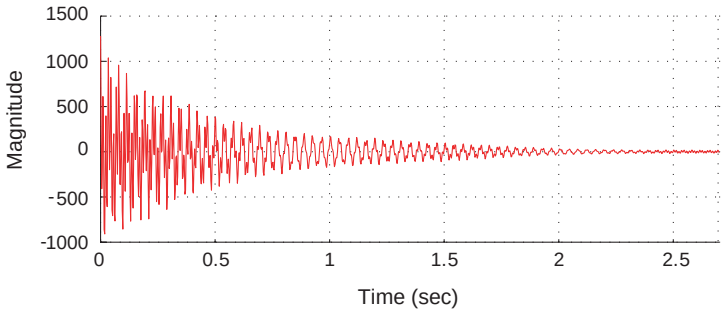

Figure 5.9: Correlation function.

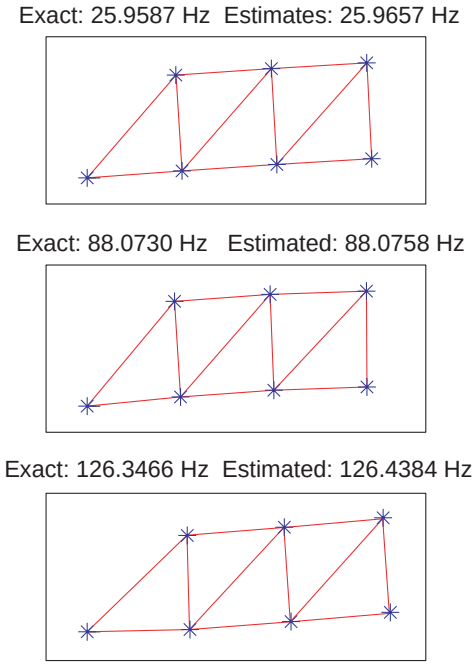

Figure 5.10: Undamaged modal parameters ($*$: identified mode shapes; —: exact mode shapes).

the identified flexibility matrices with the exact one at the measured DOFs in the *x*- and *y*-direction of nodes 3 and 5 is shown in Table 5.2. As can be seen, accurate results have been obtained using the modal normalization constants identified from either forced or ambient vibration.

5.4.2 Damage detection results

For this specific truss structure and sensor configuration, a cut-off value of 0.3 for normalized cumulative stress has been found to work well for a wide range of damage

Table 5.2: Comparison of undamaged flexibility matrices using the first three modes ($\times 10^{-6}$ m/N).

Exact flexibility matrix				*Estimated flexibility matrix*							
				Initialization based on forced vibration				*Initialization based on ambient vibration*			
0.0038	-0.0083	0.0072	-0.0128	0.0032	-0.0089	0.0063	-0.0145	0.0034	-0.0082	0.0065	-0.0130
-0.0083	0.1428	-0.0201	0.2710	-0.0089	0.1460	-0.0215	0.2766	-0.0082	0.1488	-0.0200	0.2832
0.0072	-0.0201	0.0139	-0.0328	0.0063	-0.0215	0.0123	-0.0360	0.0065	-0.0200	0.0126	-0.0332
-0.0128	0.2710	-0.0328	0.5169	-0.0145	0.2766	-0.0360	0.5264	-0.0130	0.2832	-0.0332	0.5417

scenarios while using a total of seven DLVs associated with the smallest singular values. This cut-off values is therefore used herein to select the damaged elements.

By constructing an approximate flexibility matrix for each community employing the locally measured information, the DLV method can be applied for continuous monitoring of the structure. Both single and multiple damage scenarios are investigated and the representative damage cases are shown in Table 5.3. The single damage scenario is studied in Cases 1-1 and 1-2, in which different damage extents are considered. Additionally, three multiple damage scenarios are illustrated. Cases 2-1 and 2-2 have a same damage extent for the damaged elements, while Case 2-3 has a different damage extent for the damaged element. Again, damage in different types of elements, including longitudinal, diagonal, and vertical elements, are studied through these selected damaged cases.

Table 5.3: Two damage scenarios: five damage cases.

Cases		*Damage extent (stiffness reduction)*	*Damaged elements*
Single damage	Case 1-1	20%	diagonal element 13
	Case 1-2	40%	longitudinal element 18
Multiple damage	Case 2-1	20%	diagonal element 17 and longitudinal element 36
	Case 2-2	20%	vertical element 11 and longitudinal element 40
	Case 2-3	40% and 30%	longitudinal element 20 and diagonal element 45

Case 1-1

The results of the normalized cumulative stress for each community when diagonal element 13 has a 20% stiffness reduction is displayed in Fig. 5.11. For both cases of initialization from forced and ambient vibration, results from communities 2 and 3 show that element 13 has a normalized cumulative stress smaller than the threshold value of 0.3. Therefore, this element is confirmed as a damage location in these communities. Results from other communities show no elements having a small normalized cumulative stress,

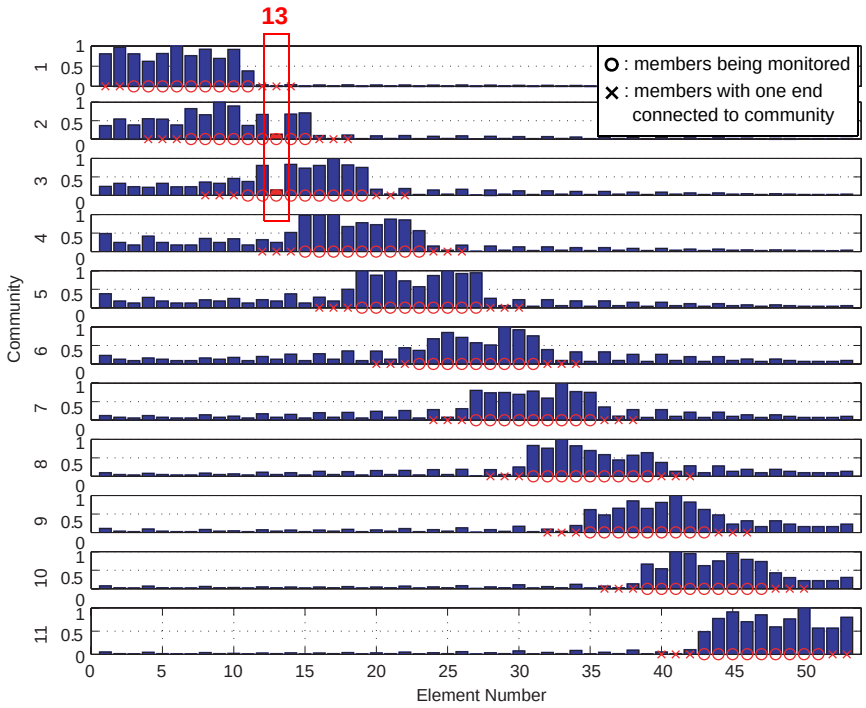

Initialization based on forced vibration

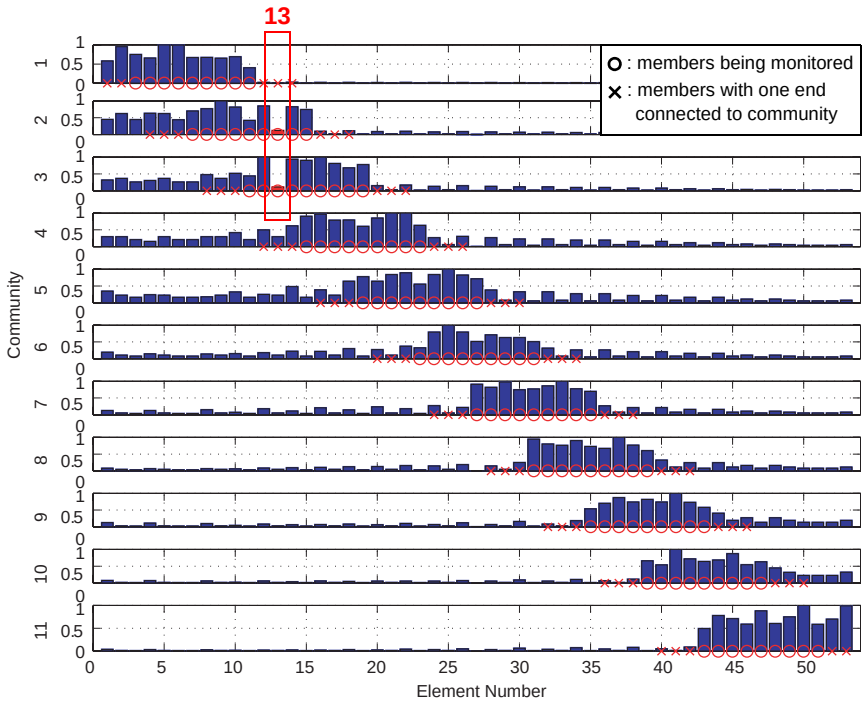

Initialization based on ambient vibration

Figure 5.11: Normalized cumulative stress when element 13 has a 20% stiffness reduction.

Note that for a densely distributed sensor network, the possibility of identifying undamaged elements as potentially damaged locations has been significantly reduced. For this specific case, the damaged element is correctly identified as the damage candidate by communities 1 and 2, and no more damage is found by the other communities.

Therefore, the manager sensors in communities 2 and 3 send the damage information to the central station; and other communities which have no damage only send an “ok” signal back to the central station.

Case 1-2

Figure 5.12. displays the results of the computed normalized cumulative stress when longitudinal element 18 has a 40% stiffness reduction. Results from communities 3 and 4 show that the normalized cumulative stress for element 18 is smaller than the threshold. Therefore, this element is confirmed as a damage location by these two communities.

For the case of initialization based on forced vibration, results from other communities show no elements having a small normalized cumulative stress. The manager sensors in communities 3 and 4 send the damage information to the central station; and other communities only send an “ok” signal back to the central station.

For the case of initialization based on ambient vibration, community 11 identifies element 43 as a damage candidate because it has a small normalized cumulative stress which is smaller than the threshold. However, communities 9 and 10 report this element as undamaged because it has a larger normalized cumulative stress. Inconsistent information has been obtained by communities 9, 10, and 11 regarding element 43. These communities need to retake data and re-conduct damage detection. The results are shown in Fig. 5.13. Because element 43 has a larger stress than the threshold in all these communities, so it is identified as an undamaged element. The manager sensors in communities 3 and 4 send the damage information regarding element 18 to the central station; and other communities only send “ok” signal back to the central station.

These results show that the proposed DCS approach works well when a single element is damaged. Multiple damage scenarios are also studied and results from three different cases will be illustrated in the following paragraphs.

Case 2-1

Figure 5.14 shows the results when diagonal element 17 and longitudinal element 36 have a 20% stiffness reduction. Communities 3 and 4 determine element 17 as a potentially damaged element; and communities 8 and 9 identify element 36 as the damage candidate.

For the case of initialization from forced vibration, community 6 reports element 23 as a damage candidate because it has a normalized cumulative stress smaller than the threshold. However, this element is determined as undamaged by communities 4 and 5. Inconsistent information is obtained by communities 4, 5, and 6 regarding element 23. These communities need to retake data and re-conduct damage detection. The results are

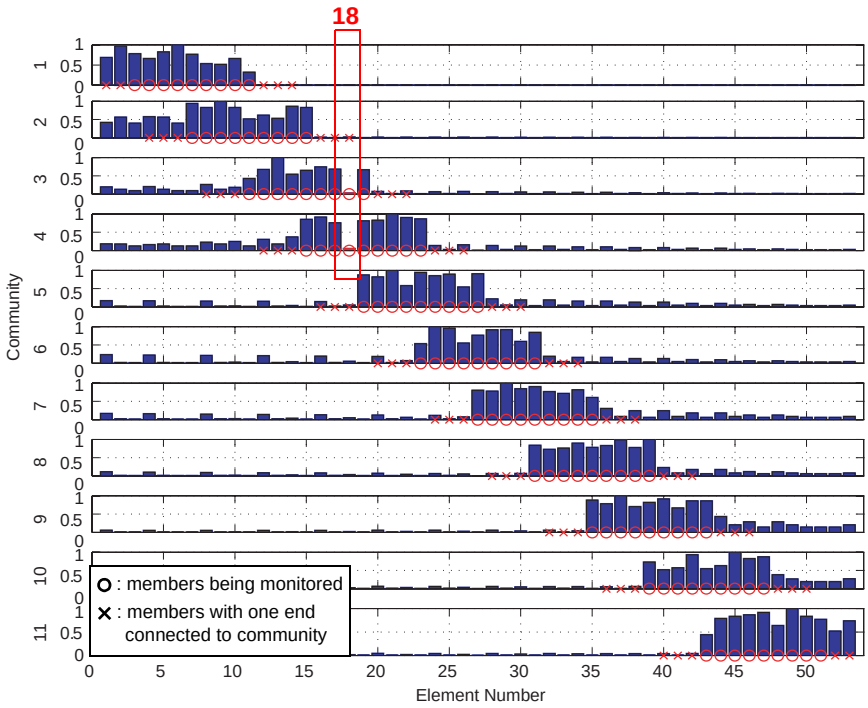

Initialization based on forced vibration

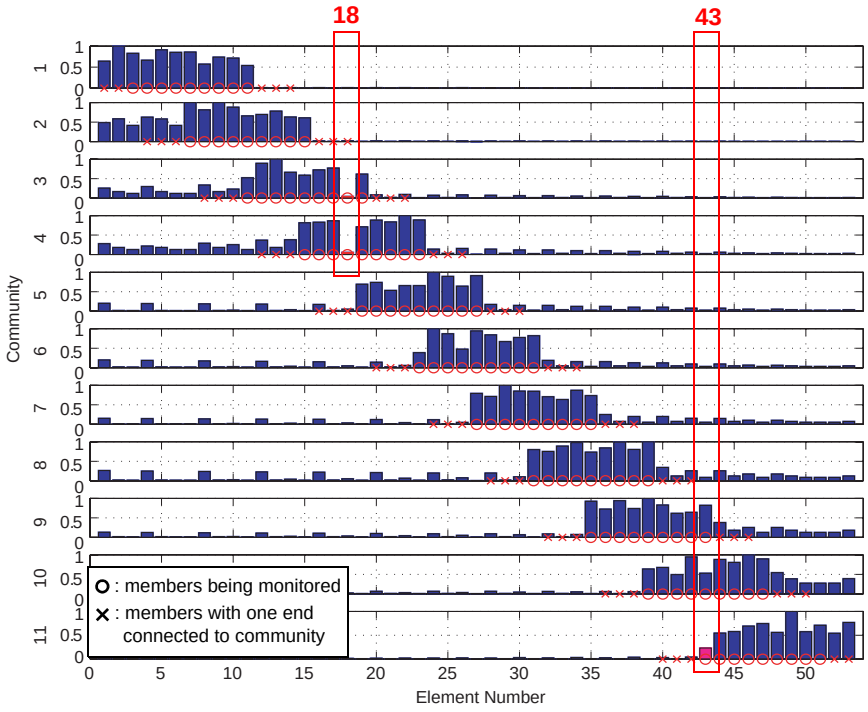

Initialization based on ambient vibration

Figure 5.12: Normalized cumulative stress when element 18 has a 40% stiffness reduction.

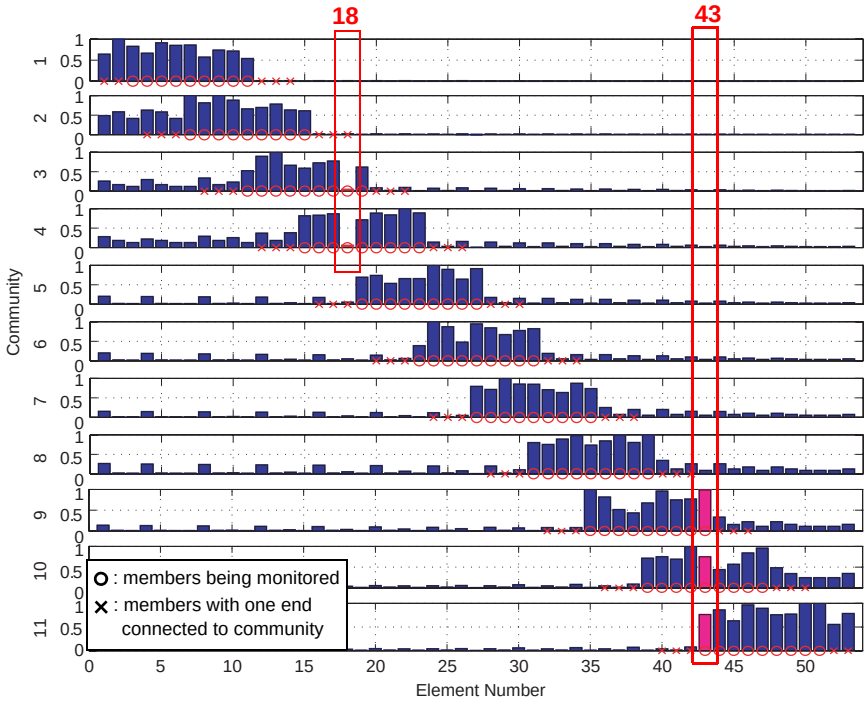

Initialization based on ambient vibration

Figure 5.13: Normalized cumulative stress when element 18 has a 40% stiffness reduction (retaking data regarding element 43).

shown in Fig. 5.15 which determines element 23 as an undamaged location as it has a large stress in all these communities.

Therefore, for both the cases of initialization based on forced and ambient vibration, communities 3 and 4 report damage information regarding element 17, and communities 8 and 9 send damage information regarding element 36 back to the central station. Other communities having no damage only send back an “ok” signal.

Case 2-2

Figure 5.16 shows the results when vertical element 11 and longitudinal element 40 have a 20% stiffness reduction. Similarly, communities 1, 2, and 3 determine that element 11 is the potentially damaged element; and communities 9 and 10 show element 40 as a damaged candidate. For both cases, these communities report damage information and other communities only send an “ok” signal back to the central station.

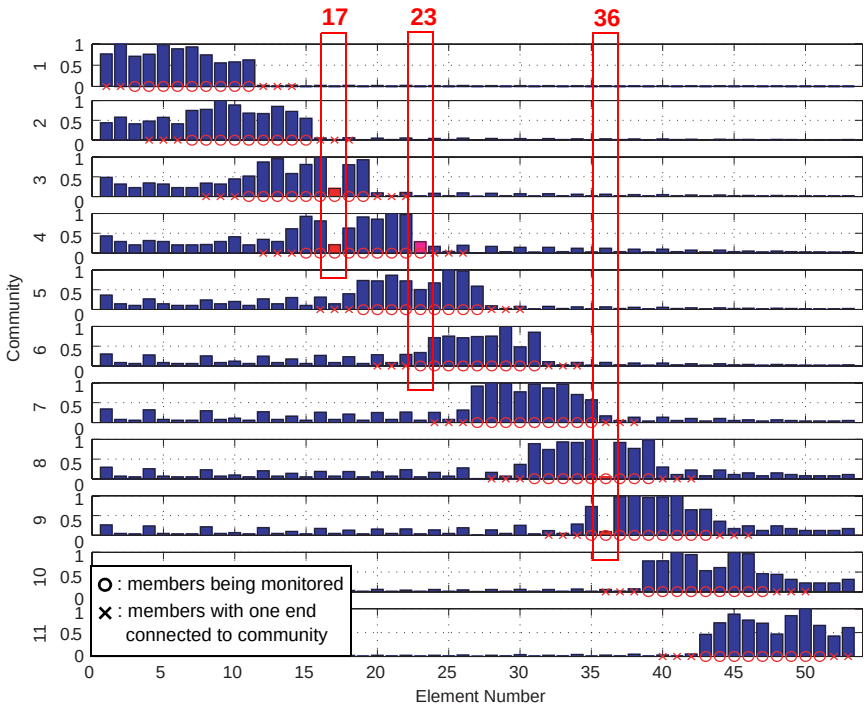

Initialization based on forced vibration

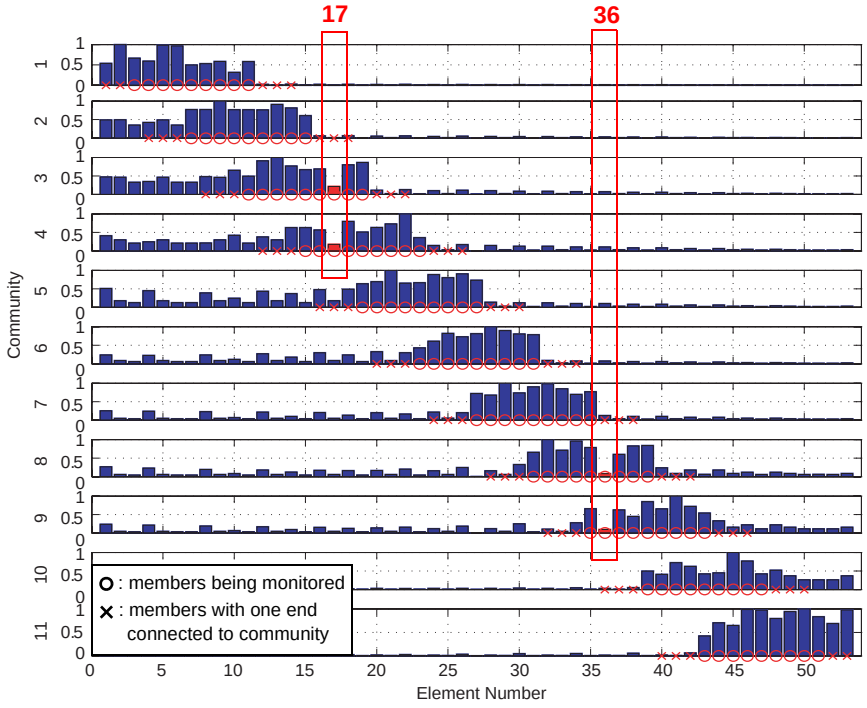

Initialization based on ambient vibration

Figure 5.14: Normalized cumulative stress when elements 17 and 36 have a 20% stiffness reduction.

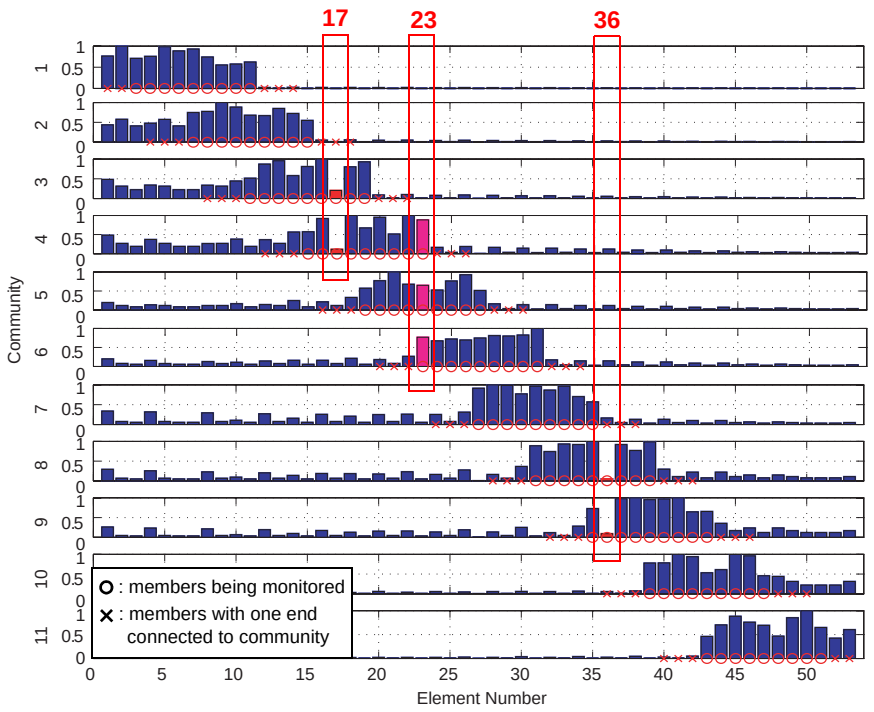

Figure 5.15: Normalized cumulative stress when elements 17 and 36 have a 20% stiffness reduction (retaking data regarding element 23).

Case 2-3

The results when longitudinal element 20 has a 40% stiffness reduction and diagonal element 45 has a 30% stiffness reduction are displayed in Fig. 5.17. Again, element 20 has been correctly identified as a damage candidate by communities 3 and 4; and element 45 is determined as a potentially damaged element by communities 10 and 11. These communities send the damage information to the central station. Communities with no damage detected only send an “ok” signal back to central station.

These simulation results demonstrate that the proposed DCS approach is promising not only for the single damage scenario but also for the multiple damage scenario. In these examples, damaged elements are consistently identified by using localized sensor groups, and retaking data and re-conducting damage detection was also studied.

5.5 Summary

In this chapter, a new distributed computing strategy (DCS) for SHM was proposed that is suitable for implementation on a network of densely distributed smart sensors. The proposed DCS approach differs from the traditional damage detection algorithms because

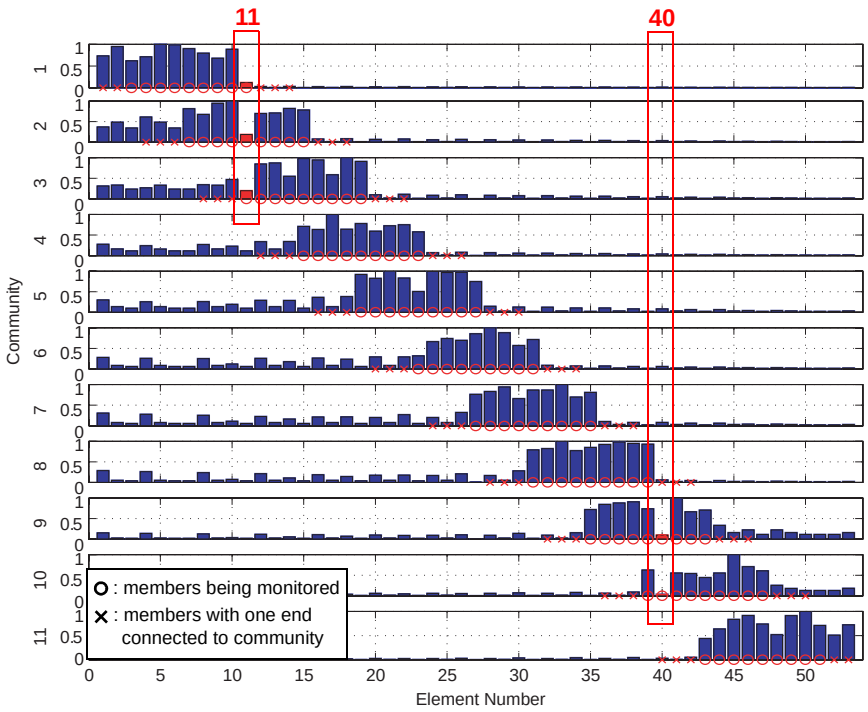

Initialization based on forced vibration

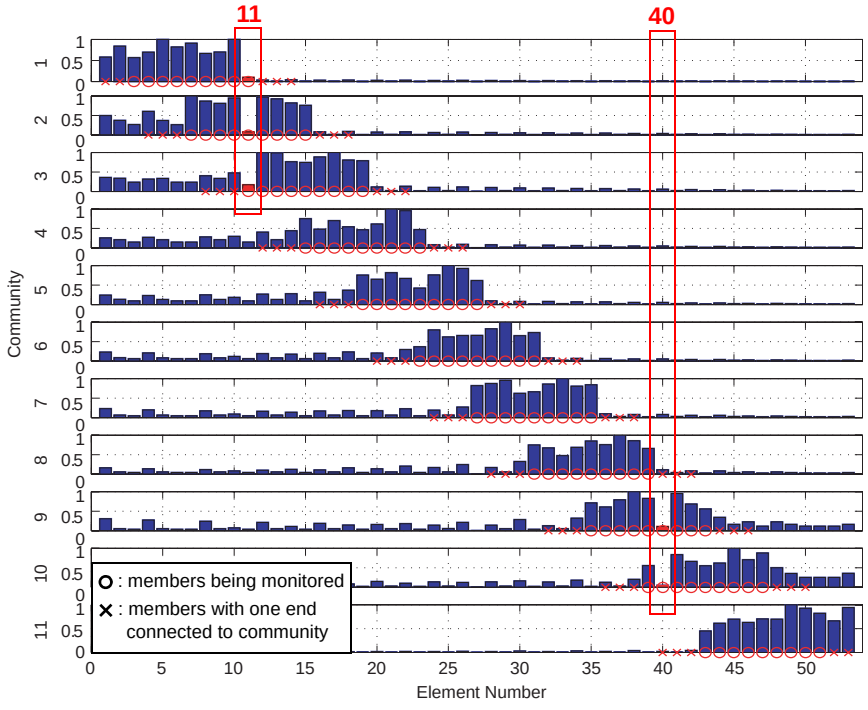

Initialization based on ambient vibration

Figure 5.16: Normalized cumulative stress when elements 11 and 40 have a 20% stiffness reduction.

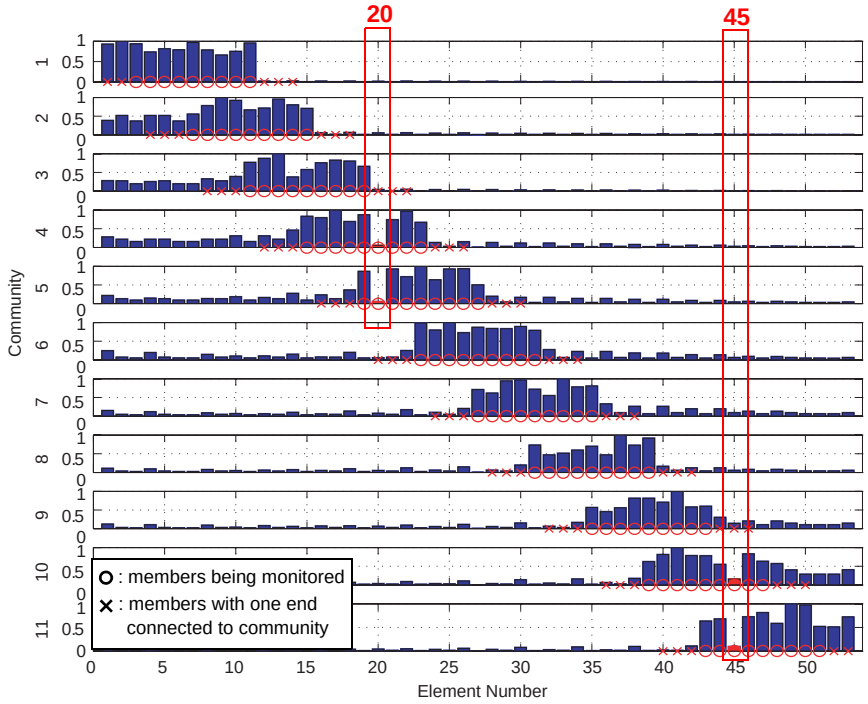

Initialization based on forced vibration

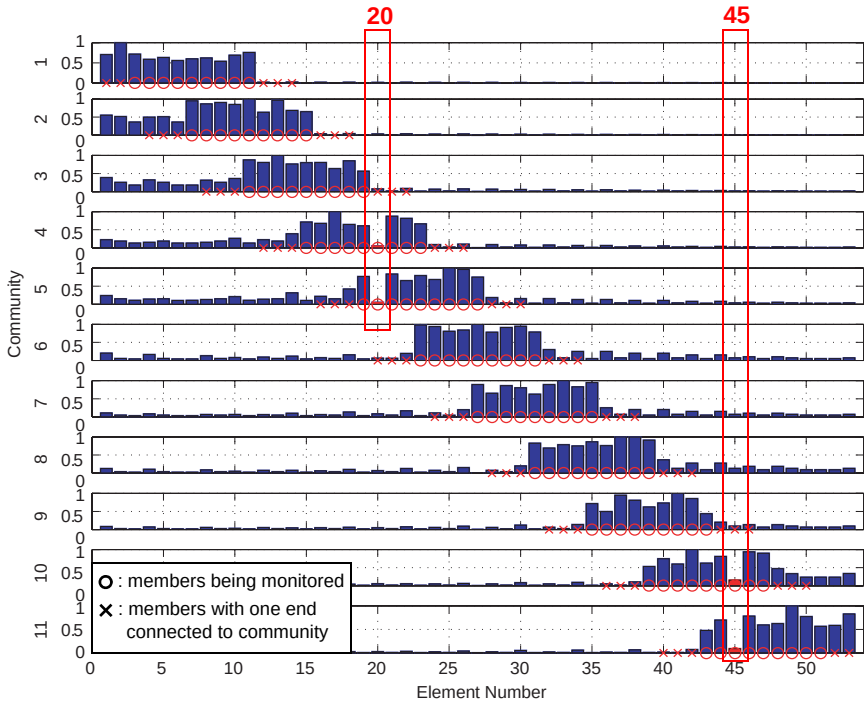

Initialization based on ambient vibration

Figure 5.17: Normalized cumulative stress when element 20 has a 40% stiffness reduction and element 45 has a 30% stiffness reduction.

it does not rely on central data acquisition and processing. In this approach, a hierarchical strategy is proposed in which adjacent smart sensors are grouped together to form sensor communities. The extended DLV method developed in Chapter 4 is employed to evaluate the condition of the local elements within these communities by utilizing only locally measured information. The damage detection results in these communities are then communicated with the surrounding communities and sent back to a central station. In this way, only limited information needs to be transferred between sensors throughout the entire structure.

Numerical simulations with noise included in measurements were conducted by employing a 14-bay truss structure. To better assess the performance of the approach, excitations were changed before and after damage. Both single and multiple damage scenarios were studied. The possibility of falsely identifying undamaged elements as the site of potential damage has been significantly reduced through the use of a dense array of sensors. Numerical results have shown the proposed DCS approach promising for continuous SHM with a densely distributed sensor network.

EXPERIMENTAL VALIDATION OF THE DISTRIBUTED COMPUTING SHM STRATEGY

To better assess the performance of the distributed computing SHM strategy proposed in Chapter 5, experimental validation of the proposed approach has been conducted at the Smart Structures Technology Laboratory of the University of Illinois at Urbana-Champaign (Gao and Spencer 2005b, 2007). Following a detailed description of the experimental setup, experimental results employing the distributed computing SHM strategy are provided which show the proposed approach to be very promising.

6.1 Experimental Setup

The distributed computing SHM strategy is experimentally verified using the 5.6 m long three-dimensional truss structure discussed in Chapter 3 and shown in Fig. 3.10. Note that the roller support has been changed in this experiment to prevent the movement in the vertical direction. This new roller support is depicted in Fig. 6.1.

The dynamic testing system shown in Fig. 6.2 has been developed to support this experiment. The magnetic shaker and the truss structure are not in the picture. Some of the components have been described in details in Chapter 3. Herein, only the new experimental components will be discussed.

A new data acquisition system from National Instruments was purchased and set up in the SSTL. The key components for this data acquisition system are the data acquisition (DAQ) board NI PCI-6052E, which has a 16-bit input and output resolution and a

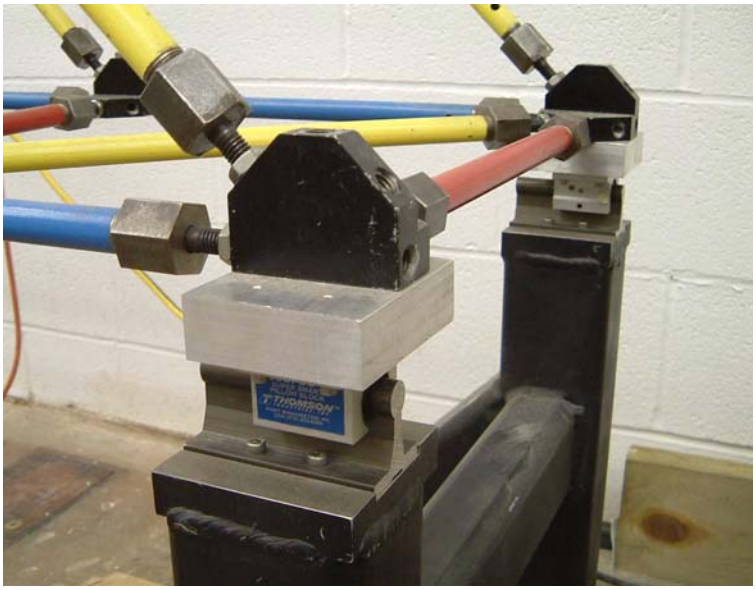

Figure 6.1: Roller support.

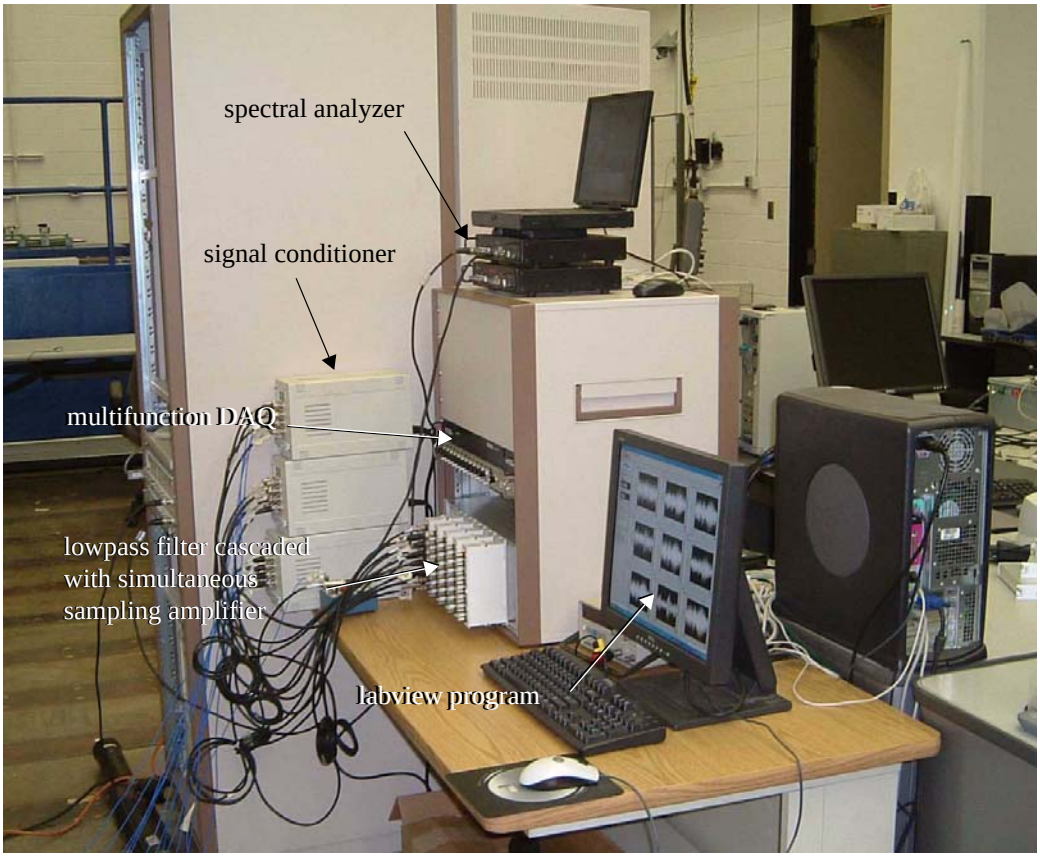

Figure 6.2: Experimental setup.

maximum sampling rate of 333 kS/s, the lowpass elliptical filter NI SCXI-1141, and the simultaneous-sampling differential amplifier NI SCXI-1140.

The National Instruments SCXI-1141 is an 8-channel, programmable 8th-order lowpass elliptical filter, which allows a sharp roll off of the response. By passing the measured data through this lowpass filter, the component of the signal at frequencies higher than the cut-off frequency will be significantly reduced. The cut-off frequency of this filter is user selectable in the range from 10Hz to 25KHz. The SCXI-1141 has a maximum sampling rate of 333KS/s and a programmable gain for each channel with a input range from ± 50 mV to ± 5 V.

The National Instruments SCXI-1140 is an 8-channel simultaneous sample and hold differential amplifier module. Simultaneous sampling is very important for dynamic testing with multiple channel measurements, because any differences in the sample times will result in artificial phase lags in the data. With the SCXI-1140, users can sample multiple signals with negligible phase delay between channels. The SCXI-1140 can be cascaded with the SCXI-1141 for applications requiring filtering and simultaneous sampling to provide high quality dynamic measurements.

A Labview program has been developed to acquire and save the data from this National Instruments data acquisition system. This program allows users to set the programmable cut-off frequencies for the lowpass filter, change the gain on each measurement channel, set sampling rate and measuring time, etc.

Ideally, all the structural members should be monitored for damage. Due to the limited experimental equipment, only elements in the outer vertical panel of the truss will be monitored employing the proposed DCS approach. A sketch of this panel is depicted in Fig. 6.3 with each node number having a circle around it.

A Ling Dynamic Systems permanent magnetic V408 shaker is attached to the bottom nodes of this panel to excite the structure vertically. Connection among the shaker, a PCB load cell (model 208B02), and a structural node is described in section 3.4.1 and shown in Figs. 3.13 and 3.14.

A steel bracket has been installed at each of the structural joints except the supports in this panel to facilitate installation of accelerometers in the *x*-direction (see Fig. 6.4). The accelerometers are attached to the bracket and structural node using magnetic bases.

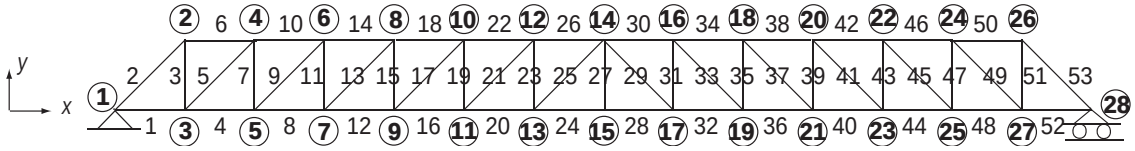

Figure 6.3: Outer vertical panel of the three-dimensional truss structure.

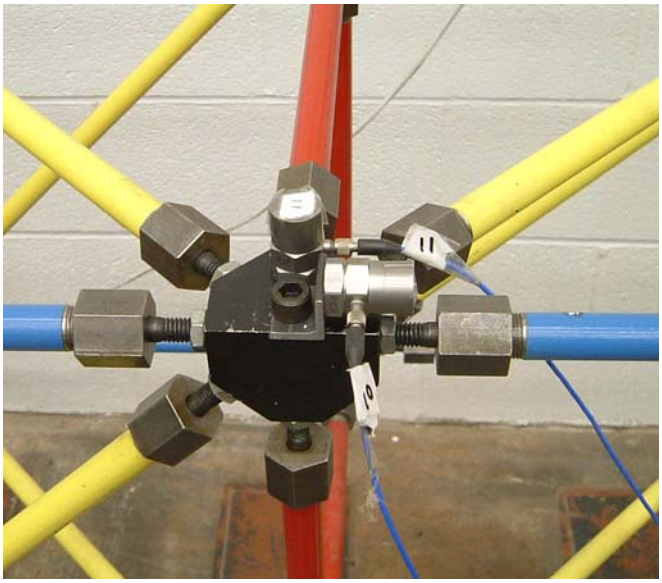

Figure 6.4: Installation of accelerometers.

Sensor communities are formed in the way same as Fig. 5.5. There are a total of 12 accelerometers in a sensor community with one accelerometer in the *x*-direction and the other in the *y*-direction at each structural node. These localized sensors are used to monitor the condition of nine local structural members which have both ends connected to the structural nodes in the same community. Again, there are a total of 11 sensor communities in this experiment.

One of the communities with a single member replaced by the damaged one is displayed in Fig. 6.5. Due to the limited experimental equipment, these 12 accelerometers shown in Fig. 6.5 have to be moved along the truss structure to measure the response for each community.

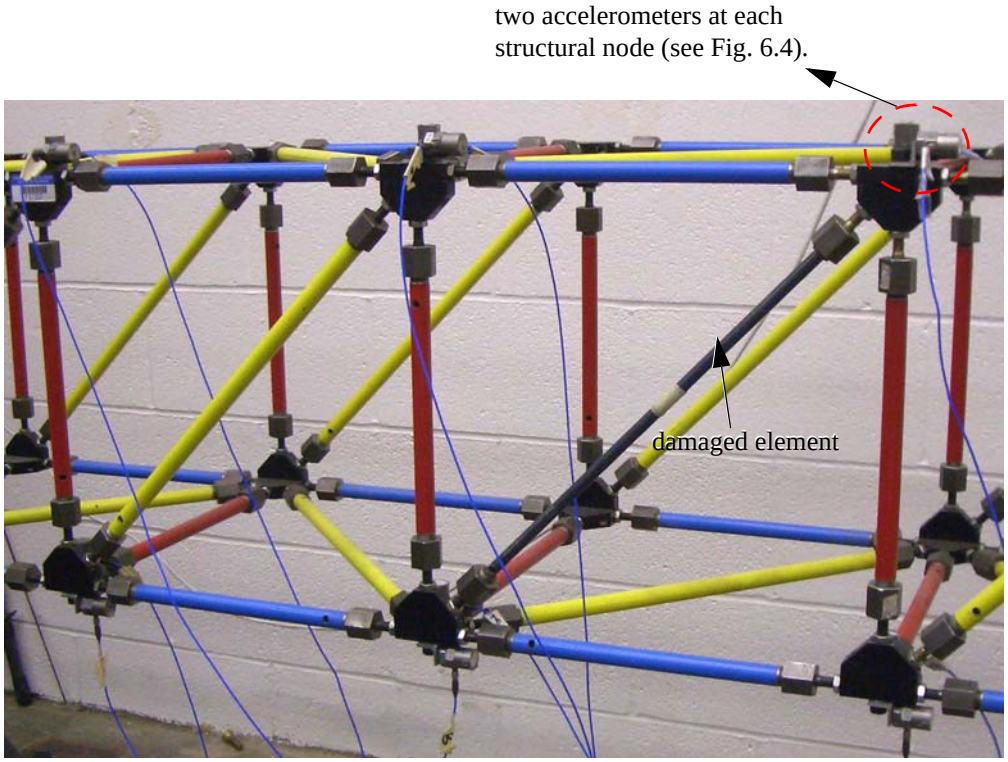

Figure 6.5: Example of a single sensor community for the outer vertical panel of the truss.

6.2 Algorithm Initialization

To detect the damage in this truss structure employing the proposed DCS approach, the undamaged flexibility matrix at the sensor communities needs to be constructed. Construction of the flexibility matrix based on both forced and ambient vibration employing experimental data will be investigated. Details of these two approaches have been reviewed in sections 4.1.

For the case of initialization based on forced vibration, dynamic testing is first conducted when seven accelerometers are installed at nodes [7, 11, 13, 17, 19, 21, 23] to

measure the acceleration in the *y*-direction and the shaker is attached to the bottom of node 17. Therefore, there is one co-located sensor and actuator pair which is at node 17. Modal normalization constants associated with these mode shapes can then be obtained from experimental data using Eq. (4.11).

For the case of algorithm initialization based on ambient vibration, a total of 11 accelerometers were installed in the *y*-direction of nodes [5, 7, 9, 11, 13, 15, 17, 19, 21, 23, 25], and two accelerometers in the *x*- and *z*-direction (perpendicular to *x*-*y* plane) of node 11. A lumped mass of 1.124 kg, which is about 48% of the original nodal mass (including the structural joint and half weight of each member connected to it), was attached to the bottom of node 11 to simulate mass perturbation. The modal normalization constants can be obtained based on the mass perturbation method using Eq. (4.20).

To verify the results from both of these approaches, undamaged flexibility matrices at the *y*-direction of nodes [7, 11, 13, 17, 19, 21, 23] have been computed using Eqs. (4.7) and (4.13) using the first six dominant modes (see Fig. 6.6, in which acceleration at node 21 is selected as the reference). Good agreement has been shown in Tables 6.1. and 6.2

Table 6.1: Undamaged flexibility matrices based on forced vibration using the first six dominant modes ($\mathrm{x}10^{-5}$ m/N).

Normalization constants based on forced vibration						
0.0533	0.0704	0.0703	0.0604	0.0533	0.0414	0.0321
0.0704	0.0958	0.0977	0.0885	0.0809	0.0651	0.0526
0.0703	0.0977	0.1012	0.0949	0.0887	0.0732	0.0604
0.0604	0.0885	0.0949	0.0960	0.0936	0.0804	0.0689
0.0533	0.0809	0.0887	0.0936	0.0935	0.0819	0.0714
0.0414	0.0651	0.0732	0.0804	0.0819	0.0730	0.0646
0.0321	0.0526	0.0604	0.0689	0.0714	0.0646	0.0579

After the modal normalization constants associated with the mode shapes at reference sensor locations were determined, a series of dynamic testing was conducted with 12

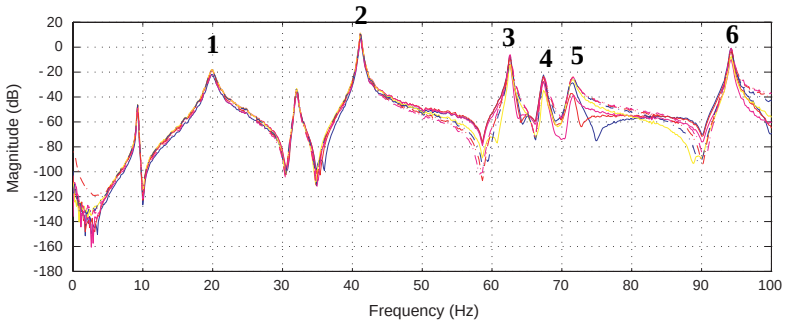

Figure 6.6: Auto- and cross-spectral density functions at nodes [7, 11, 13, 17, 19, 21, 23].

Table 6.2: Undamaged flexibility matrices based on ambient vibration using the first six dominant modes ($\mathrm{x}10^{-5}$ m/N).

Normalization constants based on ambient vibration						
0.0539	0.0695	0.0690	0.0568	0.0489	0.0375	0.0286
0.0695	0.0930	0.0951	0.0838	0.0756	0.0609	0.0488
0.0690	0.0951	0.0993	0.0917	0.0850	0.0705	0.0579
0.0568	0.0838	0.0917	0.0930	0.0906	0.0788	0.0674
0.0489	0.0756	0.0850	0.0906	0.0906	0.0805	0.0700
0.0375	0.0609	0.0705	0.0788	0.0805	0.0728	0.0642
0.0286	0.0488	0.0579	0.0674	0.0700	0.0642	0.0572

sensors installed in each community to obtain the mode shapes in these communities under ambient vibration. The associated modal normalization constants in each of these communities can then be obtained from Eq. (5.1) and the undamaged flexibility matrix at each community can be constructed using Eq. (4.7) or (4.13).

Based on contribution of the frequency modes to the measurements in each community, different communities might need to utilize different frequency modes to construct the flexibility matrix. Fig. 6.7 shows a total of 12 cross spectral density functions for communities 4 and 8, respectively. These cross spectral density functions are

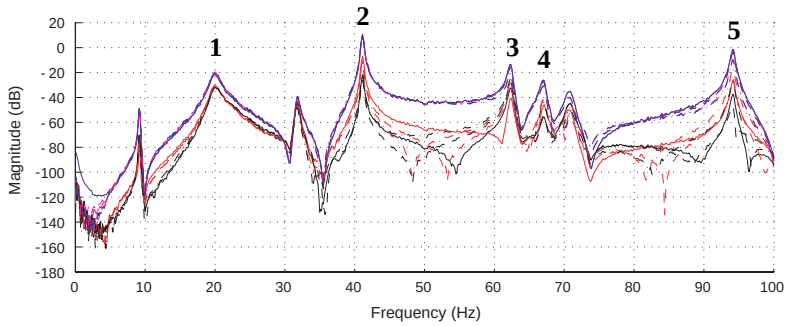

Community 4

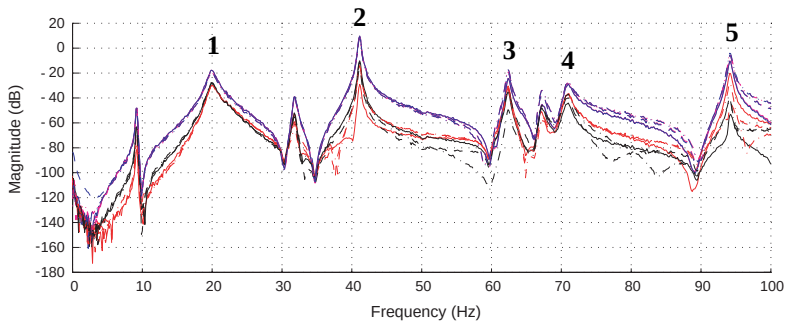

Community 8

Figure 6.7: Auto- and cross-spectral density functions.

computed from the measurements of the 12 accelerometers in each community, with the vertical acceleration at node 9 being selected as the reference output for community 4 and the vertical acceleration at node 21 being selected as the reference output for community 8. The first five dominant modes are identified for both communities 4 and 8. As shown in Fig. 6.7, the fourth dominant mode is different for these two communities.

In this experimental validation, flexibility matrices in communities 1 through 5 are constructed using the same dominant modes as community 4, and communities 6 through 11 use the same dominant modes as community 8. Therefore, the flexibility matrix in each community is constructed using the first five dominant modes identified from the measurements.

6.3 Damage Detection and Decision Making

Once the algorithm initialization is finished, the sensors can start collecting data from the structure to monitor its condition.

A finite element model of the truss structure has been developed using Matlab with a total of 160 elements and 56 nodes (see Fig. 6.8). Pin supports are defined at nodes 1 and 29 and roller supports are defined at nodes 28 and 56. For the roller supports, translation is only allowed in the *x*-direction, and rotation around *x*-axis is also permitted. Matching the dynamic properties between the finite element model and this experimental structure is difficult. However, the proposed approach is not sensitive to the dynamic properties of this structure as the analytical model is utilized for a static computation after the DLVs are obtained.

A series of damage detection tests have been conducted using the three-dimensional 14-bay truss structure located at SSTL of UIUC. Structural damage is simulated by replacing the original elements with ones having a 52.7% cross section reduction, which results in a slightly different axial stiffness reduction for different members (see Table 6.3)

Three excitation conditions (see Table 6.4) have been investigated. As shown in the table, excitation condition 1 has a same excitation location, magnitude, and bandwidth before and after damage. To better simulate the real ambient vibration condition in which the excitation contents can be changed, performance of the proposed approach under excitation condition 2 and 3 is also studied. Condition 2 has a different magnitude and

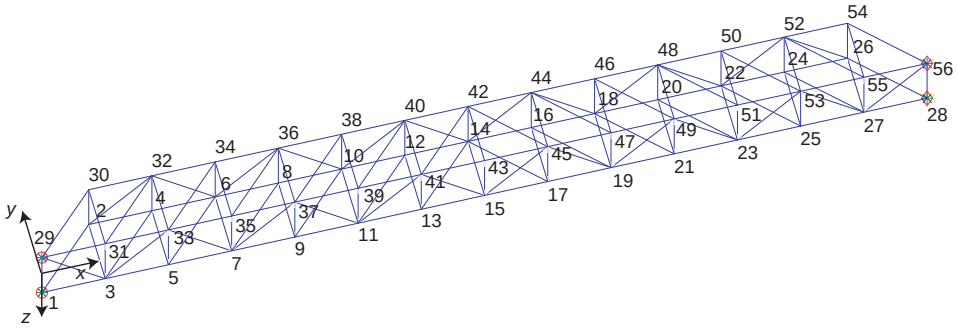

Figure 6.8: Three-dimensional finite element model.

Table 6.3: Structural damage.

	Longitudinal element	*Vertical element*	*Diagonal element*
Cross section reduction	52.7%	52.7%	52.7%
Equivalent axial stiffness reduction	44%	43.5%	46.9%

Table 6.4: Various excitation conditions before and after damage.

	Location	*Magnitude*	*Bandwidth*
Condition 1	same	same	same
Condition 2	same	different	different
Condition 3	different	different	different

bandwidth, and condition 3 has a different location, magnitude, and bandwidth before and after damage.

A cut-off value of 0.3 for the normalized cumulative stress is used and provides good performance for a wide range of damage cases by using a total of five DLVs associated with the smallest singular values. This cut-off value will be used to select the damaged elements from the detection results.

6.3.1 Excitation condition 1

Under this excitation condition, the Ling Dynamic Systems permanent magnetic V408 shaker is attached to the bottom of node 17 to excite the structure vertically. A band-limited white noise with a 0.1 RMS value of magnitude and a bandwidth of 100 Hz is sent from the Siglab spectral analyzer to drive the shaker.

Single and multiple damage scenarios, as well as damage in different types of elements, are studied. The process of retaking data when there is inconsistent damage information is not investigated in this stage. Instead it will be studied under excitation conditions 2 and 3. Results of three damage detection cases (see Table 6.5) are illustrated and discussed herein to demonstrate the performance of the proposed DCS approach.

Table 6.5: Excitation condition 1: three damage cases.

Cases	*Damaged elements*
Case 1-1	diagonal element 17
Case 1-2	longitudinal element 12 and diagonal element 41
Case 1-3	vertical element 7 and longitudinal element 36

Case 1-1

Figure 6.9 shows the results when element 17 is damage. For both the cases of

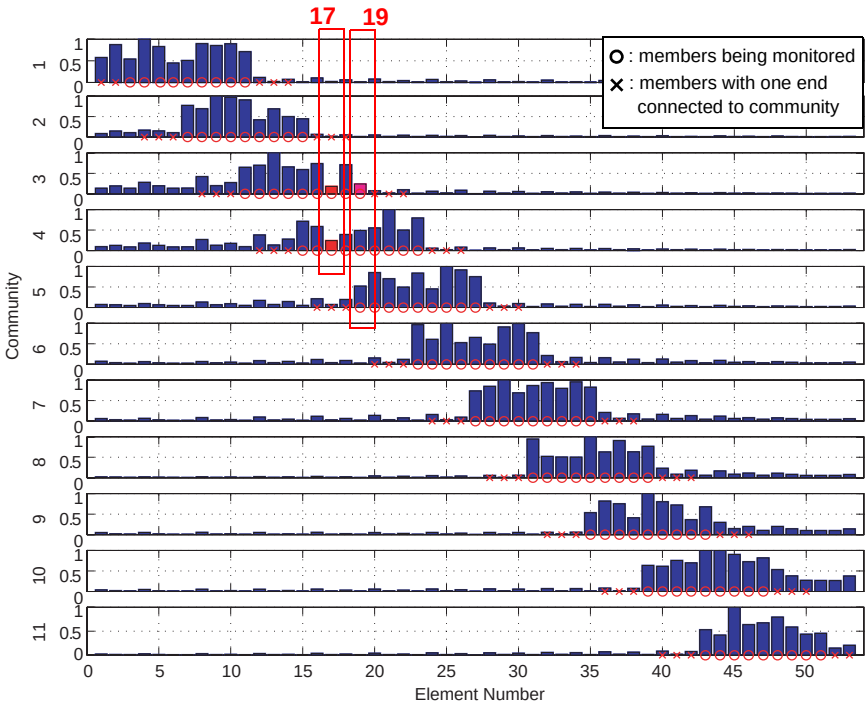

Initialization based on forced vibration

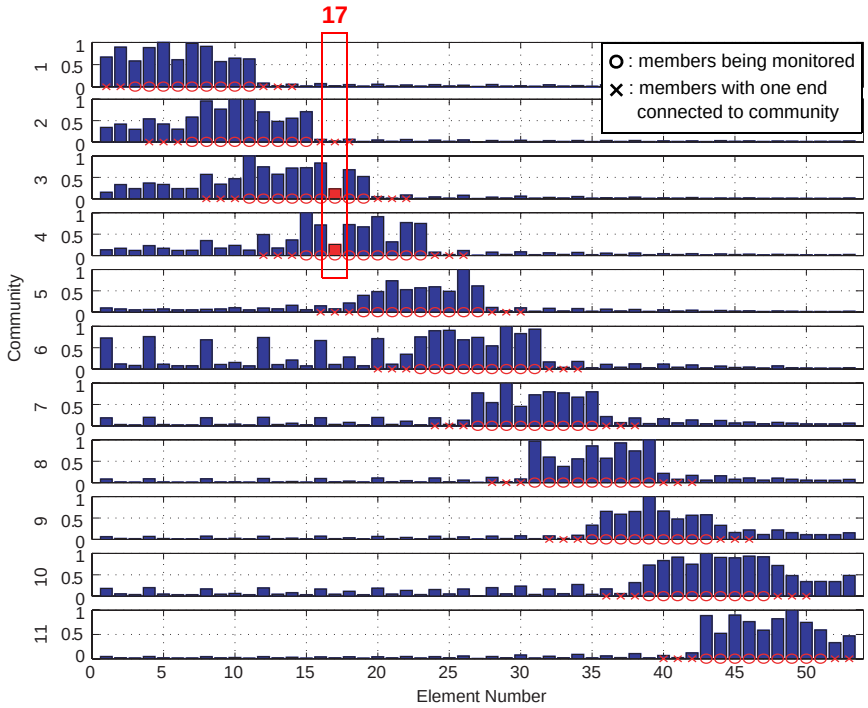

Initialization based on ambient vibration

Figure 6.9: Normalized cumulative stress when element 17 is damaged.

cumulative stress smaller than the threshold of 0.3 and therefore is determined as a damage candidate.

For the case of initialization from forced vibration, community 3 identifies element 19 as possibly having damage because its normalized cumulative stress is smaller than the threshold. However, communities 4 and 5 report this element as undamaged because its stress is larger than the threshold in both these communities. Inconsistent information regarding the condition of element 19 is obtained in communities 3, 4, and 5, therefore these communities need to retake data and re-conduct damage detection. As mentioned above, the process of re-conducting damage detection is not investigated under excitation condition 1, but it will be studied under excitation conditions 2 and 3.

Figure 6.9 shows that elements 52 and 53 also have a small normalized cumulative stress for the case of initialization based on forced vibration. These elements are not part of community 11. Instead, they have one end connected to community 11 and the other end connected to the support. Numerical simulation in Chapter 5 shows that these type of elements can still be monitored by the adjacent community (*i.e.*, elements 1 and 2 are monitored by community 1 and elements 52 and 53 are monitored by community 11). However, the experimental results do not confirm that assumption. Part of the reason may be due to the difficulty to model the real support condition. In this experiment, only the elements which have both ends connected to structural nodes in the same community will be monitored.

Case 1-2

Multiple damage scenarios are also investigated. Figure 6.10 shows the damage detection results when longitudinal element 12 and diagonal element 41 are damaged. As can be seen from the figure, element 12 is determined as a potentially damaged element by communities 2 and 3, and element 41 is identified as a damage candidate by communities 9 and 10.

For the case of initialization from forced vibration, communities 8, 9, and 10 need to retake data and re-conduct damage detection as inconsistent information regarding the condition of element 39 is obtained. Similarly, for the case of initialization based on ambient vibration, communities 6 and 7 need to re-conduct damage detection as inconsistent information regarding element 28 is obtained.

Case 1-3

The detection results regarding damage in vertical element 7 and longitudinal element 36 are shown in Fig. 6.11. The damaged elements have been correctly identified for both cases of initialization based on forced and ambient vibration. For the case of initialization based on ambient vibration, communities 1 and 2 need to re-conduct damage detection regarding element 9, and communities 9 and 10 need to retake data and re-conduct damage detection regarding element 40.

These experimental results show that the proposed DCS approach works well when excitation remains the same before and after damage. To better evaluate the performance

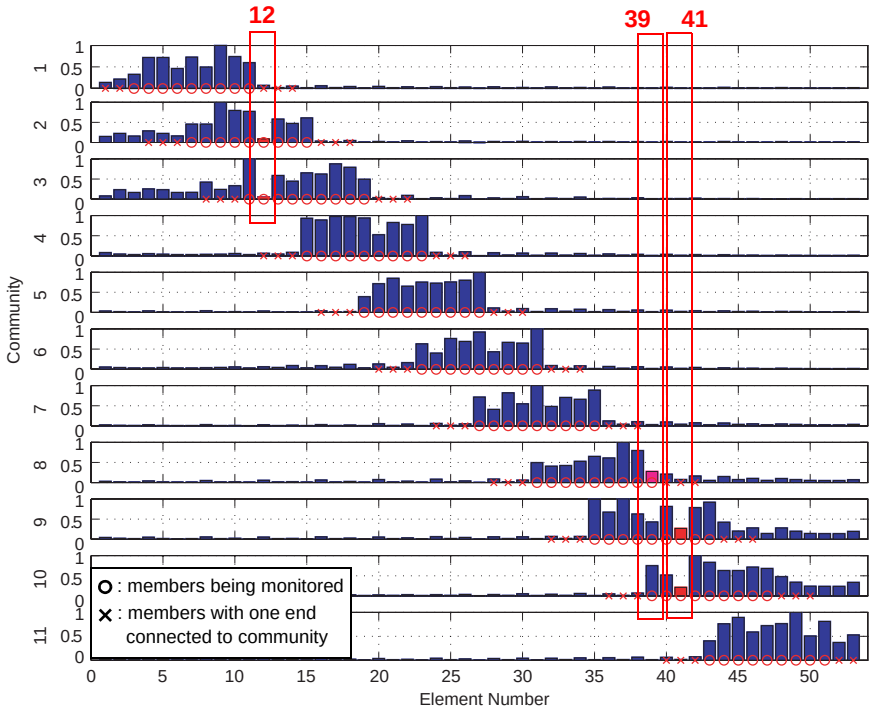

Initialization based on forced vibration

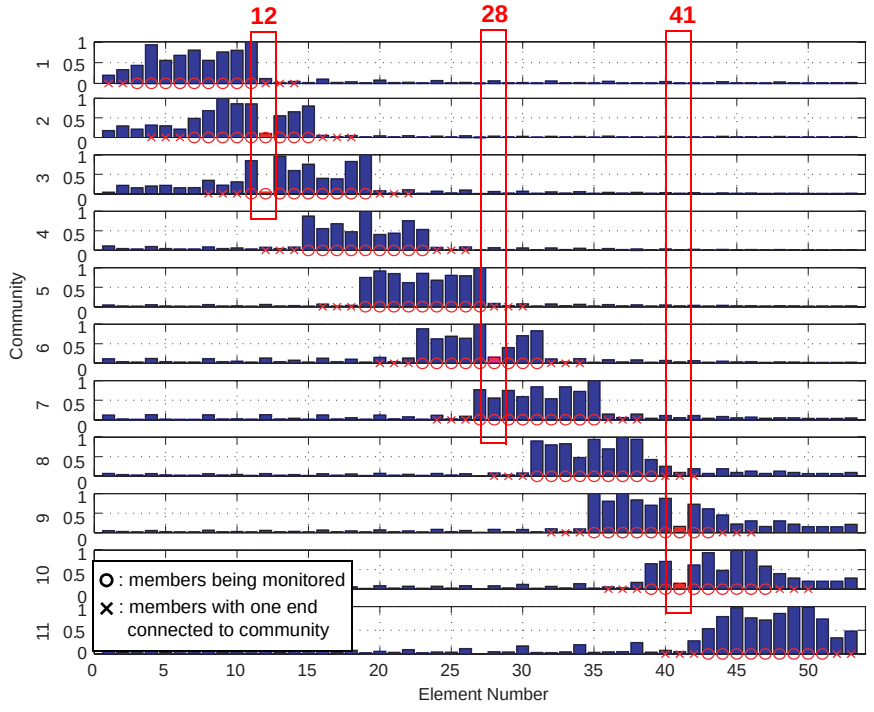

Initialization based on ambient vibration

Figure 6.10: Normalized cumulative stress when elements 12 and 41 are damaged.

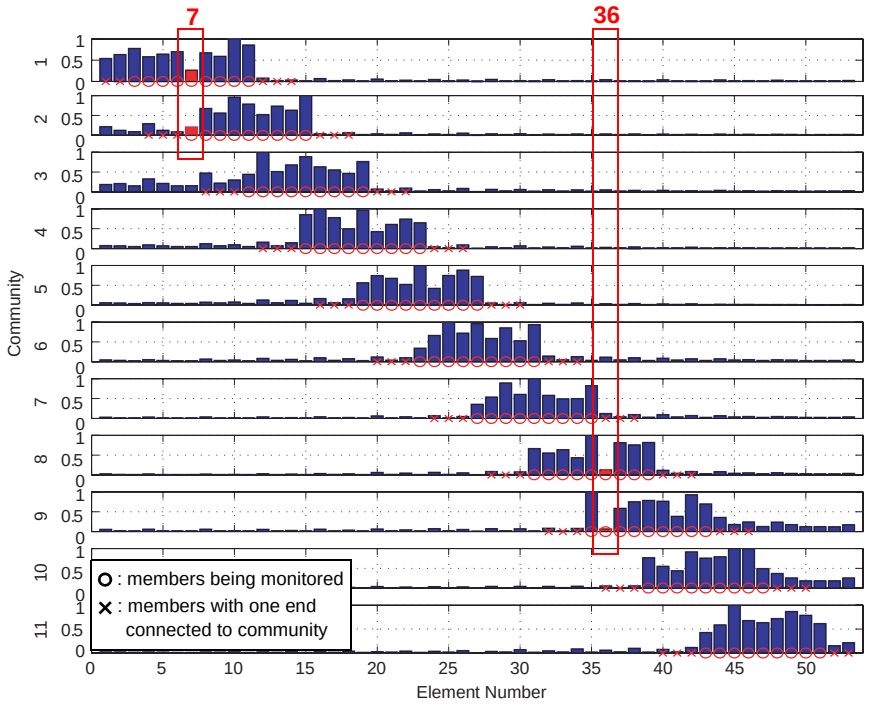

Initialization based on forced vibration

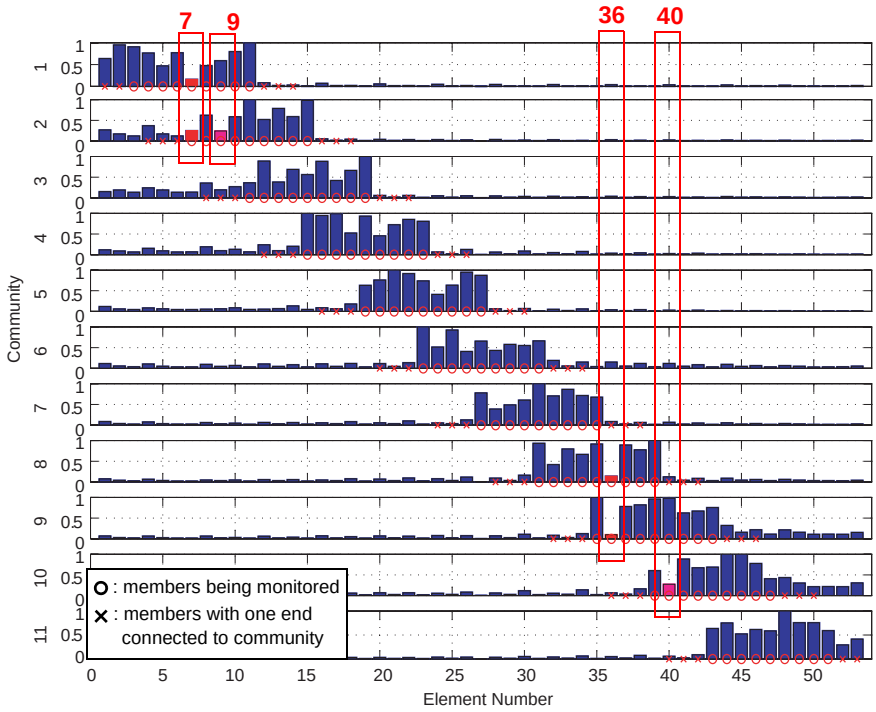

Initialization based on ambient vibration

Figure 6.11: Normalized cumulative stress when elements 7 and 36 are damaged.

of the proposed approach, experiments with excitation contents being changed before and after damage are also studied.

6.3.2 Excitation condition 2

For excitation condition 2, the magnitude of the band-limited white noise excitation is changed from a RMS value of 0.1 to 0.08, and the bandwidth is changed from 100 Hz to 200 Hz before and after damage. Two damage scenarios (see Table 6.6) are studied under this excitation condition.

Table 6.6: Excitation condition 2: two damage cases.

Cases	*Damaged element*
Case 2-1	no damage
Case 2-2	longitudinal element 8

Case 2-1

Experiments have been conducted employing the DCS approach when there is damage in the structure and good damage detection results are obtained. Questions arise regarding its performance when there is no damage in the structure.

Figure 6.12 shows the computed normalized cumulative stress when there is no damage in the structure. As shown in the figure, the normalized cumulative stresses in each community are larger than the threshold, so no damage is detected. All sensor communities send “ok” signal to the central station.

This example demonstrates that the proposed approach also works well when there is no damage in the structure.

Case 2-2

This case demonstrates the process of retaking data and re-conducting damage detection when inconsistent information has been obtained. Damage detection results when longitudinal element 8 is damaged are shown in Fig. 6.13. Element 8 is successfully identified as the damage candidate in both cases as its computed normalized cumulative stress is smaller than the threshold.

For the case of initialization based on forced vibration, community 6 reports that element 24 is damaged as it has a normalized cumulative stress smaller than the threshold 0.3. However, community 5 identify element 24 as having no damage as its stress exceeds the threshold. Inconsistent information is obtained by communities 5 and 6 regarding the condition of element 24, therefore these two communities need to retake data and re-conduct damage detection to determine its condition. Fig. 6.14 shows the results after re-conducting damage detection in these two communities, element 24 is determined as undamaged because both communities report that it has a normalized cumulative stress larger than the threshold.

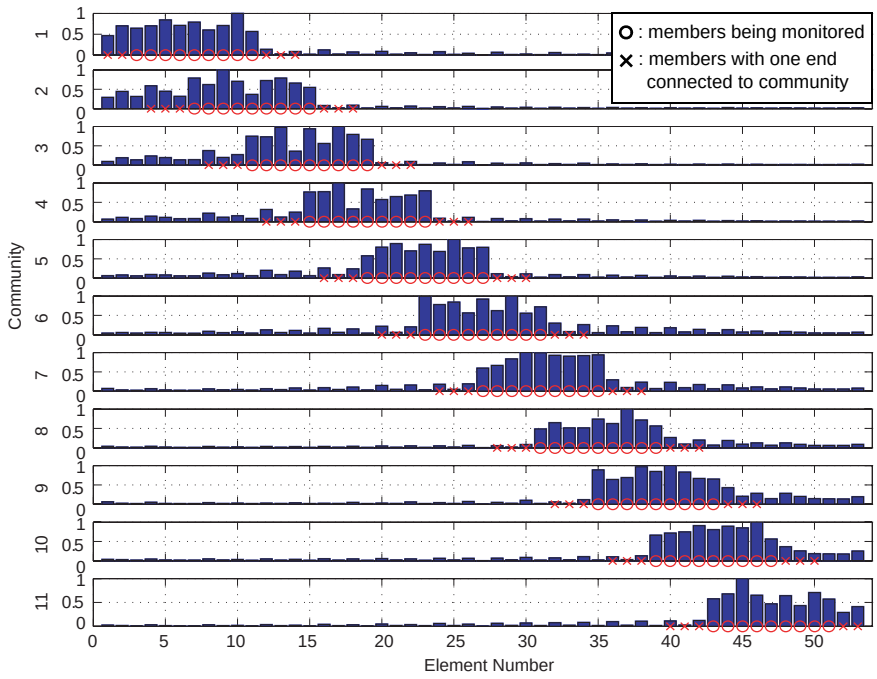

Initialization based on forced vibration

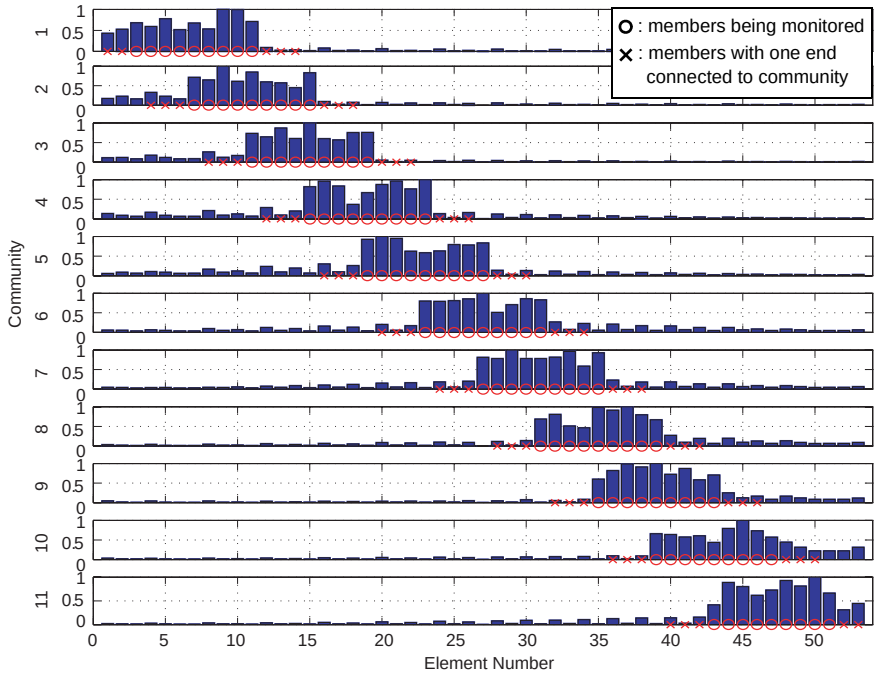

Initialization based on ambient vibration

Figure 6.12: Normalized cumulative stress when there is no damage in the structure.

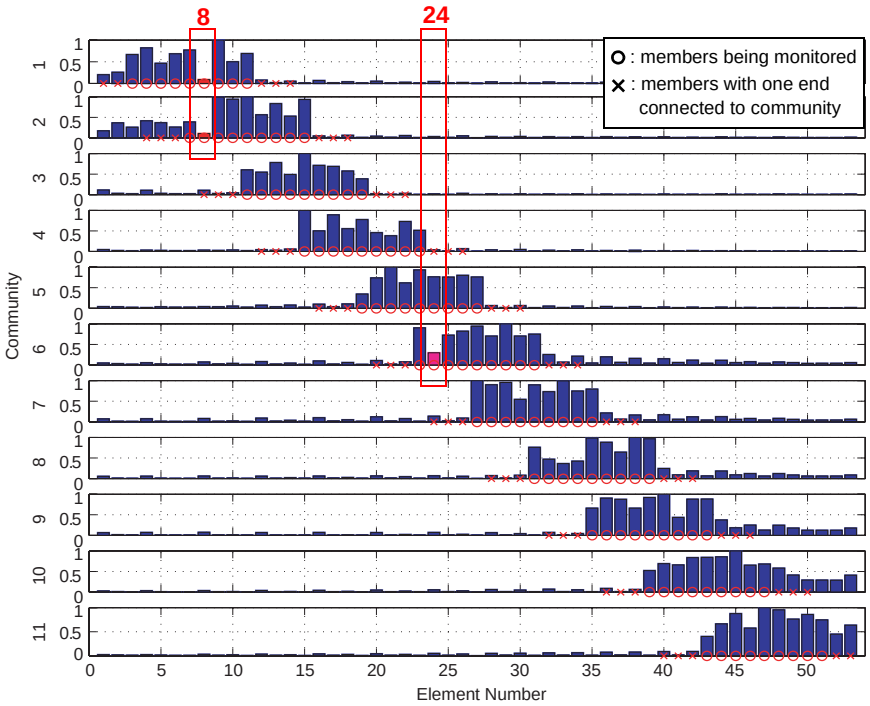

Initialization based on forced vibration

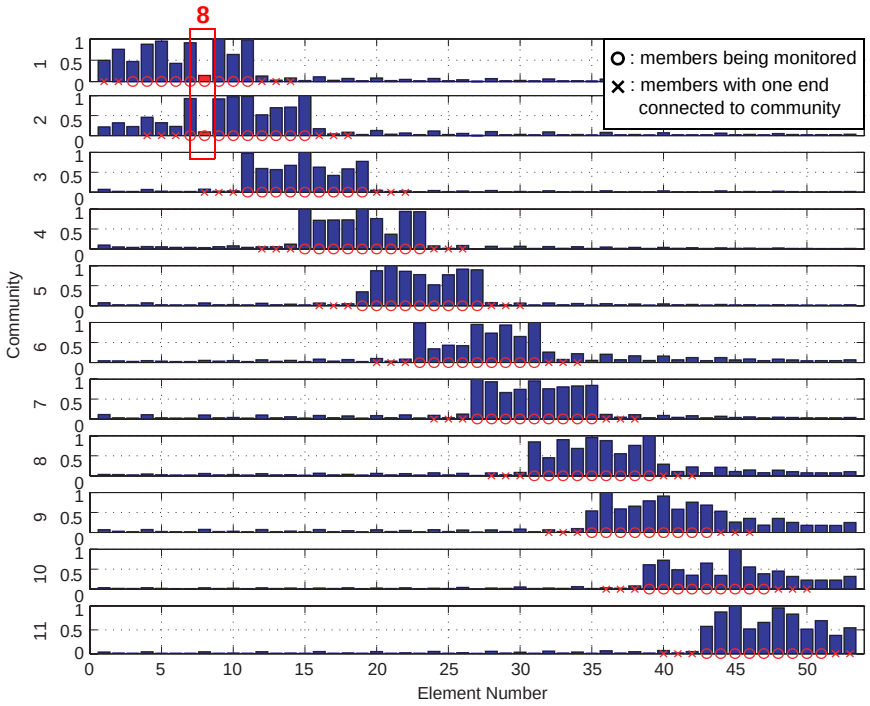

Initialization based on ambient vibration

Figure 6.13: Normalized cumulative stress when element 8 is damaged.

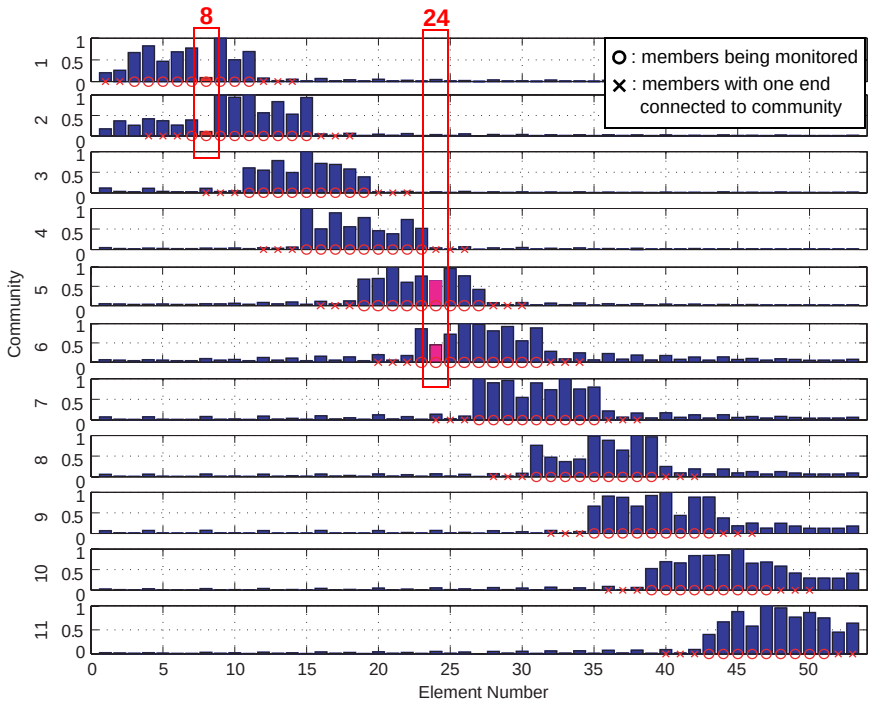

Figure 6.14: Normalized cumulative stress when element 8 is damaged (retaking data regarding element 24).

Therefore, only communities 1 and 2 report damage information to the central station, while other communities send “ok” signal back to the central station.

6.3.3 Excitation condition 3

For excitation condition 3, not only are the excitation magnitude and level changed before and after damage, but the shaker location is also moved from node 17 to node 23 to simulate the change of the excitation location. Two damage scenarios (see Table 6.7) are considered under this excitation condition, with case 3-2 illustrating the process of retaking data and re-conducting damage detection.

Table 6.7: Excitation condition 3: two damage cases.

Cases	*Damaged element*
Case 3-1	diagonal element 9
Case 3-2	longitudinal element 16

Case 3-1

Figure 6.15 shows the damage detection results when element 9 is damaged. In both cases, element 9 is consistently identified as the damage candidate and there is no other damage. Therefore, only communities 1 and 2 report the damage information and other communities only need to send a “ok” signal back to the central station.

Case 3-2

Detection results when element 16 is damaged is shown in Fig. 6.16, where element 16 is correctly identified as the damage candidate by communities 3 and 4 for both cases.

For the case of initialization based on forced vibration, communities 9, 10, and 11 report inconsistent information regarding the condition of element 43. These communities need to retake data and re-conduct damage detection regarding element 43. Fig. 6.17 illustrates the results after communities 9, 10, and 11 re-conduct damage detection. These results confirmed that element 43 is not damaged.

For the case of initialization based on ambient vibration, inconsistent information regarding elements 20 and 34 is obtained. Fig. 6.18 shows results when communities 4 and 5 retake data regarding element 20, and communities 7 and 8 retake data regarding element 34. Again, these elements are identified as having no damage as their normalized cumulative stresses are larger than the threshold.

These experimental results demonstrate that the proposed DCS approach not only works robustly when excitation remains the same before and after damage, it also performs well when excitation contents have been changed. Therefore, the proposed approach is a promising algorithm which has the potential application to practice with a dense array of smart sensors.

6.4 Discussions

In this experiment, inconsistent damage information is obtained in various damage cases. Questions arise how frequently this situation happens, as well as how reliably the proposed algorithms can detect structural damage. This section provides some insights on these questions.

To investigate the situation of inconsistent damage information, let’s consider Case 2-2 in which element 8 is damaged. As shown in Fig. 6.12, for the case of initialization from forced vibration, inconsistent information regarding element 24 is obtained by community 6. For this specific community, a total of ten sequential tests of retaking data and re-conducting damage detection for the damaged structure and have been conducted under various excitation conditions (see Table 6.8). The damage detection results for community 6 that includes elements [23, 24, 25, 26, 27, 28, 29, 30, 31] are shown in Fig. 6.19. As can be seen, among these ten tests, only tests 1 and 7 reports possible damage information for a different location. Although these results are problem dependent, they indicate that the

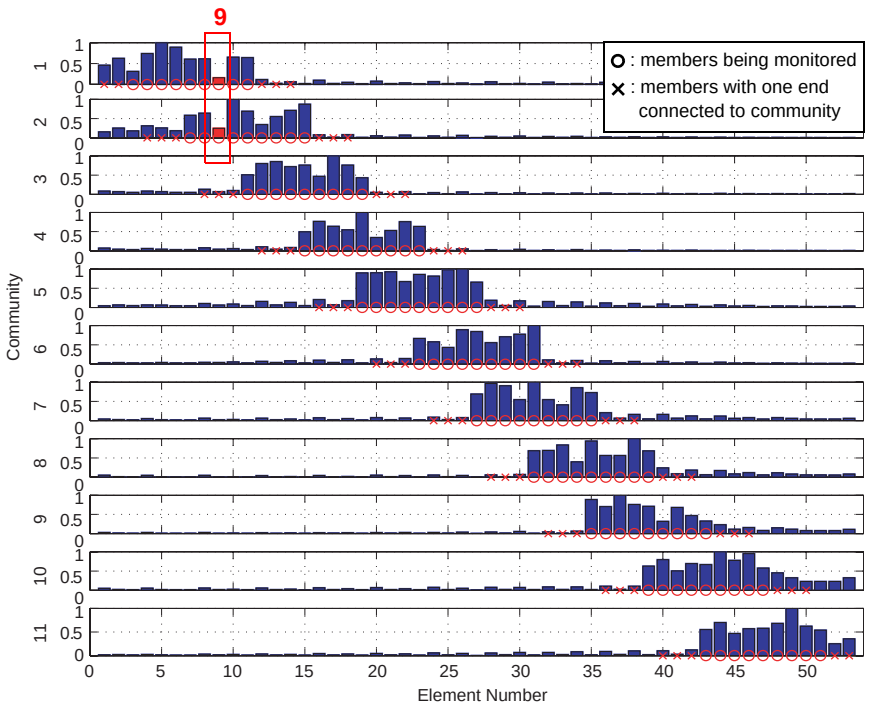

Initialization based on forced vibration

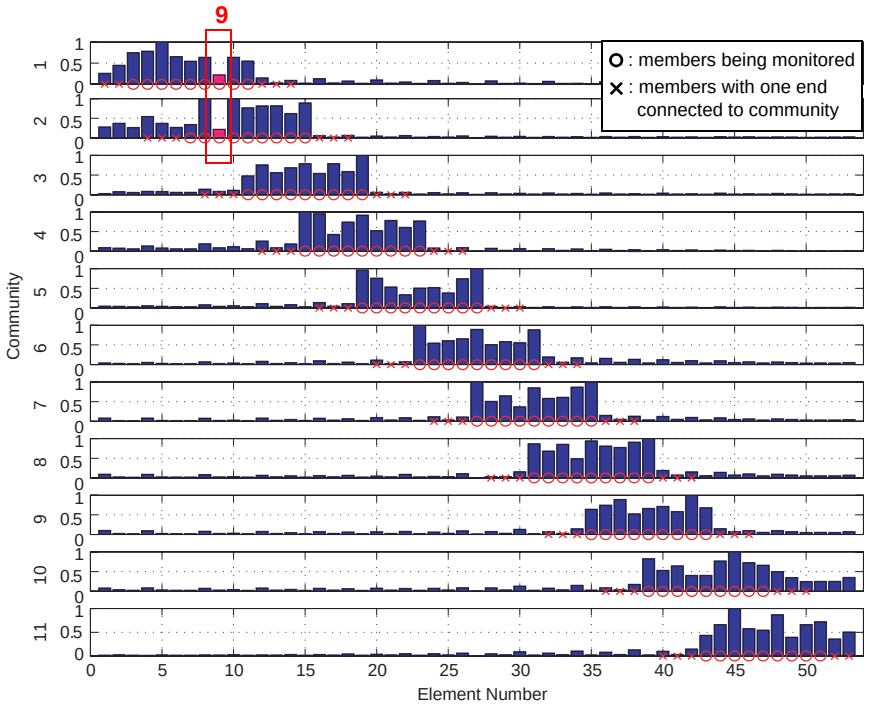

Initialization based on ambient vibration

Figure 6.15: Normalized cumulative stress when element 9 is damaged.

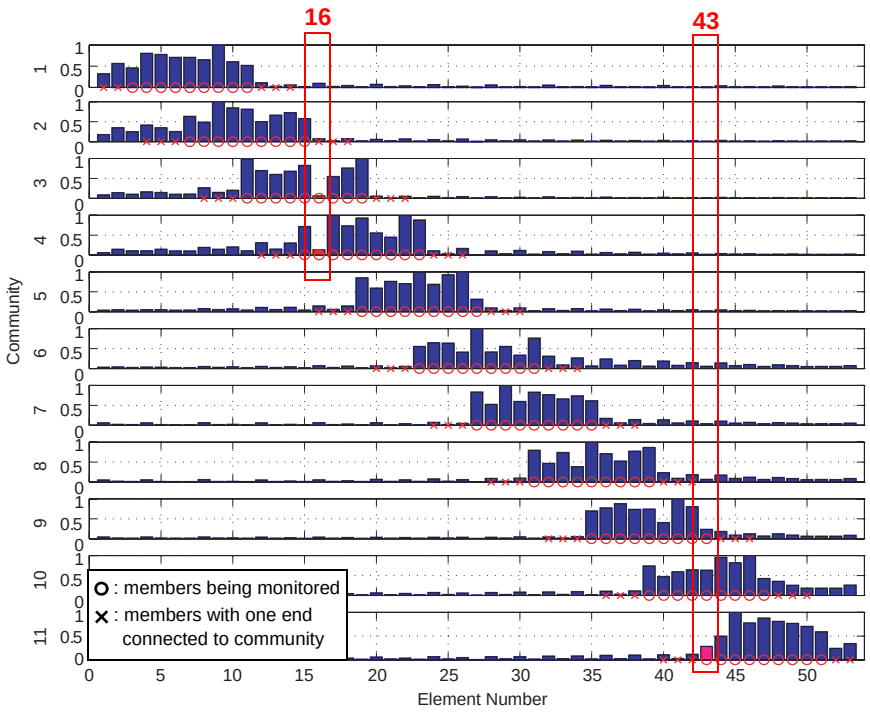

Initialization based on forced vibration

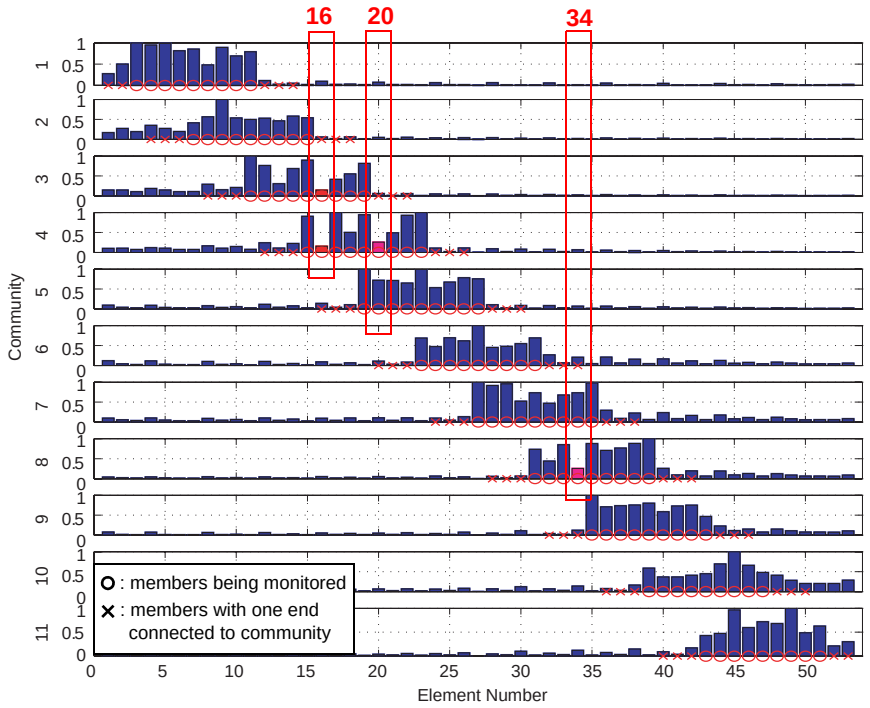

Initialization based on ambient vibration

Figure 6.16: Normalized cumulative stress when element 16 is damaged.

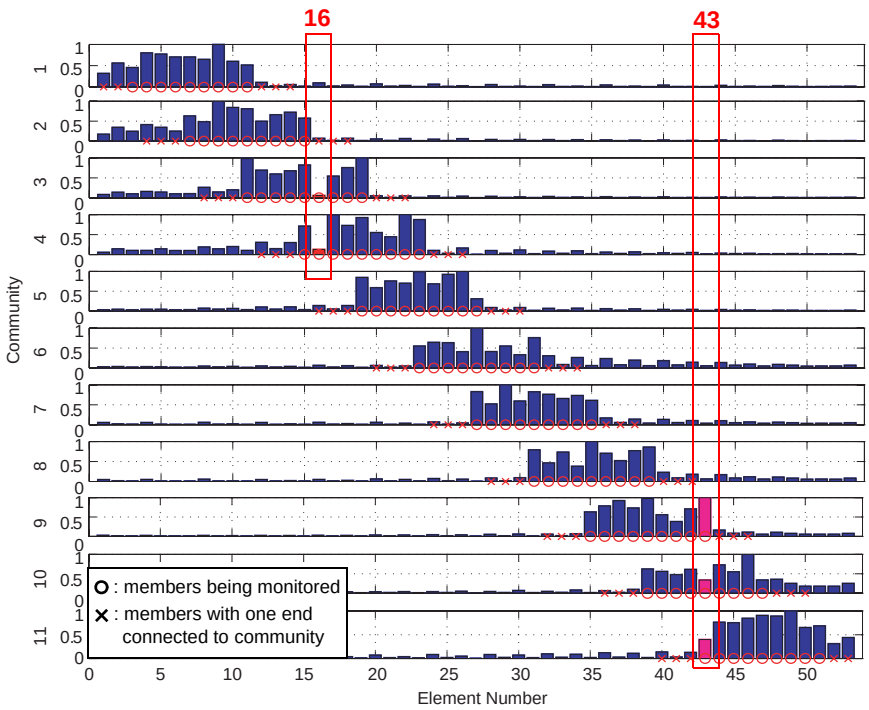

Figure 6.17: Normalized cumulative stress when element 16 is damaged (retaking data regarding element 43).

situation of inconsistent damage information is rather random and does not occur in the majority of the tests.

To provide some insights on how reliably the proposed DCS approach detects structural damage, Case 2-2 is considered again. Ten sequential tests are conducted for community 2 that includes elements [7, 8, 9, 10, 11, 12, 13, 14, 15]. The excitation conditions are the same as Table 6.8. The damage detection results are displayed in Fig. 6.20, which shows element 8 is identified as the damage candidate. These results indicate the proposed DCS approach can consistently identify the damage location, in this case, element 8.

6.5 Summary

In this chapter, the distributed computing strategy for SHM was experimentally verified using a three-dimensional 14-bay truss structure. Structural damage was simulated by replacing various truss elements with ones having a 52.7% cross section reduction. Both single and multiple damage scenarios were studied. Various excitation conditions, including changing excitation level, bandwidth and location before and after damage, were also investigated. Retaking data and re-conducting damage detection when there is inconsistent information were studied using experimental data.

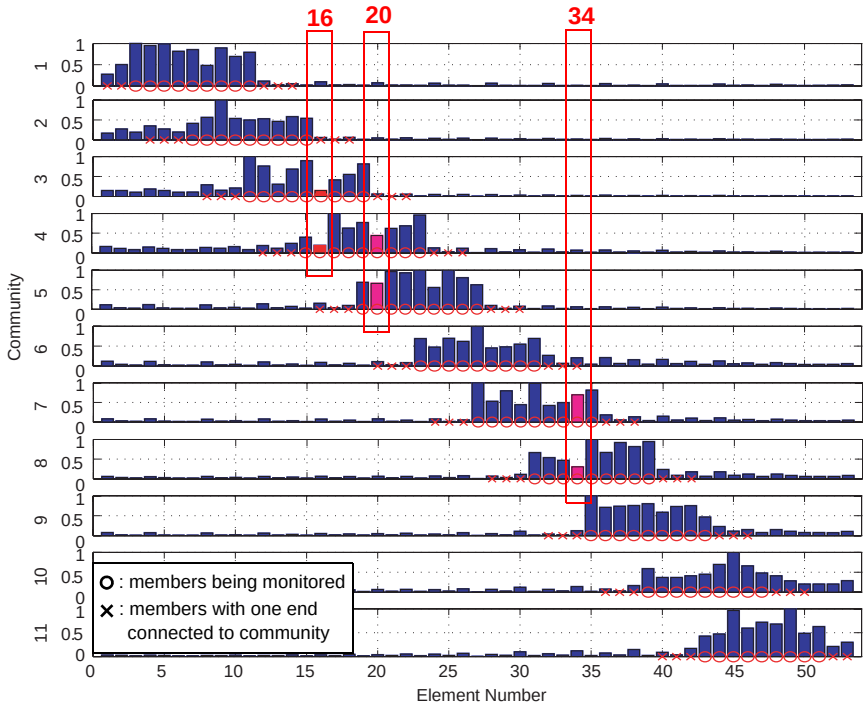

Initialization based on ambient vibration

Figure 6.18: Normalized cumulative stress when element 16 is damaged (retaking data regarding elements 20 and 34).

Table 6.8: Excitation conditions for ten sequential experiments: element 8 is damaged.

Tests		*Excitation bandwidth (Hz)*	*Excitation magnitude (RMS value)*
Undamaged		100	0.10
Damaged	Test 1	200	0.06
	Test 2	200	0.08
	Test 3	200	0.10
	Test 4	200	0.12
	Test 5	200	0.14
	Test 6	100	0.06
	Test 7	100	0.08
	Test 8	100	0.10
	Test 9	100	0.12
	Test 10	100	0.14

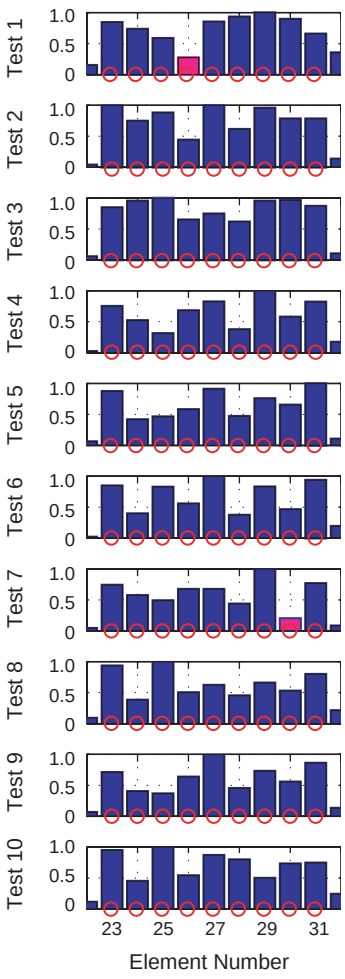

Figure 6.19: Normalized cumulative stress when element 8 is damaged (community 6)

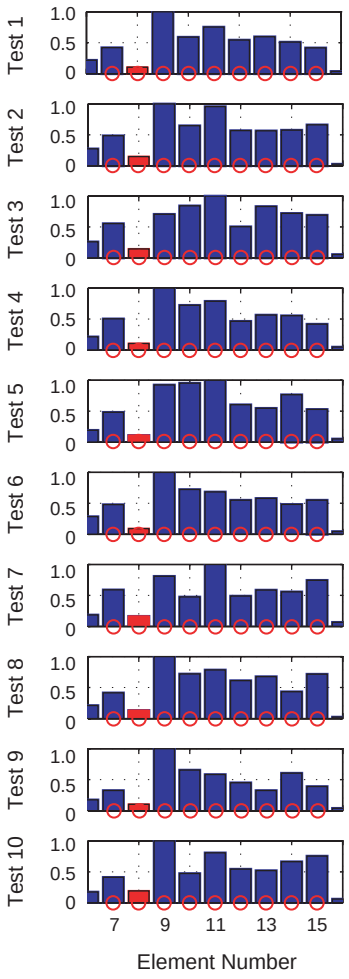

Figure 6.20: Normalized cumulative stress when element 8 is damaged (community 2)

The experimental results have shown that the proposed DCS approach can successfully monitor local community members only utilizing locally measured information for various damage scenarios under different excitation conditions. The proposed DCS approach was shown promising for application of SHM on a densely distributed sensor network.

IMPLEMENTATION OF THE DCS APPROACH ON A SIMULATED SMART SENSOR NETWORK

To better illustrate the implementation of the proposed DCS approach, a Simulink model with the support of Stateflow (MathWorks, Inc., 2004) has been developed that simulates a smart sensor network. In Chapters 5 and 6, the proposed DCS approach was shown to be promising through numerical and experimental examples. However, the flowchart shown in Fig. 5.7 needs to be implemented in an autonomous manner so that important implementation issues for the DCS approach can be studied. These issues include: how sensor communities communicate with each other to exchange damage information, and when and how they automatically initiate retaking data and re-conduct damage detection, etc. The Simulink and Stateflow model, which has been developed and will be presented in this chapter, is used to address these issues.

In this chapter, following brief introduction of Simulink and Stateflow, an overview of the proposed Simulink and Stateflow model is provided. Implementation of the proposed DCS approach in this Simulink model employing both numerical and experimental measurements is then presented.

7.1 Background

Simulink is an extension to Matlab which provides a graphical interface for the construction of a block diagram representation of dynamic systems. It can represent either linear or nonlinear systems whether they are in continuous or discrete time domain. It has a wide range of pre-programmed block libraries which allow users to accurately design, simulate, and analyze different dynamic systems.

Stateflow is a graphical design and development tool for control and supervisory logic used with Simulink (The MathWorks, Inc. 2004). Stateflow is a finite state machine, which means it is a representation of an event-driven system. This system reacts to events by making a transition from one state to another state if the condition of this transition is true (see Fig. 7.1). Programming for smart sensors is based on event-driven language, therefore Stateflow in conjunction with Simulink is a suitable tool to simulate a smart sensor network.

Some practical issues pertaining to the smart sensor technology will not be studied herein due to the technical limitation of Simulink and Stateflow. The wireless transmission between smart sensors is replaced by the direct link between Simulink or Stateflow blocks. Therefore, communication of sensor communities through radio frequency technology is not studied. Data loss or confliction which may happen in practice can not be modeled. In addition, synchronization of the measurements is not simulated because Simulink cannot run under different clocks.

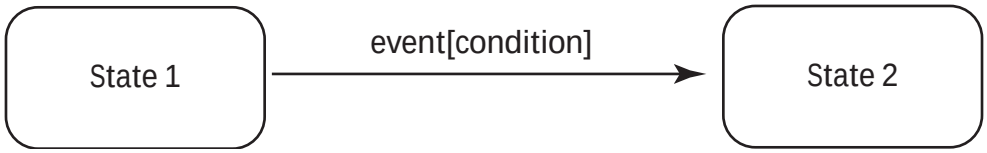

Figure 7.1: Stateflow example.

7.2 Overview of the Simulink and Stateflow Model

A Simulink and Stateflow model that simulates a smart sensor network consisting of eleven sensor communities has been developed (see Fig. 7.2). Sensor communities are formed in the manner same as Fig. 5.5. This sensor network can be initiated to detect damage upon the user's request, and provide damage information and the inconsistent information regarding condition of structural members. It has the capability to allow adjacent sensor communities to communicate with each other in order to share damage information, and automatically initiate those communities with inconsistent damage information to retake data and re-conduct damage detection. This sensor network is capable of detecting both single and multiple damage scenarios, but only a single damage is allowed in one community. Herein, each sensor community communicates with the communities immediately before and after it. Major components of this Simulink and Stateflow model will be introduced in the remainder of this section.

Figure 7.3 shows the user switch and output scopes of the Simulink and Stateflow model. The user switch, which is at the lower left corner of the graph, can simulate sending a request from a central station to the sensor network to initiate a process of damage detection. This is done by broadcasting an event throughout the sensor network whenever the user switch changes its output value. There are a total of 11 columns LEDs/ scopes. Each column represents outputs from one sensor community, e.g., LED1 is associated with community 1, and LED2 is associated with community 2, and so on.

The green LED at the first row turns to red if there is damage confirmed in the associated sensor community, and turns to half green and half red if there is inconsistent information. For example, LED7 changes to half green and half red because inconsistent damage information is obtained in community 7.

The second row from the top in Fig. 7.3 shows the final damage detection results by displaying a number bearing a specific meaning (see Table 7.1). For example, scope F_dele3 displays a value of 17, which means element 17 has been determined as a damage candidate in community 3.

The third row from the top shows the same value as the one in the second row if there is no inconsistent information. Otherwise, it displays the number of the element which has inconsistent damage information. For example, scope dele10 displays a number of 41. This result means inconsistent information has been obtained in community 10 regarding

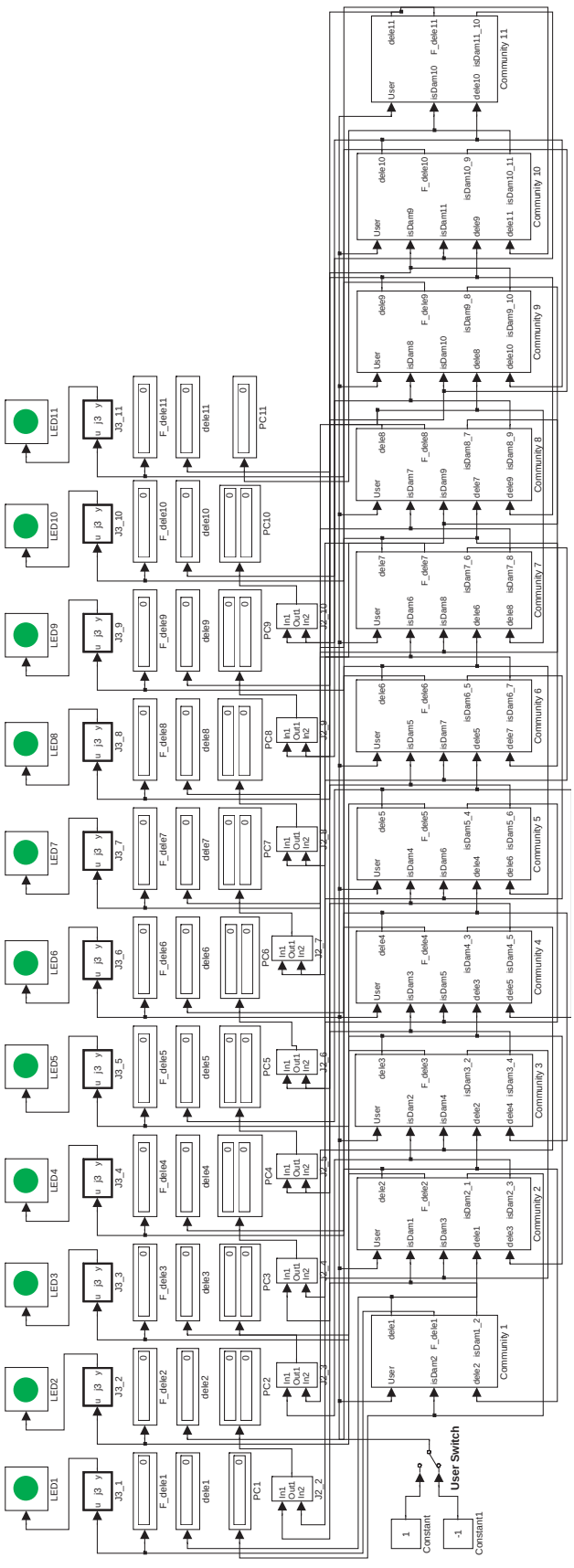

Figure 7.2: Simulink and Stateflow model.

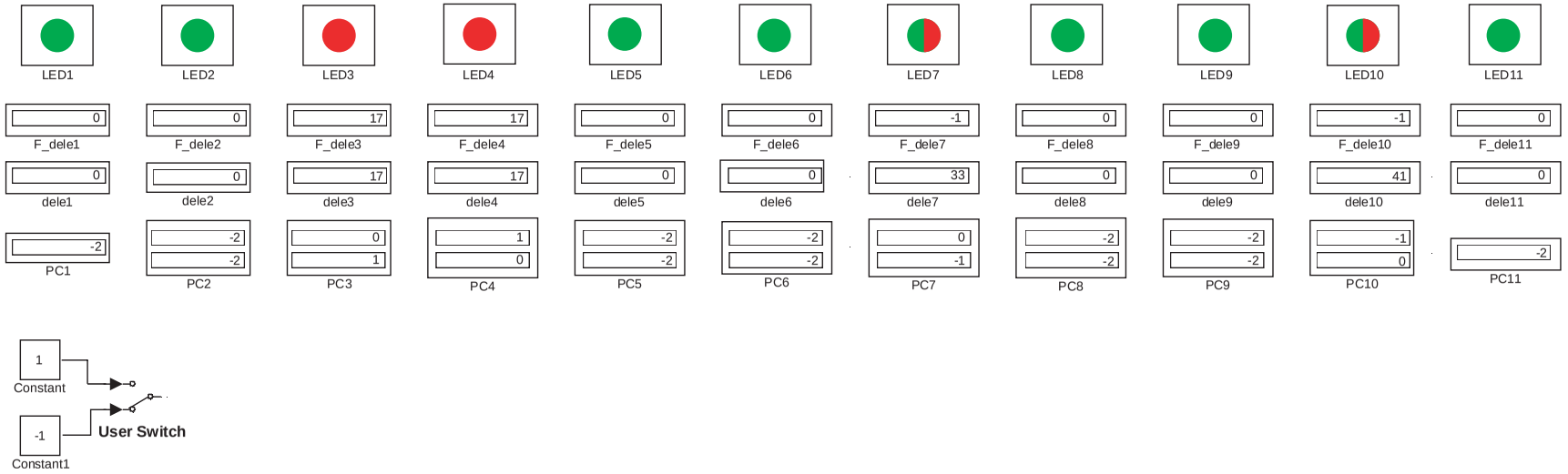

Figure 7.3: User switch and output scopes.

element 41, because LED10 turns to half green and half red and F_dele10 displays a value of -1.

Table 7.1: Final damage detection result in a community.

Number	*Meaning*
0	no damage in this community
-1	inconsistent information obtained in this community
other	damaged element number

The last row in Fig. 7.3 shows the query results from adjacent communities. The top scope shows the query result from the left community and the bottom one displays the result from the right community with a different number bearing a different meaning (see Table 7.2). For example, the top scope in PC7 shows a value of 0 representing that the damage candidate 33 is not a member of community 6. The bottom scope displays a value of -1, which means element is a member of community 7 but it is not identified as a damage location.

Table 7.2: Query result from an adjacent community.

Number	*Meaning*
0	damage candidate is not a member of the adjacent community
1	damage candidate is a member of the adjacent community and is confirmed as having damage
-1	damage candidate is a member of the adjacent community but is not identified as having damage
-2	no query sent to this adjacent community

A total of 11 sensor communities have been formed (see Fig. 7.4) and the content of a typical sensor community, e.g. community 4, is shown in Fig. 7.5. There are four different Stateflow blocks to simulate different functions of the manager sensor, including detecting damage, determining the condition of local elements based on detection results in this community and query results from adjacent communities, and processing queries from adjacent communities. There is an embedded Matlab function that advises community 4 to retake data and re-conduct damage detection when inconsistent damage information is obtained.

The Stateflow block “Detect 4” (see Fig. 7.6) simulates damage detection in the sensor community. There are two states in this block: Off and Detect4 (see Table 7.3). State Off is the default state for a manger sensor. There are two possibilities when the manager sensor transits from state Off to Detect4 (see Table 7.4). In this table, y = -1 means there is inconsistent information; and $n <= 2$ means that the manager sensor will at most re-conduct damage detection for two times. In state Detect4, a Matlab program is

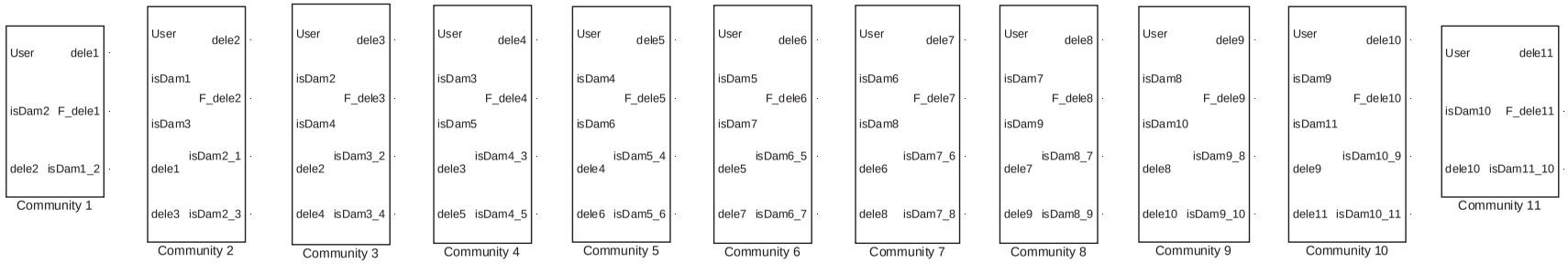

Figure 7.4: Sensor communities.

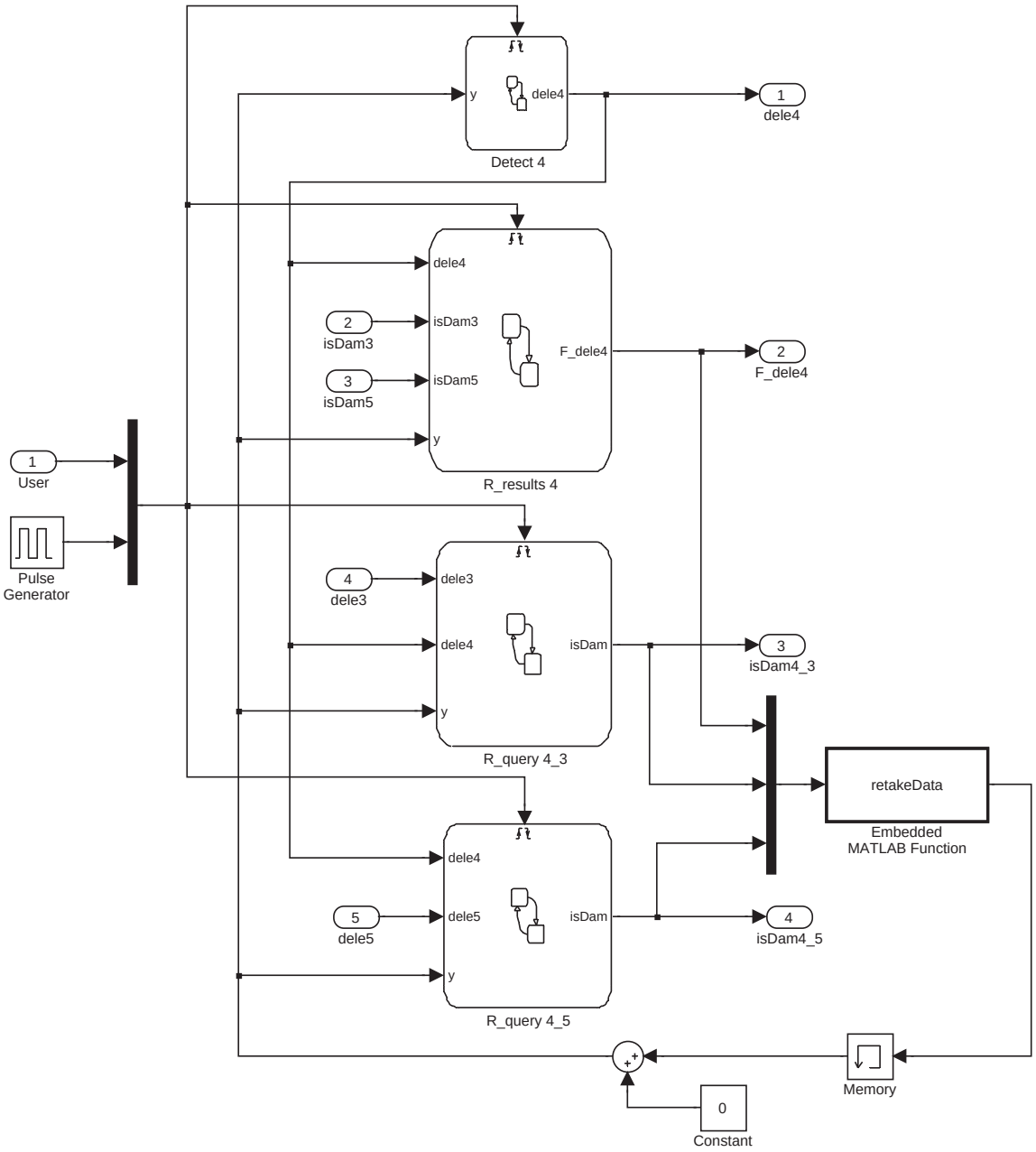

Figure 7.5: A typical sensor community:
community 4.

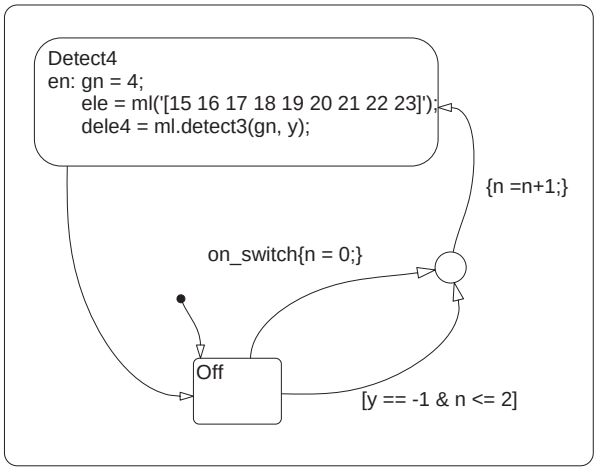

Figure 7.6: Typical Stateflow block in Simulink model: Detect 4.

invoked to load the measured data and implement the damage detection algorithm for the community. The manager sensor automatically returns from state Detect4 to Off after a damage detection process is finished.

Table 7.3: Two states in Stateflow block “Detect 4”.

States	*Meaning*
Off	manager sensor is not detecting damage
Detect4	manager sensor is detecting damage

Table 7.4: Two possibilities of transition from state Off to Detect4.

Possibility	*Condition*	*Meaning*
First	on_switch{n = 0}	an on_switch event is generated from the central station to advise the manager sensor to conduct damage detection
Second	[y = -1 & n <= 2]	inconsistent damage information has been obtained, therefore this community is required to re-conduct damage detection

The Stateflow block “R_results 4” (see Fig. 7.7) receives the query results from adjacent communities and processes these results to provide condition of local elements in community 4. There are three states in this Stateflow block: Off, R_results4, and No_results (see Table 7.5); and there are three possibilities that the manager sensor needs

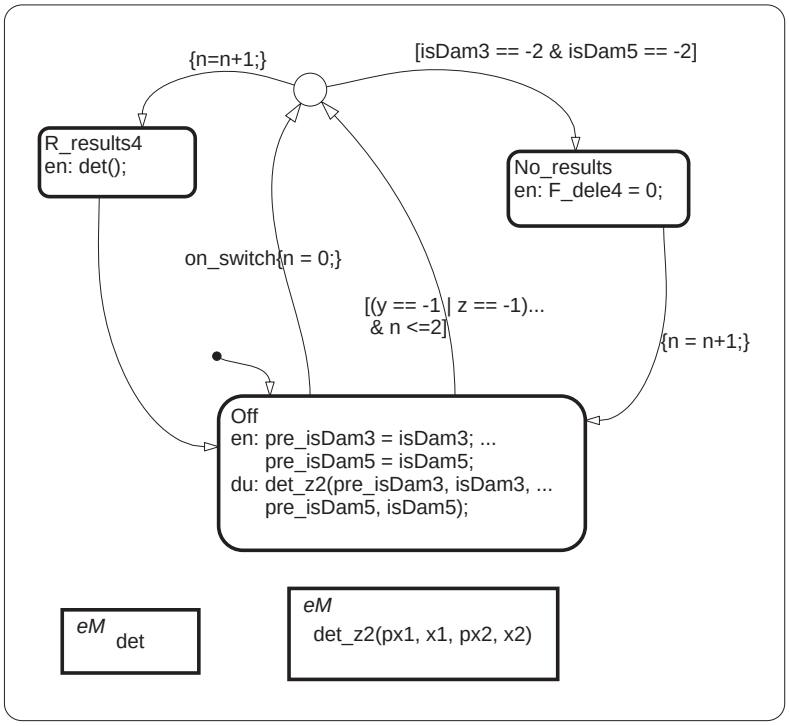

Figure 7.7: Typical Stateflow block in
Simulink model: R_results 4

to re-evaluate the condition of local elements, *i.e.*, transit from state Off to either state R_results4 or No_results (see Table 7.6). Under all these three conditions, the manager sensor exits the Off state. If there is damage in community 4, it transits to state R_results4 which makes final judgements on which element is damaged. Otherwise, it moves to state No_results which assigns a value of 0 to variable F_dele4.

Table 7.5: Three states in Stateflow block “R_results 4”.

State	*Meaning*
Off	manager sensor is not processing damage detection and query results
R_results4	manager sensor is processing the damage detection and query results, and damage is found in this community
No_results	manager sensor is processing the damage detection and query results and no damage is found in this community

Table 7.6: Three possibilities to exit state Off.

Possibility	*Condition*	*Meaning*
First	on_switch{$n = 0$}	new damage detection has been conducted in this community reacting to event on_switch
Second	[$y = -1$ & $n <= 2$]	new damage detection has been conducted in this community because inconsistent information is obtained
Third	[$z = -1$ & $n <= 2$]	new damage detection has been conducted in adjacent communities therefore query results from adjacent communities may be changed

The Stateflow block "R_query 4_3" (see Fig. 7.8) receives query from adjacent community 3, processes the query, and sends the results back to community 3. Similarly, there are three states in this block: Off, R_query4_3, and No_query (see Table 7.7); and there are three possibilities when the manager sensor exits state Off (see Table 7.8). After the manager sensor exits the Off state, it enters state R_query4_3 if a query is detected, otherwise it enters state No_query. The query results from this Stateflow block are then sent back to community 3.

Table 7.7: Three states in Stateflow block "R_query 4_3".

State	*Meaning*
Off	manager sensor is not detecting and processing query
R_query4_3	manage sensor detects there is query and is processing it
No_query	manager sensor detects no query and is assigning a value -2 to variable isDam which means no query is received from community 3

Table 7.8: Three possibilities to exit state Off.

Possibility	*Condition*	*Meaning*
First	on_switch{$n = 0$}	new damage detection has been conducted in this community due to event on_switch, so the damage information in community 4 may be changed and the query from community 3 needs to be re-valuated
Second	[$y = -1$ & $n <= 2$]	new damage detection has been conducted in this community due to inconsistent damage information
Third	[$z = -1$ & $n <= 2$]	new damage detection has been conducted in the adjacent communities whose damage information may have been changed

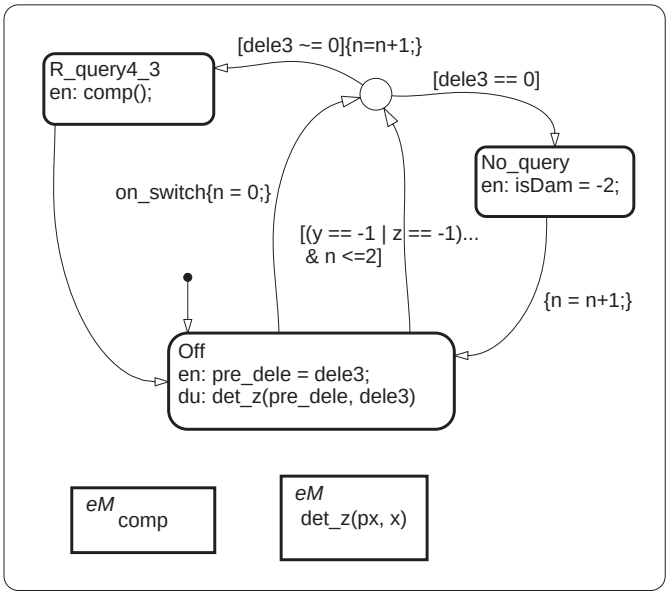

Figure 7.8: Typical Stateflow block in Simulink model: R_query 4_3.

Similarly, the Stateflow block “R_query 4_5” receives query from adjacent community 5, processes it, and sends the results back to community 5.

The embedded Matlab function “retakeData” collects outputs from Stateflow blocks “R_results 4”, and “R_query 4_3”, and “R_query 4_5” to determine whether re-conducting damage is needed. If any of the results from these three Stateflow blocks is -1, then “retakeData” generates a value of -1 to advise the community to re-conduct damage detection. A number of -1 from these three Stateflow blocks means that inconsistent information has been obtained either in community 4 or the adjacent community (see Table 7.9), therefore re-conducting damage detection is needed in community 4.

Table 7.9: Meaning of a number of -1 from different Stateflow blocks.

-1	*Meaning*
From “R_results 4”	inconsistent information has been obtained in community 4
From “R_query 4_3”	inconsistent information is obtained in community 3 whose damage candidate is a member of community 4.
From “R_query 4_5”	inconsistent information is obtained in community 5 whose damage candidate is a member of community 4

This section illustrated major components of the proposed Simulink and Stateflow model. Implementation of the DCS approach employing both simulation data and experimental measurements utilizing the proposed Simulink and Stateflow model will be presented in the next section.

7.3 Numerical and Experimental Validation

Damage detection results of two damage cases (see Table 7.10) employing the proposed Simulink and Stateflow model are illustrated herein. In both cases, algorithm initialization in the proposed DCS approach is based on forced vibration.

Table 7.10: Numerical and experimental validation.

Cases	*Case type*	*Structure*	*Damaged elements*
Case 1	Simulation	14-bay planar truss (see Fig. 5.1)	longitudinal element 20 has a 40% stiffness reduction, and diagonal element 45 has a 30% stiffness reduction
Case 2	Experiment	outer vertical panel of a three-dimensional 14-bay truss structure (see Figs. 3.10 and 6.3)	longitudinal element 8 has a 52.7% cross section reduction

Case 1

In this case, structural damage in elements 20 and 45 is investigated using simulation data from a 14-bay planar truss (see Fig. 5.1). Details regarding this structural and the computer simulation have been presented in Chapter 5.

The damage detection results without employing the Simulink and Stateflow model are shown in Fig. 5.17, where communities 4 and 5 identify element 20 as a potentially damaged element and communities 10 and 11 determine element 45 as a damage candidate.

The damage detection results employing the Simulink and Stateflow model are shown in Fig. 7.9. As can be seen, the LEDs for community 4, 5, 10, and 11 turn to red which means damage has been detected in these sensor communities. The second row from the top shows the final damage detection results, where communities 4 and 5 show that element 22 is the damaged element and communities 10 and 11 show that element 45 is the damaged element. The third row from the top displays the same element numbers as the second row as there is no inconsistent damage information. In the fourth row, the top scope of PC4 shows a number of 0, which means damaged element 20 is not a member of community 3. The bottom scope of PC4 displays a number 1 indicating element 20 is a member of community 5 and is confirmed as a damage candidate. Scopes in PC5, PC10 and PC11 display the similar information. Therefore, the damaged elements have been consistently identified using the proposed Simulink and Stateflow model.

Case 2

In this case, structural damage in element 8 is studied using experimentally measured data from the outer vertical panel of a three-dimensional 14-bay truss structure (see Figs.

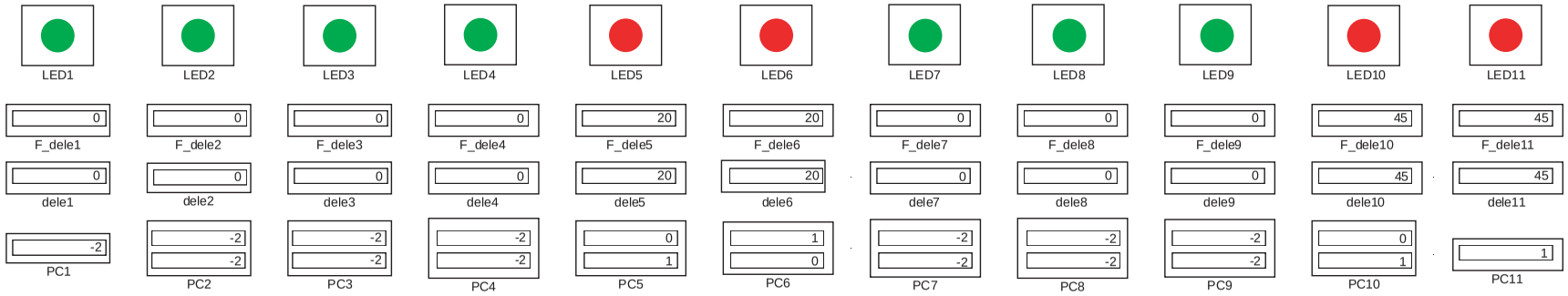

Figure 7.9: Outputs from Simulink and Stateflow model
when elements 20 and 45 are damaged.

3.10 and 6.3). Details regarding the experimental set up have been presented in Chapters 3 and 6.

The damage detection results without employing the Simulink and Stateflow model are shown in Figs. 6.13 and 6.14. Damage detection results in Fig. 6.13 show that communities 1 and 2 identify element 8 as a potentially damaged element and communities 5 and 6 obtain inconsistent damage information regarding element 24. The results after retaking data in these two communities are displayed in Fig. 6.14 which identifies element 24 as undamaged.

The damage detection results employing the proposed Simulink and Stateflow model are illustrated in Figs. 7.10 and 7.11. The LEDs in communities 1 and 2 turn to red in Fig. 7.10 and the associated scopes in the second and third rows display element 8 is identified as a damage candidate. PC1 and PC2 in the fourth row indicate element 8 is only a member of communities 1 and 2. As can be seen from Fig. 7.10, the LED in community 6 turns to half red and half green and the associated scope in the second row shows a value of -1, which indicate inconsistent damage information has been obtained in this community. Output scope in the third row shows that element 24 is identified as damaged in community 6. Top scope of PC6 shows a value of -1 indicating element 24 is a member of community 5 but is not identified as damaged; and bottom scope of PC6 displays value of 0 which means element 24 is not a member of community 7. Therefore, communities 5 and 6 are required to re-conduct damage detection.

Figure 7.11 shows the results after retaking data and re-conducting damage in communities 5 and 6. Both LEDs in communities 5 and 6 turn to green which means element 24 is determined by these communities as undamaged after re-conducting damage detection.

7.4 Summary

A Simulink and Stateflow model, which simulates a smart sensor network consisting of eleven sensor communities, has been developed. The proposed DCS approach was successfully implemented on this sensor network employing both numerical and experimental data. An detailed overview of major components of the proposed model was provided. This Simulink and Stateflow model has been shown capable of demonstrating important features, such as damage information exchange between sensor communities, providing inconsistent damage information, automatically initiating the process of retaking data, etc. Numerical and experimental results indicate that the proposed DCS approach is promising for SHM application on densely distributed sensor networks.

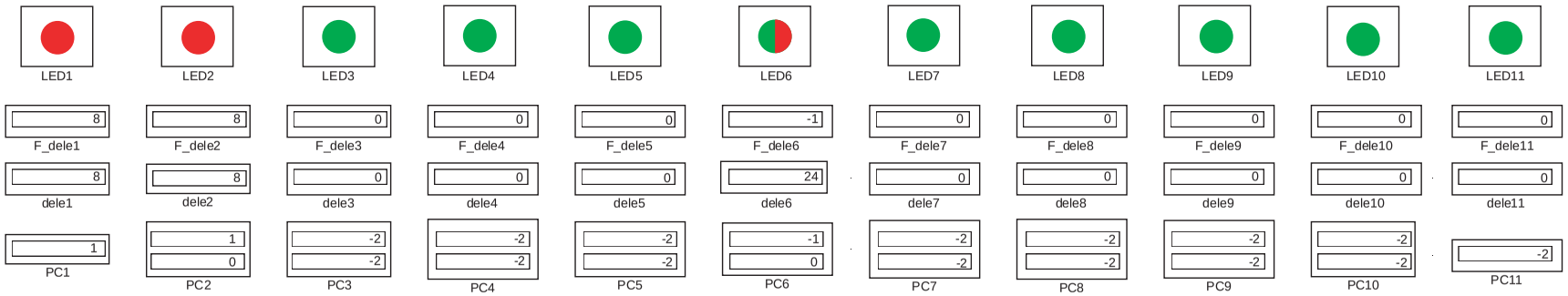

Figure 7.10: Outputs from Simulink and Stateflow model when 8 is damaged.

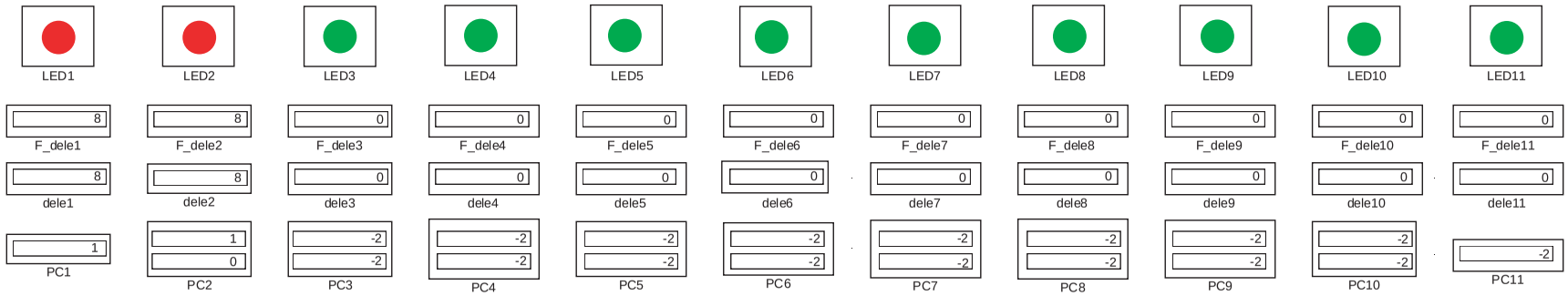

Figure 7.11: Outputs from Simulink and Stateflow model when 8 is damaged (retaking data in communities 5 and 6 regarding element 24).

CONCLUSIONS AND FUTURE STUDIES

8.1 Conclusions

The research detailed in this report has addressed some of the challenges of applying SHM to civil infrastructure. Focus has been placed on development of SHM algorithms suitable for application on densely distributed sensor networks.

An extensive literature review of vibration-based damage detection methods, as well as recent developments in smart sensor technology, have been provided. To effectively detect damage at an arbitrary location in a structure, sensors must be densely distributed throughout the structure. However, most of existing SHM methodologies assume the measured data to be centrally acquired and processed. Implementation of SHM systems with central data processing on densely distributed sensor networks is challenging either using traditionally wired or wireless sensors. By offering distributed computing capacities and environment, recent fast-growing smart sensor technology has made structural health monitoring using a dense array of sensors feasible, and therefore has the potential to change fundamentally the way how civil infrastructure is monitored. SHM algorithms which can take advantage of the smart sensor technology are desired but currently very limited. Therefore, development of new SHM algorithms that mesh well with the smart sensor technology is very important.

A flexibility-based damage localization method, the DLV method that has been shown to be quite promising, was investigated. Motivation of flexibility-matrix-based methods was first presented. Because an inverse relationship exists between the flexibility matrix and the square of the modal frequencies, the flexibility matrix is frequently insensitive to high frequency modes, which are typically quite difficult to determine experimentally. Numerical examples were employed to demonstrate this unique characteristic with results indicating significant potential for practical application of flexibility-based damage detection approaches. Concepts of the DLV method were then introduced. The essence of the DLV method is to compute a set of load vectors which produce zero stress at the damaged region. Numerical examples have been provided to better understand this method. As the flexibility matrix needs to be constructed for implementation of the DLV method, formulation of the flexibility matrix for proportionally damped structures was reviewed. This formulation is based on the assumption that input excitations are measured and there is at least one co-located sensor and actuator pair. To assess the efficacy of the DLV method in practice, this method was experimentally verified using a three-dimensional 14-bay truss structure. Damage was simulated by replacing the original element with one having a 52.7% cross section reduction, which results in around a 45% axial stiffness reduction. Structural damage was successfully identified using only a limited number of frequency modes.

The DLV method was then extended for continuous online damage diagnosis employing ambient vibration. The essence of the extended DLV method is to construct an

approximate flexibility matrix for the potentially damaged structure utilizing the modal normalization constants from the undamaged structure. The DLV method can be then applied for continuos online damage diagnosis employing ambient vibration. Different formulations of the flexibility matrix were reviewed. For the case when input excitations are measured, the flexibility matrix can be constructed for structures with general viscous damping; while a mass perturbation method was introduced to compute the flexibility matrix for proportionally damped structures when input excitations are not available. Changes of the modal normalization constants due to structural damage were then studied with results implying that the undamaged normalization constants may provide a reasonable approximation to the damaged ones when damage is small. Based on these results, the extension of the DLV method was proposed and illustrated with flow charts. Finally, the proposed approach was numerically validated using a 14-bay planar truss structure.

A new distributed computing strategy for SHM based on the extended DLV methods was then proposed which is suitable for implementation on a network of densely distributed smart sensors. In this approach, a hierarchical strategy is proposed in which adjacent smart sensors are grouped together to form sensor communities. The extended DLV method is employed to evaluate the condition of local elements within these communities by utilizing only locally measured information. Therefore, only limited information needs to be transferred to a central station. The concept of locating damage using local information was first presented, followed by the development of the DCS approach. Numerical simulations with noise included in measurements were then presented. Both the excitation magnitude and location were changed before and after damage to better simulate ambient vibration. Different damage extents were investigated. Both single and multiple damage scenarios have been studied with results showing the proposed DCS approach promising for online SHM with a densely distributed sensor network.

Experimental verification of the proposed DCS approach for SHM was carried out using a three-dimensional 14-bay truss structure. Damage was simulated by replacing structure members with the ones having a 52.7% cross section reduction that results in around a 45% axial stiffness reduction. Both single and multiple damage scenarios were studied in this experiment. Various excitation conditions, including changing excitation level, bandwidth and location before and after damage, were also investigated. The process of retaking data and re-conducting damage detection when there is inconsistent damage information was studied using experimental data. The experimental results show that the proposed DCS approach can successfully monitor local community members only utilizing locally measured information for various damage scenarios under different excitation conditions.

A Simulink and Stateflow model which simulates a smart sensor network consisting of eleven sensor communities was then developed to better understand application of the proposed DCS approach in practice. Numerical and experimental verification of the proposed DCS approach were successfully conducted in Chapter 5 and 6. However, some important issues of implementation of the proposed approach in smart sensor networks were not studied in those two chapters. The proposed Simulink and Stateflow model

simulated a smart sensor network, which can be initiated to detect damage upon the user's request, and provide damage information and the inconsistent damage information. It has the capability to allow adjacent sensor communities to communicate with each other, and automatically initiate those communities with inconsistent damage information to re-conduct damage detection. This Simulink and Stateflow model is also capable of illustrating damage detection of both single and multiple damage scenarios. Both simulation data from a 14-bay planar truss and experimental measurements from a three-dimensional 14-bay truss structure have been utilized to successfully demonstrate important features for implementation of the DCS approach on densely distributed sensor networks.

8.2 Future Studies

Although this research has successfully addressed some of the challenges for application of SHM algorithms to civil infrastructure, several questions remain. This section presents a few directions for further research in the future.

8.2.1 Effect of excitation conditions and damage scenarios

The effect of various excitation conditions on the proposed DCS approach should be further studied. In this research, numerous simulations and experiments have been successfully carried out to evaluate the performance of the DCS approach. Band-limited white noise was utilized as excitations for these simulations and experiments. The proposed DCS approach performed well under these excitations. Questions arise about how well this method works under different excitations from band-limited white noise, e.g. non-stationary excitations. More efforts should be directed to the study using various excitation conditions.

In addition, different damage scenarios should be studied to gain more insight on the performance of the proposed approach. In both the simulations and experiments which were conducted in this research, structural damage was simulated by uniformly reducing the member stiffness along its length. Elastic modulus of structural members was changed to simulate the damage during simulations; while this goal was achieved in experiments by replacing original elements with ones having a uniformly smaller cross section. Other types of damage scenarios, e.g. cracks on structural members, loose-joint at the structural node, etc. were not studied. Performance of the proposed approach should be studied for these type of damage scenarios to obtain a better understanding.

8.2.2 Probability analysis

Probability analysis should also be performed to better assess the efficacy of the proposed DCS approach in practice. Many uncertainties exist when detecting damage under real conditions. Excitations of real structures can be quite different from the simulated ones in numerical examples and experiments. Environmental conditions (e.g. temperature, humidity contents, etc.) can change from time to time. Development of analytical model for real structures is certainly more difficult than modelling relatively

simpler structures in laboratory. Therefore, modelling errors are inevitable. All these factors create uncertainties which affect the performance the proposed approach. Modeling these uncertainties and evaluating their effects on the performance of the proposed DCS approach using numerical methods, e.g. Monte Carlo simulation, is certainly desired and very useful for better understanding this approach.

8.2.3 Implementation of the DCS approach on smart sensor networks

Implementation of the DCS approach on real smart sensor networks is important to gain insight on application of the proposed approach in practice. The research detailed in this report has established the feasibility of the proposed DCS approach through simulations and experiments. A Simulink model with the support of the Stateflow was also developed to demonstrate important features of implementing this approach with a dense array of smart sensors. However, due to the technical limitations of Simulink and Stateflow, practical issues, such as sensor communications through radio frequency technology, data synchronization among community sensors, data loss during communication and so on, could not have been studied. Effects of these practical issues need to be investigated by implementing the proposed DCS approach on real smart sensor networks.

8.2.4 Extension of the DCS approach to more complicated structures

Extending the proposed DCS approach to more complicated structures is important. The proposed DCS approach has been shown to work well for truss structures. However, real structures consist of different types of members, such as truss members, frame members, plate members, and so on. It is desirable to extend the proposed approach to handle more complicated structures.

The essence of the extension is to define appropriate member stresses which are produced by the DLVs for different type of elements. For truss members, the axial force can be defined as the generalized member stress when applying the DLV method. For other type members, different generalized member stress is needed. For example, Bernal (2002) suggested to define the member stress for a planar beam element as $(M_i^2 + M_j^2 + 2M_iM_j)^{1/2}$ where M_i and M_j are the two end moments. After appropriate generalized stresses are defined, the proposed DCS approach can still be applied to detect damage for different types of structures.

8.2.5 Optimal sensor topology

Optimizing sensor topology in a single community is also desired. For the relatively simple truss structures studied herein, each community was developed employing a total of 12 sensors on six structural nodes to monitor nine local structural members, and good results have been reported. For more complicated structures, each community may need to cover a larger portion of the structure, and therefore includes more localized sensors. It is important to study the effect of different sensor topology on the proposed DCS approach. With an optimal sensor topology, good results can potentially be achieved with less smart

sensors. Therefore, communication and computation in a single community can be reduced, and the efficiency of the sensor network can be improved.

8.2.6 SHM strategies employing multi-scale information

Detecting damage in some structural members is more difficult than others due to their different contributions to the dynamic behavior of the structure. During the experimental verification using the DCS approach, detecting damage in the vertical and diagonal elements located close to the mid-span of the truss structure was found to be more difficult than other elements. A rational explanation of this phenomenon can be sought by analyzing the structure under its self-weight. For those elements that carry more forces under self-weight, their damage is expected to have larger impact on structural dynamic behavior, and therefore is easier to be detected. Fig. 8.1 shows actual axial forces in vertical panel of the truss structure (see Fig. 3.10). In this figure, for illustration purpose, the member width represents magnitude of the axial force. As can be seen, the vertical and diagonal elements close to the mid-span of the truss carry much smaller forces compared with others. Therefore, detecting damage in these elements is more challenging. A detailed sensitivity analysis should be conducted to identify those elements in which damage is more difficult to detect, so that different SHM strategies could be possibly developed to monitor these type of structural members.

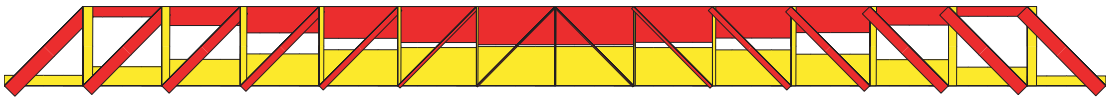

Figure 8.1: Axial forces under self-weight.

Development of new SHM strategies which do not rely only on dynamic property changes is therefore desired. As discussed above, damage in some structural elements can be difficult to detect by vibration-based damage detection methods. These structural members do not contribute significantly to structural stiffness, but they may still be critical to the structure (e.g. to maintain the structural stability). Monitoring the condition of these structural members is also an important issue. Using different types of measurements other than accelerations (e.g. strain gage measurement) might be more effective in monitoring these elements. To optimize performance of a SHM system, more effort should be directed to the development of new SHM strategies which take advantage of multi-scale information from different types of measurements.

REFERENCES

Adams, R.D., Cawley, P., Pye, C.J., and Stone, B.J. (1978). “A vibration technique for nondestructive assessing the integrity of structures.” *J. of Mech. Engrg. Science*, 20:93–100.

Agre, J.R., Clare, L.P., Pottie, G.J., and Romanov, N.P. (1999). “Development platform for self-organizing wireless sensor networks.” *Proc. of SPIE - The International Society for Optical Engineering*, Orlando, Florida, 3713:257–267.

Aktan, A.E., Lee, K.L., Chuntavan, C., and Aksel, T. (1994). “Modal testing for structural identification and condition assessment of constructed facilities.” *Proc. of the 12th International Modal Analysis Conf.*, Honolulu, Hawaii, Vol.I, 462–468.

Aktan, A.E., Chase, S., Inman D.J., and Pines, D.J. (2001). “The paradigm of monitoring and managing the health of infrastructure systems.” *A Workshop on Health Monitoring of Long Span Bridges*, Irvine, CA, 1–14.

Akyildiz, I.F., Su, W., Sankarasubramaniam, Y., and Cayirci, E. (2002). “Wireless sensor networks: a survey.” *Computer Networks*, 38:393–422.

Alvin, K.F., and Park, K.C. (1994). “Second-order structural identification procedure via state-space-based system identification.” *AIAA J.*, 32(2):397–406.

Baruh, H., and Ratan, S. (1993). “Damage detection in flexible structures.” *J. of Sound and Vibration*, 166:21–30.

Bernal, D. (2000). “Extracting flexibility matrices from state-space realizations.” *COST F3 Conf.*, Madrid, Spain, 127–135.

Bernal, D. (2002). “Load vectors for damage localization.” *J. of Engrg. Mech.*, 128(1):7–14.

Bernal, D., and Gunes, B. (2004). “Flexibility based approach for damage characterization: benchmark application”, *J. of Engrg. Mech.*, 130(1), 61–70.

Bernal, D. (2004). “Modal Scaling from Known Added Masses,” *J. of Engrg. Mech.*, 130(9), 1083–1088.

Brincker, R., Andersen, P., Kirkegaard, P.H., and Ulfkjær, J.P. (1995). “Damage detection in laboratory concrete beams.” *Proc. of the 13th International Modal Analysis Conf.*, Nashville, Tennessee, Vol.I, 668–674.

Brinker, R., and Andersen, P. (2002). “A way of getting scaled mode shapes in output-only modal testing”, *IMAC-XXI*, Orlando, Florida, paper #141.

Brooks, T. (1999). “Using smart accelerometers and wireless interfaces for condition monitoring.” *Machine Plant and System Monitoring*, May/June issue.

Carlin, R.A., and Garcia, E. (1996). “Parameter optimization of a genetic algorithm for structural damage detection.” *Proc. of the 14th International Modal Analysis Conf.*, Dearborn, Michigan, Vol.2, 1292–1298.

Carrasco, C.J., Osegueda, R.A., Ferregut, C.M., and Grygier, M. (1997a). “Damage localization in a space truss model using modal strain energy.” *Proc. of the 15th International Modal Analysis Conf.*, Orlando, Florida, Vol.II, 1786–1792.

Carrasco, C.J., Osegueda, R.A., Ferregut, C.M., and Grygier, M. (1997b). “Localization and quantification of damage in a space truss model using modal strain energy.” *Smart Structures and Materials 1997: Smart Systems for Bridges, Structures, and Highways*, SPIE, Vol.3043, 181–192.

Cawley, P., and Adams, R.D. (1979). “The location of defects in structures from measurements of natural frequencies.” *J. of Strain Analysis*, 14:49-57.

Chen, H.L., Spyrakos, C.C., and Venkatesh, G. (1995). “Evaluating structural deterioration by dynamic response.” *J. of Struct. Engrg.*, 121:1197–1204.

Chen, S.S., and Kim, S. (1994). “Neural network based signal monitoring in a smart structural system.” *Smart Structures and Materials 1994: Smart Sensing, Processing, and Instrumentation*, SPIE, Vol.2191, 176–186.

Clayton, E.H., and Spencer, B.F., Jr. (2001). “Development of an experimental model for the study of infrastructure preservation.” *Proc. of the National Conf. on Undergraduate Research (NCUR)*, Whitewater, WI.

Crossbow Technology Inc. “MICAz wireless measurement system.” http://www.xbow.com, June, 2004.

Doebling, S.W., Farrar, C.R., Prime, M.B., and Shevitz, D.W. (1996). “Damage identification and health monitoring of structural and mechanical systems from changes in their vibration characteristics: a literature review.” Los Alamos National Laboratory Report LA-13070-MS.

Dos Santos, J.M.C., and Zimmerman, D.C. (1996). “Structural Damage Detection Using Minimum Rank Update Theory and Parameter Estimation,” *Proc. of the AIAA/ASME/AHS Adaptive Structures Forum*, 168–175, AIAA-96-1282.

Dyke, S.J., Caicedo, J.M., and Johnson, E.A. (2000). “Monitoring a benchmark structure for damage identification.” *Proc. of the Engineering Mechanics Specialty Conference*, Austin, Texas.

Farrar, C.R., Doebling, S.W., and Duffey, T.A. (1999). “Vibration-based damage detection.” *Proc. of the Structural Dynamics Forum SD2000*, Los Alamos, NM, 11–17.

Friswell, M.I., Penny, J.E.T., and Lindfield, G. (1995). “The location of damage from vibration data using genetic algorithms.” *Proc. of the 13th International Modal Analysis Conf.*, Nashville, Tennessee, Vol.II, 1640–1646.

Fox, C.H.J. (1992). “The location of defects in structures: a comparison of the use of natural frequency and mode shape data.” *Proc. of the 10th International Modal Analysis Conf.*, Las Vegas, Nevada, Vol.I, 522–528.

Frampton, K.D. (2001). “Decentralized control of structural acoustic radiation.” *Proc. of International Mechanical Engineering Congress and Exhibition*, New York, NY, Vol.28, 232–238.

Gao, Y., and Spencer, B.F., Jr. (2002). “Damage localization under ambient vibration using changes in flexibility.” *J. of Earthquake Engineering and Earthquake Vibration*, 1(1):136–144.

Gao, Y., and Spencer, B.F., Jr. (2005a). “Flexibility-based approach for continuous monitoring of civil infrastructure.” *Proc. of the 9th International Conference on Structural Safety and Reliability*, Rome, Italy, June 19-23.

Gao, Y., and Spencer, B.F., Jr. (2005b). “Damage diagnosis of a truss structure employing a distributed computing algorithm.” *Proc. of the 2nd International Conference on Structural Health Monitoring of Intelligent Infrastructure*, Shenzhen, China, November 16-18.

Gao, Y. and Spencer, B.F., Jr. (2006). “Online damage diagnosis of civil infrastructure employing a flexibility-based approach.” *J. of Smart Materials and Structures*, 15:9–19.

Gao, Y., and Spencer, B.F. Jr. (2007). “Experimental verification of a distributed computing algorithm for structural health monitoring.” *J. of Smart Structures and Systems*, Vol. 3, No. 4.

Gao, Y., Spencer, B.F., Jr., and Bernal, D. (2004). “Experimental verification of the damage locating vector method.” *Proc. of the 1st International Workshop on Advanced Smart Materials and Smart Structures Technology*, Honolulu, Hawaii.

Gao, Y., Spencer, B.F., Jr., and Bernal, D. (2007). “Experimental verification of the damage locating vector method.” *J. of Eng. Mech.*, 133(10):1043–1049.

Gao, Y., Spencer, B.F. Jr., and Ruiz-Sandoval, M. (2006). “Distributed computing algorithm for structural health monitoring.” *J. of Structural Control and Health Monitoring*, 13(1): 488–507.

Garcia, G., Osegueda, R., and Meza, D. (1998). “Comparison of the damage detection results utilizing an ARMA model and a FRF model to extract the modal parameters.” *Proc. of SPIE: Smart Systems for Bridges, Structures, and Highways*, San Diego, CA, Vol.3325, 244–252.

Hill, J. and Culler, D. (2002). “Mica: a wireless platform for deeply embedded networks.” *IEEE Micro*, Vol. 22, No. 6, November/December, 12–24.

Hjelmstad, K.D. (1996). “On the uniqueness of modal parameter estimation.” *J. Sound Vib.*, 192(2):581–598.

Ho, Y.K., and Ewins, D.J. (1999). “Numerical evaluation of the damage index.” *Proc. of 2nd Int. Workshop on Structural Monitoring*, Stanford, CA, 995–1011.

Ho, Y.K., and Ewins, D.J. (2000). “On the structural damage identification with mode shapes.” *European COST F3 Conf. on System Identification and Structural Health Monitoring*, Madrid, Spain, 677–686.

Hollar, S. (2000). “COTS Dust.” Master of Science Thesis, University of California at Berkeley.

James, G.H. III, Carne, T.G., and Lauffer, J.P. (1993). “The natural excitation technique (NExT) for modal parameter extraction from operating wind turbines.” SAND92-1666, UC-261, Sandia National Laboratories.

Juang, J.N., and Pappa, R.S. (1985). “An eigensystem realization algorithm for modal parameter identification and model reduction.” *J. of Guidance Control and Dyn.*, 8:620–627.

Juang, J.N. (1994). *Applied System Identification*, New Jersey:Prentice Hall PTR.

Kim, K., Ryu, J., Lee, S., and Choi, L. (1997). “In-situ monitoring of Sungsan Bridge in Han River with a optical fiber sensor system.” *Proc. of SPIE: Smart Systems for Bridges, Structures, and Highways*, San Diego, CA, Vol.3043, 72–76.

Kim, J.-H., Jeon, H.-S., and Lee, C.-W. (1992). “Application of the modal assurance criteria for detecting structural faults.” *Proc. of the 10th International Modal Analysis Conf.*, Las Vegas, Nevada, Vol.I, 536–540.

Kling, R. (2003). Intel Research Mote. Intel Corporation Research, Santa Clara, California.

Ko, J.M., Wong, C.W., and Lam, H.F. (1994). “Damage detection in steel framed structures by vibration measurement approach.” *Proc. of 12th International Modal Analysis Conf.*, Honolulu, Hawaii, 280–286.

Lam, H.F., Ko, J.M., and Wong, C.W. (1995). “Detection of damage location based on sensitivity analysis,” *Proc. of the 13th International Modal Analysis Conf.*, Nashville, Tennessee, 1499–1505.

Liu, R.C., Zhou, L., Cheng X., and Mau. S.T. (2001). “Wireless sensors for structural monitoring.” *Strong Motion Instrumentation for Civil Engineering Structures*, 253–266.

Luo, H., and Hanagud, S. (1997). “Dynamic learning rate neural network training and composite structural damage detection.” *AIAA J.*, 35:1522–1527.

Lynch, J.P. (2002). Decentralization of wireless monitoring and control technologies for smart civil structures. PhD Thesis, Stanford University, CA.

Lynch, J.P., Law, K.H., Kiremidjian, A.S., Kenny, T.W., Carryer, E., and Patridge, A. (2001). “The design of a wireless sensing unit for structural health monitoring.” *3rd International Workshop on Structural Health Monitoring*, Stanford, California, 1041–1050.

Maeck, J., and De Roeck, G. (1999). “Damage detection on a prestressed concrete bridge and RC beams using dynamic system identification.” *Proc. of the International Conf. on Damage Assessment of Structures (DAMAS 99)*, Dublin, Ireland, 320–327.

Mares, C., and Surace, C. (1996). “An application of genetic algorithms to identify damage in elastic structures.” *J. of Sound and Vibration*, 195:195–215.

Maser, K., Egri, R., Lichtenstein, A., and Chase, S. (1997). “Development of wireless global bridge evaluation and monitoring system (WGBEMS).” *Proc. of the Specialty Conf. on Infrastructure Condition Assessment: Art, Science, Practice*, 91–100.

Masri, S.F., Nakamura, M., Chassiakos, A.G., and Caughey, T.K. (1996). “Neural network approach to detection of changes in structural parameters.” *J. of Engrg. Mech.*, 122:350–360.

Messina, A., Jones, I.A., and Williams, E.J. (1996). “Damage detection and localization using natural frequency changes.” *Identification in Engrg. Systems: Proc. of the International Conf.*, Swansea, U.K., 67–76.

Mitchell, K., Sana, S., Balakrishnan, V.S., Rao, V., and Pottinger, H.J. (1999). “Micro sensors for health monitoring of smart structures.” *SPIE Conf. on Smart Electronics and MEMS*, 3673:351–358.

Mitchell, K., Dang, N., Liu, P., Rao, V., and Pottinger H.J. (2001). “Web-controlled wireless network sensors for structural health monitoring.” *Proc. of SPIE the International Society for Optical Engrg.*, 4334:234–243.

National Bridge Inventory Data (NBID) (1998). Rep. No.FHWA-PD-96-001, Washington D.C.

National Research Council Computer Science and Telecommunications Board (2002). Embedded everywhere, a research agenda for networked systems of embedded computers. *National Research Council, National Academy Press*; Washington, D.C. 236.

Ni, Y.Q., Wang, B.S., and Ko, J.M. (1999). “Selection of input vectors to neural networks for structural damage identification.” *Smart Structures and Materials 1999: Smart Systems for Bridges, Structures, and Highways*, SPIE, 3671:270–280.

Pandey, A.K., and Biswas, M. (1994). “Damage detection in structures using changes in flexibility.” *J. of Sound and Vibration*, 169(1):3–17.

Pandey, A.K., and Biswas, M. (1995a). “Damage diagnosis of truss structures by estimation of flexibility change.” *Modal Analysis*, 10:104–117.

Pandey, A.K., and Biswas, M. (1995b). “Experimental verification of flexibility difference method for locating damage in structures.” *J. of Sound and Vibration*, 184:311–328.

Parloo, E., Verboven, P. Cuillame, P., and Overmeire, M.V. (2001). “Sensitivity-based mass normalization of mode shape estimates from output-only data.” *Proc. of the International Conf. on Structural System Identification*, Kassel, Germany, 627–636.

Parloo, E., Verboven, P. Cuillame, P., and Overmeire, M.V. (2002). “Iterative calculation of nonlinear changes by first order approximations.” *Mechanical Systems and Signal Proc.*, 16(5):757–767.

Peeters, B., Maeck, J., and Roeck, G.D. (2001). “Vibration-based damage detection in civil engineering: excitation sources and temperature effects,” *Smart Materials and Structures*, 10(3):518–527

Polastre, J., Szewczyk, R., and Culler, R. (2005). “Telos: enabling ultra-low power wireless research.” *Proc. of the Fourth International Conf. on Information Processing in Sensor Networks: Special track on Platform Tools and Design Methods for Network Embedded Sensors (IPSN/SPOTS)*, April 25-27.

Pothisiri, T., and Hjelmstad, K.D. (2003). “Structural damage detection and assessment from modal response.” *J. of Engrg. Mech.*, 129(2):135–145.

Ricles, J.M., and Kosmatka, J.B. (1992). “Damage detection in elastic structures using vibratory residual forces and weighted sensitivity.” *AIAA Journal*, 30:2310–2316.

Salawu, O.S., (1995). “Nondestructive assessment of structures using the integrity index method applied to a concrete highway bridge.” *Insight*, 37(11):875–878.

Salawu, O.S. (1997). “Detection of structural damage through changes in frequency: a review.” *Engrg. Struct.*, 19:718–723.

Sheinman, I. (1996). “Damage detection and updating of stiffness and mass matrices using mode data.” *Computers & Structures*, 59:149–156.

Shi, Z.Y., and Law, S.S. (1998). “Structural Damage Localization from Modal Strain Energy Change.” *J. of Sound and Vibration*, 218(5):825–844.

Shi, Z.Y., Law, S.S., and Zhang, L.M. (2000). “Structural Damage Detection from Modal Strain Energy Change.” *J. of Engrg. Mech.*, 126(12):1216–1223.

Shi, Z.Y., Law, S.S., and Zhang, L.M. (2002). “Improved Damage Quantification from Elemental Modal Strain Energy Change.” *J. of Engrg. Mech.*, 128(5):521–529.

Shin, S., and Hjelmstad, K.D. (1994). “Damage detection and assessment of structural systems from measured response.” *Civil Engrg. Studies*, SRS 593, UILU-ENG-94-2013, Univ. of Illinois at Urbana-Champaign, IL.

Sohn, H., Farrar, C.R., Hemez, F.M., Shunk, D.D., Stinemates, D.W., and Nadler, B.R. (2003). “A review of structural health monitoring literature: 1996-2001.” Los Alamos National Laboratory Report LA-13976-MS.

Spencer, B.F., Jr., Ruiz-Sandoval, M., and Gao, Y. (2002). “Frontiers in structural health monitoring.” *Proc. of China-Japan Workshop on Vibration Control and Health Monitoring of Structures and 3rd Chinese Symposium on Structural Vibration Control*, Shanghai, China.

Spencer, B.F., Jr., Ruiz-Sandoval, M.E. and Krata, N. (2004). “Smart sensing technology: opportunities and challenges.” *J. of Structural Control and Health Monitoring*, 11:349–368.

Spencer, B.F., Jr., and Gao, Y. (2005). “New paradigms for structural health monitoring employing smart sensor technology.” *Proc. of the 2nd International Workshop on Advanced Smart Materials and Smart Structures Technology*, Gyeong-ju, Korea, July 21-24.

Spyrakos, C.C., Chen, H.L., Stephens, J., and Govindaraj, V. (1990). “Evaluating structural deterioration using dynamic response characterization.” *Intelligent Struct.*, edited by K.P. Chong, S.C. Liu and J.C. Li, Elsevier Applied Science, London, 137–154.

Straser, E.G., and Kiremidjian A.S. (1996). “A modular visual approach to damage monitoring for civil structures.” *Proc. of SPIE v2719, Smart Structures and Materials*, 112–122.

Straser, E.G., and Kiremidjian A.S. (1998). “A modular wireless damage monitoring system for structures.” The John A. Blume Earthquake Engineering Center, Report No. 128.

Stubbs, N. (1985). “A general theory of non-destructive damage detection in structures.” *Proc. of the 2nd International Symposium on Struct. Control*, Ontario, Canada, 694–713.

Stubbs, N., and Osegueda, R. (1987). “Global nondestructive damage evaluation of offshore platforms using modal analysis.” *Proc. of the 6th International Offshore Mech. and Arctic Engrg. Symposium*, Houston, Texas, Vol.II, 517–524.

Stubbs, N., and Osegueda R. (1990a). “Global non-destructive damage evaluation in solids.” *Modal Analysis: The International J. of Analytical and Experimental Modal Analysis*, 5(2):67–79.

Stubbs, N., and Osegueda R. (1990b). “Global damage detection in solids–experimental verification.” *Modal Analysis: The International J. of Analytical and Experimental Modal Analysis*, 5(2):81–97.

Toksoy, T., and Aktan, A.E. (1994). “Bridge-condition assessment by modal flexibility.” *Experimental Mech.*, 34:271–278.

Vandiver, J.K. (1975). “Detection of Structural Failure on Fixed Platforms by Measurement of Dynamic Response,” *Proc. of the 7th Annual Offshore Technology Conf.*, 243–252.

West, W.M. (1984). “Illustration of the use of modal assurance criterion to detect structural changes in an orbiter test specimen.” *Proc. Air Force Conf. on Aircraft Struct. Integrity*, 1–6.

Williams, E.J., Messina, A., and Payne, B.S. (1997). “A frequency-change correlation approach to damage detection.” *Proc. of the 15th International Modal Analysis Conf.*, Orlando, Florida, Vol.I, 652–657.

Wu, X., Ghaboussi, J., and Garrett, J.H. (1992). “Use of neural networks in detection of structural damage.” *Computers & Structures*, 42:649–659.

Yao, G.C., Chang, K.C., and Lee, G.C. (1992). “Damage diagnosis of steel frames using vibrational signature analysis.” *J. of Engrg. of Mech.*, 118(9):1946–1961.

Zimmerman, D.C., Yap, K.C., and Hasselman, T. (1997). “Evolutionary approach for model refinement.” *Proc. of the 15th International Modal Analysis Conf.*, Orlando, Florida, Vol.I, 551–557.

List of Recent NSEL Reports

No.	*Authors*	*Title*	*Date*
001	Nagayama, T. and Spencer, B.F.	Structural Health Monitoring Using Smart Sensors	Nov. 2007
002	Sun, S. and Kuchma, D.A.	Shear Behavior and Capacity of Large-Scale Prestressed High-Strength Concrete Bulb-Tee Girders	Nov. 2007
003	Nagle, T.J. and Kuchma, D.A.	Nontraditional Limitations on the Shear Capacity of Prestressed, Concrete Girders	Dec. 2007
004	Kwon, O-S. and Elnashai, A.S.	Probabilistic Seismic Assessment of Structure, Foundation, and Soil Interacting Systems	Dec. 2007
005	Nakata, N., Spencer, B.F., and Elnashai, A.S.	Multi-dimensional Mixed-mode Hybrid Simulation: Control and Applications	Dec. 2007
006	Carrion, J. and Spencer, B.F.	Model-based Strategies for Real-time Hybrid Testing	Dec. 2007
007	Kim, Y.S., Spencer, B.F., and Elnashai, A.S.	Seismic Loss Assessment and Mitigation for Critical Urban Infrastructure Systems	Jan. 2008
008	Gourley, B.C., Tort, C., Denavit, M.D., Schiller, P.H., and Hajjar, J.F.	A Synopsis of Studies of the Monotonic and Cyclic Behavior of Concrete-Filled Steel Tube Members, Connections, and Frames	April 2008
009	Xu, D. and Hjelmstad, K.D.	A New Node-to-node Approach to Contact/Impact Problems for Two Dimensional Elastic Solids Subject to Finite Deformation	May 2008
010	Zhu, J. and Popovics, J.S.	Non-contact NDT of Concrete Structures Using Air Coupled Sensors	May 2008
011	Gao, Y. and Spencer, B.F.	Structural Health Monitoring Strategies for Smart Sensor Networks	May 2008